1992

Gas Phase And Surface Reactions In Organometallic Chemical Vapour Deposition Of Platinum

Eric Chuan-whatt Ou

GAS PHASE AND SURFACE REACTIONS IN ORGANOMETALLIC CHEMICAL VAPOUR DEPOSITION OF PLATINUM

by

Eric Chuan-Whatt Ou

Department of Chemistry

Submitted in partial fulfilment
of the requirements for the Degree of
Doctor of Philosophy

Faculty of Graduate Studies
The University of Western Ontario
London, Ontario
June 1992

ISBN 0-315-75354-4

ABSTRACT

Organometallic chemical vapour deposition (OMCVD) films usually have carbon as an impurity. This comes from the decomposition of the ligands in the organometallic precursor. Understanding the chemical reactions in the decomposition will greatly enhance our ability to control the impurity level in these films and also the epitaxial growth of the films. Depending on the pressure in the reactor, the important reactions could be in the gas phase or on the surface.

Decomposition of the precursor, *cis*-dimethyl platinum diisocyanide in presence of hydrogen shows reduction in carbon impurity. The decomposition was carried out in an infrared gas cell so that infrared light could be used in a transmission experiment as an in-situ probe of the reaction. It was found that the methyl platinum groups reacted with the hydrogen to give an increased yield of methane. The isocyanide ligand appears to leave the complex in one piece in an initial reversible equilibrium step. Subsequently they reacted with hydrogen gas to give ammonia. Kinetic measurements demonstrate a heterogenous component to the reaction.

Surface reactions were carried out in an ultra high vacuum (UHV) chamber. The main surface tools used in the study were Infrared Reflection Absorption Spectroscopy (IRRAS) and Temperature Programmed Desorption (TPD). The interaction of acetonitrile with methyl isocyanide with Pt(111) was also studied to

assist in the overall understanding of the decomposition mechanism of *cis*-dimethyl platinum diisocyanide. When the precursor is adsorbed on a Pt(111) surface at 110 K, it does so dissociatively to give terminally bonded methyl isocyanide and some platinum hydrocarbon fragments. Thermochemistry of the complex on Pt(111) involved decomposition to H_2 and HCN. The effect of surface carbon on Pt(111) appears to turn off the reactivity of the surface. When it was sufficiently turned off, monolayer adsorption was molecular. The thermal chemistry was also changed as dehydrogenation was greatly reduced. Loss of methyl isocyanide at 525 K was turned on instead and is consistent with decomposition studies at 580 K in the infrared cell where methyl isocyanide loss was also observed.

ACKNOWLEDGEMENTS

I would like to take this opportunity to thank many people who helped bring this study to completion. I would like to thank my supervisor Prof. P. R. Norton, who has provided excellent supervision. From him, I emulate all the qualities of an excellent scientist. I wish to thank Prof. R. J. Puddephatt for his many discussions in organometallic chemistry. My thanks also go to Dr. K. Griffiths for his help in initiating the construction of the ultra high vacuum chamber and his supervision in the construction of the Kelvin probe for measurements of work function change. I thank Prof. M. Trenary of the University of Illinois for assistance and advice in setting up the infrared reflection absorption experiment. I thank Dr. S. Roy for his help in the gas phase experiments, Dr. P.A. Young for his help in the surface experiments and Dr. N. Dryden for the synthesis of the organometallic precursors. I also thank every member of Interface Science Western for a great working environment. Support from the Ontario Centre of Materials Research is greatly appreciated.

The support my family gave me during the preparation of the thesis goes beyond the written pages. I would especially like to thank my wife for support and for typing the manuscript despite her busy schedule and Jesse for never a dull moment. Finally, I thank my God, the El Shuddai, for the rich supply of His life in meeting my every need.

TABLE OF CONTENTS

Page

LIST OF ABBREVIATIONS

ADC : analog-to-digital converter

AES : Auger electron spectroscopy

a.u. : absorbance unit

CVD : chemical vapour deposition

DPt : *cis*-dimethyl platinum diisocyanide, where the 6 hydrogens on the 2 methyl attached to the platinum have been deuterated.

D'Pt : *cis*-dimethyl platinum diisocyanide, where the 6 hydrogens on the 2 methyl attached to the nitrogen have been deuterated.

$D_{12}Pt$: *cis*-dimethyl platinum diisocyanide where all 12 hydrogens have been deuterated.

EELS : electron energy loss spectroscopy

FTIR-RAS : fourier transform infrared-reflection absorption spectroscopy

FWHM : full width at half maximum

HPt : *cis*-dimethyl platinum diisocyanide

IR : infrared

LEED : low energy electron diffraction

Ligand : methyl isocyanide

OMCVD : organometallic chemical vapour deposition

SNR : signal to noise ratio

TD-$\Delta\phi$: temperature desorption work function change

TD-FTIR-	temperature desorption fourier transform infrared reflection
RAS:	absorption spectroscopy
TPD :	temperature programmed desorption
UHV :	ultra high vacuum

LIST OF FIGURES

LIST OF TABLES

CHAPTER 1

INTRODUCTION

1.1 Introduction

Thin films are very important to modern technology. They are important as protective coatings for steel turbines.[1] Cobalt-platinum bimetallic thin films are also increasingly finding applications as magnetic materials, because this system has been found to exhibit large perpendicular magnetic anisotropies, and has allowed for high density magnetic recording of information.[2] Furthermore, they play a big part in the miniaturization of components in very large scale integration (VLSI) of electronic devices.[3]

Thin films can be deposited by physical methods as well by chemical vapour deposition.

1.2 Physical Methods of Deposition

1.2.1 Cathode Sputtering

This technique uses an inert gas, xenon or argon at a pressure of 10^{-1} or 10^{-2}

---

[1] Prof. Puddephatt has a patent with Liburdi Engineering for coating steel turbines using CVD.

[2]Zeper, W.B., Greidanus, F.J.A.M., and Carcia, P.F., **IEEE Transactions on Magnetics**, 25/5 (1989), 3764-66

[3]Blech, I., Sello, H and Gregor, L.V., in "Handbook of Thin Film Technology" (Maissel L.I. and Glang R., eds.), (1970), 23-1.

torr. A potential drop of several kilovolts is applied to this gas. A glow discharge is created in the inert gas from which positive ions are accelerated towards the cathode (target) and material is removed from the cathode and deposited on the substrates.[4] If substrates are placed at the anode, only negatively charged ions or neutrals will arrive at the substrate.

1.2.2 Evaporation

The material to be deposited is heated to its evaporation point which results in deposition on the substrate. The pressure in the chamber is typically at about 10^{-6} torr.

1.2.3 Molecular Beam Epitaxy

The availability of ultra high vacuum systems has allowed the growth of thin films using molecular beam epitaxy. Successful growth of III/V semiconductors has been achieved where molecular beams of gallium and arsenic have been directed at the substrate under UHV conditions and GaAs films grown epitaxially.[5] In contrast to high vacuum techniques operating at pressures of 10^{-6} torr, contamination of the films is greatly reduced in molecular beam epitaxy. Typical pressure is in the 10^{-10}

---

[4]Spencer, E.G., and Schmidt, P.H., **J. Vac. Sci. Technol.**, 8 (1971), S52.

[5]Brillson, L.J., Viturro, R.E., Mailhiot, C., Shaw, J.L., Tache, N., McKinley, J., Margaritondo, G., Woodall, J.M., Kirchner, P.D., Pettit, G.D., and Wright, S.L., **J. Vac. Sci. Technol. B**, 6 (1988), 1263.

torr range.

1.3 Chemical Vapour Deposition (CVD)

In contrast to physical methods, CVD is a chemical process whereby a chemical precursor containing the element to be deposited is transported in the vapour phase to the substrate and decomposed, with the element deposited as a thin film on the substrate. Features particular to the CVD processes are good conformal step coverage, low temperature deposition, absence of radiation damage and high wafer throughput, which are important in very large scale integration (VLSI). Many experimental variables during CVD growth can be changed leading to different types of film with respect to morphology, composition and properties. The variables are: pressure, temperature, energy source for decomposition, carrier gas, type of precursor and surface. For an adequate description of CVD, the chemistry involved must be understood. Changing any one of the variables will change the chemistry of the process. Obviously changing the precursor (not changing the element to be deposited) will change the chemistry as each precursor will have its own properties. The different energy source used usually results in different decomposition pathways for the same precursor. For example, thermally induced decomposition is different from laser decomposition, which in turn is different from plasma decomposition. Even changing the pressure causes the decomposition pathways to change; under high pressures the precursor basically interacts with itself in the gas phase while at low pressures, surface interactions with the growing surface become important.

1.3.1 Silicon CVD.

Silicon is usually deposited from the pyrolysis of silane gas (SiH_4). Joyce and Bradley[6] performed one of the earliest studies of silicon CVD. Silicon deposition rates were studied as a function of substrate temperature and silane partial pressure. They found that the process was thermally activated with an activation energy of 37 kcal/mole. Second order desorption of hydrogen from the growing film surface was thought to be the rate-limiting step. The generation of silylene SiH_2 from the decomposition of silane[7]

is generally thought to be the first step in film growth. Silylene is a very reactive intermediate and is known to insert readily into Si-H bonds[8] and gives amorphous silicon hydride films.

Farnaam and Olander[9] have studied SiH_4 decomposition on Si(111) at temperatures above 900 °C. They proposed that SiH_4 chemisorbs by reacting with a surface silicon atom to produce two bound SiH_2 species and these decompose with the evolution of molecular hydrogen to deposit silicon.

1.3.2 GaAs OMCVD

Organometallic Chemical Vapour Deposition (OMCVD) is similar to CVD,

---

[6]Joyce, B.A., Bradley, R.R, **J. Electrochem. Soc.**, 110 (1963), 1235-40.

[7]Purnell, J.H., Walsh, R., **Chem.Phys.Lett.**, 110 (1984), 330-34.

[8]Gaspar, P.P., **Reactive Intermed.**, 3 (1985), 333-427

[9]Farnaam, M.J., Olander, D.R., **Surf. Sci.**, 145 (1984), 390-406

except that the precursor molecule is an organometallic molecule. Kuech and Veuhoff[10] have investigated the incorporation of carbon during the OMCVD of GaAs from trimethylgallium (TMG) and arsine. They suggested that methyl groups, produced by the heterogenous decomposition of TMG, recombine on the surface with atomic hydrogen, produced in the heterogenous decomposition of AsH_3 to yield methane. Carbon incorporation declined rapidly with increased AsH_3 partial pressure, consistent with the proposal. Recently Memmert and Yu[11] investigated the pyrolysis of TMG on GaAs(100) surfaces and found that CH_3, and not CH_4 is the major product with and without arsine. The presence of arsine did accelerate the CH_3 desorption process.

1.3.3 Aluminum OMCVD

Bent et al[12] have investigated the decomposition of triisobutylaluminum (TIBA) on Al(111) and Al(100) surfaces in the OMCVD of aluminum films. TIBA decomposes both these surfaces at surface temperatures less than 600 K by a β-hydride elimination reaction to give hydrogen and isobutylene and leads to carbon free aluminum films. In contrast above 600 K, the β-methyl elimination reaction and subsequent α-hydrogen abstractions from the surface methyl group become important and are the source of carbon incorporation in the aluminum film.

---

[10]Kuech, T.F., Veuhoff, E., J. Cryst. Growth, 68 (1984), 148-56

[11]Memmert, U., Yu, M.L., Appl. Phys. Lett., 56/19 (1990), 1883-85

[12]Bent, B.E., Nuzzo, R.G., Dubois, L.H., J. Am. Chem. Soc., 111/5 (1989), 1634-44

1.3.4 Platinum OMCVD

Aluminum silicon interfaces could be ruined by aluminum diffusion into silicon. Well defined (i.e. sharp) platinum silicon interfaces[13] have been reported and platinum may be a viable alternative to aluminum in metal-semiconductor contacts.

a. Pt(II) Organometallic Complexes As Precursors for the OMCVD of Platinum

Prof. R.J. Puddephatt, an organometallic chemist at University of Western Ontario has synthesized Pt(II) organometallic complexes and has studied the platinum OMCVD films from the decomposition of *cis*-$Me_2Pt(MeNC)_2$. The following paragraphs briefly summarizes the work that he has done.[14] The following complexes have been synthesized as possible precursors for platinum OMCVD:

(1) *cis*-$Me_2Pt(MeNC)_2$ -- labelled as HPt

(2a) *cis*-$(CD_3)_2Pt(MeNC)_2$ -- labelled as DPt

(2b) *cis*-$Me_2Pt(CD_3NC)_2$ -- labelled as D'Pt

(2c) *cis*-$(CD_3)_2Pt(CD_3NC)_2$ -- labelled as $D_{12}Pt$

(3) *cis*-$Me_2Pt(XyNC)_2$ (Xy = 2,6-$Me_2C_6H_3$)

(4) $Me_2Pt(COD)$ (COD = 1,5-cyclo-octadiene)

(5) *cis*-$Me(\sigma\text{-}CH_2CH{=}CH_2)Pt(MeNC)_2$

(6) *cis*-$Me(\sigma\text{-}CH_2CH{=}CH_2)Pt(XyNC)_2$

(7) *cis*-$Me(\sigma\text{-}CH_2CH{=}CH_2)Pt(^tBuNC)_2$

---

[13]Morgen, P., Szymonski, M., Onsgaard, J., Jorgensen, B., Rossi, G., **Surf. Sci.**, 197 (1988), 347.

[14]Dryden, N.H., Kumar, R., Ou E., Rashidi, M., Roy, S., Norton, P.R., Puddephatt, R.J., Scott, J.D., **Chem. Mater.**, 3 (1991), 677-85

(8) $Me(\sigma\text{-}CH_2CH{=}CH_2)\text{-}Pt(COD)$

(9) *cis*-$Me(CH{=}CH_2)Pt(MeNC)_2$

(10) $Me(^tBuC{\equiv}C)Pt(MeNC)_2$

The precursors are colorless or pale-yellow solids except for 7 which is an oil. The thermal stability of the compounds varies depending on the ligands. Compounds 1 to 4 are air stable. 5,6 and 8 to 10 can be stored indefinitely at 0 °C in the absence of light and 7 decomposes slowly at 0 °C.

The thermolysis of dialkylplatinum(II) complexes in the presence of hydrogen has been found to give platinum films of high purity. These precursors therefore offer a viable alternative to the use of the platinum(IV) precursors $PtMe_3(C_5H_5)$ and $PtMe_3(MeC_5H_4)$. In contrast to Pt(IV) complexes, the thermal stability of Pt(II) complexes can be modified by choice of alkylplatinum groups. The photochemical stability can be modified by changing the supporting ligands. Unfortunately, they have lower volatility than the Pt(IV) precursors. Both classes of precursor give excellent purity of the platinum films when OMCVD is carried out in the presence of hydrogen.

Cis-dimethyl platinum diisocyanide could be decomposed by UV heating at 150 °C in the presence of UV radiation. Since thermolysis of HPt does not occur at this temperature, the OMCVD is clearly photochemically enhanced when the ligand is MeNC. In all cases, the thermolysis temperature could be lowered to 100 - 150 °C from 250 °C when OMCVD was carried out in the presence of hydrogen.

The allylplatinum complex *cis*-Me(σ-$CH_2CH{=}CH_2$)Pt(MeNC)$_2$ gave efficient OMCVD at 180 °C whereas the complex *cis*-$Me_2Pt(MeNC)_2$ required 250 °C for efficient OMCVD. Thus the σ-allyl group provides a weak link and allows decomposition at a significantly lower temperature, presumably due to lower Pt-C bond energy for the allyl-platinum compared to the methyl-platinum group. The vinyl derivative also decomposed at lower temperature, but its synthesis is more difficult and it decomposed on storage.

b. Nature of Carbon Impurities in the Platinum Film from OMCVD of *cis*-[$Me_2Pt(MeNC)_2$]

X-ray Photoelectron Spectroscopy (XPS) analysis determined that the carbon content decreased considerably for films prepared with hydrogen as carrier gas. Narrow scan XPS analysis was carried out in the 275-295 (C(1s)) and 65-85 (Pt(4f)) eV regions, of two films prepared by OMCVD without hydrogen using the precursors $Me_2Pt(MeNC)_2$ and $(CD_3)_2Pt(MeNC)_2$ respectively. The films were deposited on silicon substrates which had the native oxide on the surface. No Si-surface pretreatment was used. The C(1s) binding energy region showed three peaks at nearly the same positions for both films. The main peak appears at 283.9 - 284.1 eV, while two other peaks appear at 283.1 - 283.7 and 285.9 - 286.0 eV respectively. Carbon fragments that give signals in the 284 eV region are graphite and hydrocarbons and the XPS data cannot easily distinguish between these. The higher binding energy peak is likely due to C-O groups. The platinum $4f_{5/2}$ and $4f_{7/2}$ peaks

Figure 1.1 : Narrow-scan XPS analysis of platinum films formed by OMCVD from *cis*-($Me_2Pt(MeNC)_2$ (A,C(1s) region; B, Pt(4f) region) in the absence of hydrogen.

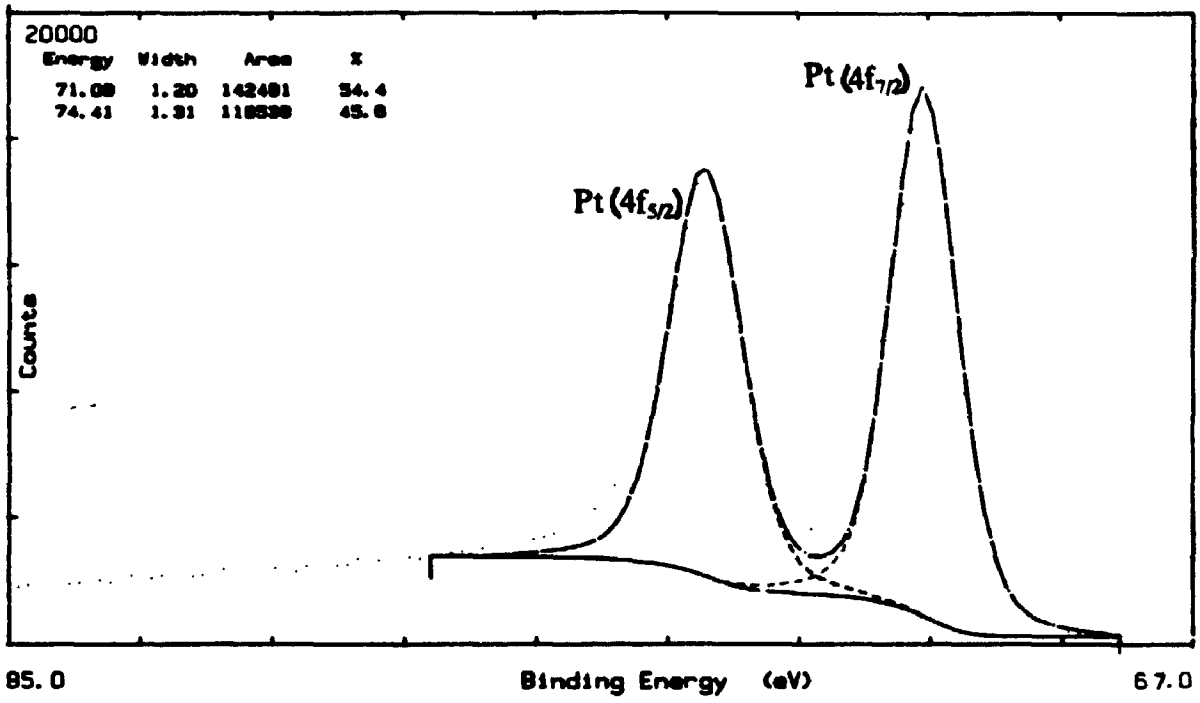
20000
Energy Width Area %
71.08 1.20 142481 54.4
74.41 1.31 118538 45.6
Pt (4f7/2)
Pt (4f5/2)
Counts
85.0
Binding Energy (eV)
67.0

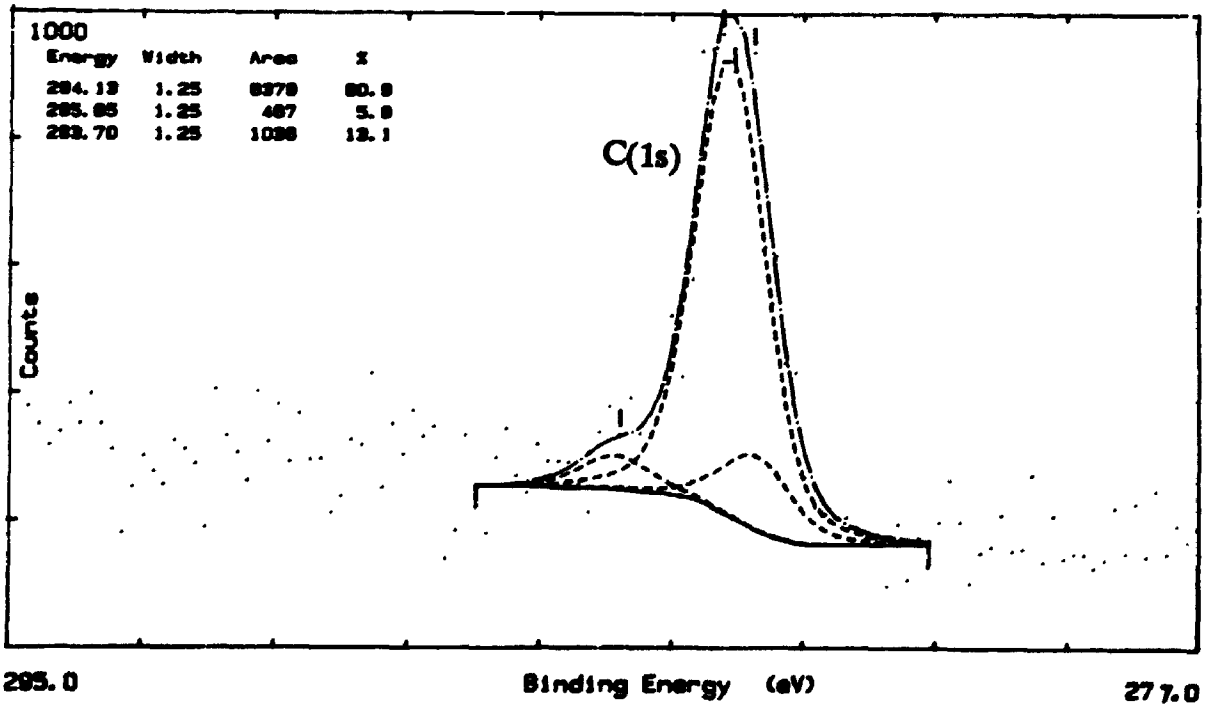
1000
Energy Width Area %
284.13 1.25 8378 80.8
285.65 1.25 487 5.8
283.70 1.25 1098 13.1
C(1s)
Counts
295.0
Binding Energy (eV)
277.0

appear consistently at 74.4 - 74.5 and 71.0 - 71.1 eV respectively, as expected for metallic platinum, (see figure 1.1).

The Secondary Ion Mass Spectroscopy (SIMS) analysis showed:

(1) Well defined interface characteristics in all cases, i.e., there was a sharp transition from platinum-rich to silicon-rich phases.

(2) Films prepared from $(CD_3)_2Pt(MeNC)_2$ showed very high count rates at m/e = 2 (the deuterium signal) whose intensity parallelled that of the platinum signal (m/e = 195) very well along the film depth; subsequently both the signals fell when the Si signal (at m/e = 30) grew in intensity.

(3) The relative intensities of the peaks at m/e = 13 and 14, corresponding in part to CH and CD respectively, were consistently higher throughout the platinum rich regions for films prepared from HPt [$I_{13}/I_{14} = 26\pm4$] compared to the DPt [$I_{13}/I_{14} = 5\pm3$] precursor. Since other contributing ions, such as nitrogen at $m/e = 14$ are likely to be constant in all samples, the presence of CH is higher in films prepared from the HPt and CD is higher in films prepared from the DPt precursor. The results from (2) and (3) indicate that the carbon impurities arise, at least in part, from the methylplatinum groups and are present as hydrocarbon and hydrocarbon fragments in the film.

1.4 Organization of the dissertation

In view of the importance of the mechanism of decomposition of the precursor

in the OMCVD process plus the thermal stability and volatility of cis-dimethyl platinum diisocyanide, a major study (described in this thesis) was undertaken to undertaken to understand the chemical reactions in the decomposition of cis-dimethyl platinum diisocyanide. Furthermore, the strong C≡N stretch in the complex would allow the use of infrared spectroscopy to be used as an in situ probe.

Chapter 1 introduces chemical vapour deposition (CVD) as one of the methods used to deposit thin films. The use of metallic thin films on semiconductor substrates in very large scale integration (VLSI) of electronic devices is very important. Abrupt metal-semiconductor interfaces can be achieved with platinum thin films, in contrast to aluminum because of the diffusion of Al in silicon. The research which has been completed prior to the current study using *cis*-$[(CH_3)_2Pt(MeNC)_2]$ as an organometallic precursor in OMCVD was described in Section 1.3.4. That work showed that decomposition of the precursor in the presence of hydrogen lowered the carbon impurity level in the film. This result motivated the study of the decomposition kinetics in the gas phase both in the presence and absence of hydrogen. It also prompted studies of surface reaction of the complex on platinum surfaces.

Chapter 2 describes the experimental tools in the investigation of the surface reaction of the precursor on a platinum surface. An ultra high vacuum (UHV) chamber with a base pressure of 1×10^{-10} torr was equipped with surface analytical

tools to study the surface reaction. This chapter describes the theory of low energy electron diffraction (LEED), Auger electron spectroscopy (AES), infrared reflection absorption spectroscopy (IRRAS), temperature programmed desorption (TPD) and work function measurements ($\Delta\phi$). Chapter 2 also outlines the considerations in the design and construction of the vibrating capacitor Kelvin probe for $\Delta\phi$ measurements, the IRRAS and the TPD experiments.

Chapter 3 studies the gas phase decomposition of the precursor. Infrared spectroscopy coupled with isotope labelling was used to study the decomposition mechanism of HPt both in the presence and absence of hydrogen gas. Kinetic measurements were also made.

The interaction of methyl isocyanide and acetonitrile with platinum (111) was studied next. This work was prompted by the gas phase studies in Chapter 3, where we show that decomposition of the complex to platinum and methane is preceded by an initial equilibrium step involving a loss of CH_3NC ligand. CH_3NC isomerizes to CH_3CN (acetonitrile) under these conditions. These molecules may interact with the growing platinum film and thus a study of the interaction of these molecules with a platinum (111) is warranted. Furthermore, the study may assist in the interpretation of the results obtained in the interaction of *cis*-dimethyl platinum diisocyanide with platinum (111), which is described in chapter 5. The acetonitrile work is described in Chapter 4 and the methyl isocyanide work is described in Section 5.3.1 in Chapter

5.

Chapter 5 studies the interaction of the precursor on Pt(111). We also examine the effect of changing the reactivity of the Pt(111) surface on this interaction. The tools used in the investigation were IRRAS, TPD and $\Delta\phi$.

Finally, Chapter 6 summarizes the main findings and discusses the areas where further investigations may be done to enhance the understanding of the mechanism of OMCVD of platinum using *cis*-$(CH_3)_2Pt(MeNC)_2$.

CHAPTER 2

EXPERIMENTAL TECHNIQUES

2.1 Ultra High Vacuum (UHV) Chamber

The stainless steel UHV chamber, called the Chemical Vapour Deposition (CVD) chamber, Figure 2.1, was specifically designed to conduct investigations in the interaction of organometallic precursors with metal and semiconductor surfaces. It is a 12-inch diameter cylindrical chamber with 3 levels of vacuum ports. At the top is an 8-inch port where a high precision long travel (HPLT) manipulator equipped with micrometer adjustments for x, y, z motions. At the bottom of the chamber, another 8-inch port would allow a high pressure cell to be introduced into the system. On the first level are eight $2^3/_4$-inch ports. A vibrating capacitor called a Kelvin probe is installed on one of these. On the second level is a $4^1/_2$-inch port used as a window for viewing the crystal. On its left is another $4^1/_2$-inch port which carries the organometallic doser. On the right is another similar port which carries a 600 amu Hiden, quadrupole mass spectrometer (QMS). Further away are four $4^1/_2$-inch ports for mounting infrared windows. The nearer two are for infrared reflection absorption experiments, while the further two are for multiple internal reflection infrared experiments for semiconductor work. The last port on this level is an 8-inch port which carries low energy electron diffraction optics for doing LEED and Auger spectroscopy.

Figure 2.1 : The Ultra High Vacuum (UHV) Chamber for the study of surface reactions in Organometallic Chemical Vapour Deposition.

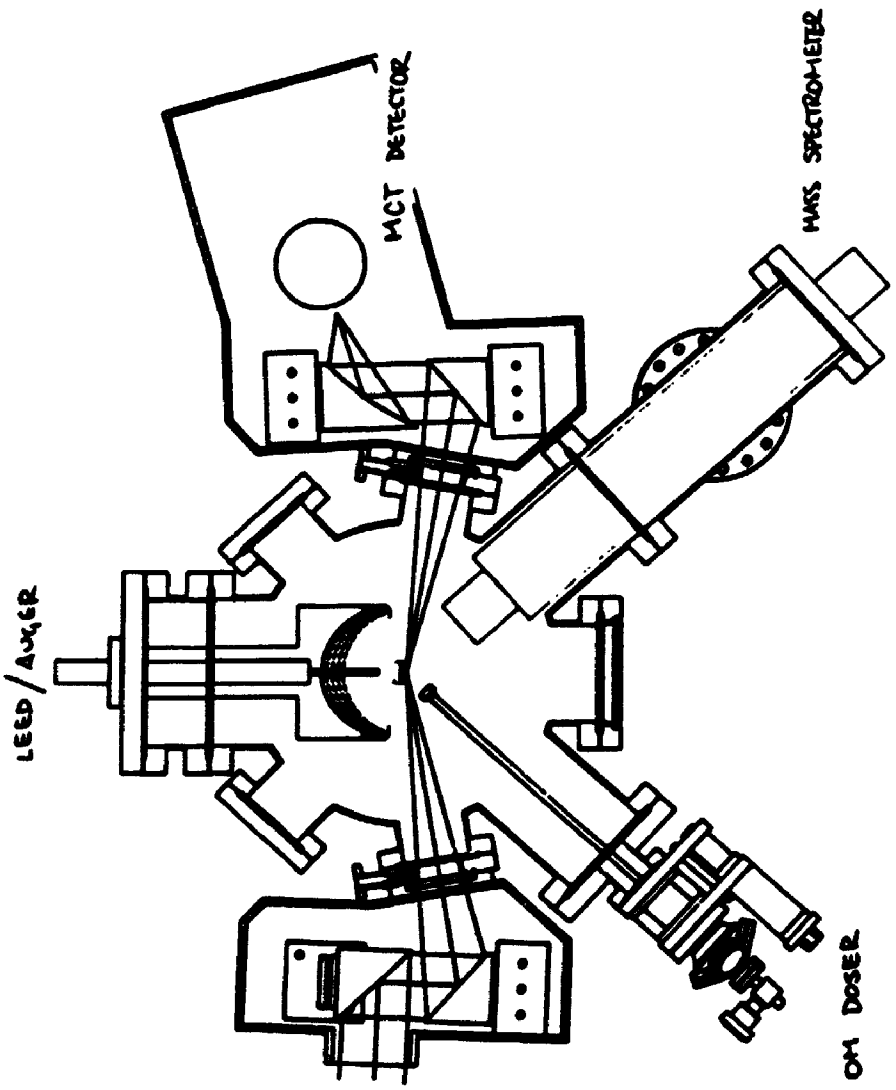

FTIR

On the last level are two 8-inch and two 6-inch ports. One 6-inch port is a pumping port for the turbomolecular pump (TMP). The other 6-inch port is for the gas manifold system. One 8-inch port is for the titanium sublimation pump (TSP) while the other one is for a planned vacuum load lock system for fast transfer of crystal samples.

The chamber is pumped by a 330 l/s turbomolecular pump (Balzers TPU330) and a titanium sublimator pump which has a pumping speed of 1000 l/s. The turbomolecular pump does not pump hydrogen well and is therefore supplemented by the sublimator pump. A safety interlock system was designed which interlocks all the switches in the various equipment ensuring that the whole vacuum system will shut down safely in the event of a power, water, air or pressure failure.

2.2 Low Energy Electron Diffraction (LEED)

High symmetry single crystal metal surfaces have a regular arrangement of atoms at the surface. The inter-atomic distances between these atoms is on the order of Å 's. The wavelength associated with an electron of energy E is expressed as:

$$\lambda = \frac{12.3}{(E_{eV})^{1/2}} \text{ Å} \qquad (2.1)$$

Thus beam energies used in LEED are about 100 eV. Beam currents are typically 0.2 - 1 μA. The crystal surface effectively behaves as a diffraction grating.

The diffraction condition for a one dimensional array of scatterers is $n\lambda = d \sin \phi$, where ϕ is the scattering angle on reflection, n is the order of diffraction and d is the inter-atomic distance. The electrons which satisfy this relation form a cone. For a two dimensional array, a second set of equations $n\lambda = d'\sin \phi'$ has to be simultaneously satisfied. The interaction of these two sets of cones produces "rods" in reciprocal space, which impinge on the phosphor screen as spots.

The LEED optics consist of four grids (Figure 2.2a). The first is held at ground to provide a field free region around the crystal which is also grounded. The middle pair of grids are held at a negative bias, close to the voltage of the primary electrons so that only elastically scattered electrons are allowed to pass. The last grid is held at ground. After passing the last grid, the elastically scattered electrons impinge on a phosphor screen, which is held at several kilovolts positive to give the electrons sufficient energy to excite the phosphor. The electrons which are allowed to arrive at the phosphor are therefore of the same energy as they all are elastically reflected off the crystal.

2.3 Auger Electron Spectroscopy

When a high energy beam of electrons (about 2000 eV) is brought to the crystal surface from an electron gun, it ejects an electron from a core level of the atom. An electron in a higher lying orbital fills the hole created, and energy is

Figure 2.2a : LEED operation * †

Figure 2.2b : Auger operation ** †

Notes:

* from lecture notes given by Prof. Schultz at the University of Western Ontario. (Chem. 657)

** obtained from J.C. Riviere (1990). "Surface Analytical Techniques", Oxford Science Publications, p. 57.

† The same optics are used in LEED and retarding field analyzer in Auger Spectroscopy. The second and the third grids are the retarding grids. During Auger operation, there is a modulation voltage superimposed on the retarding voltage.

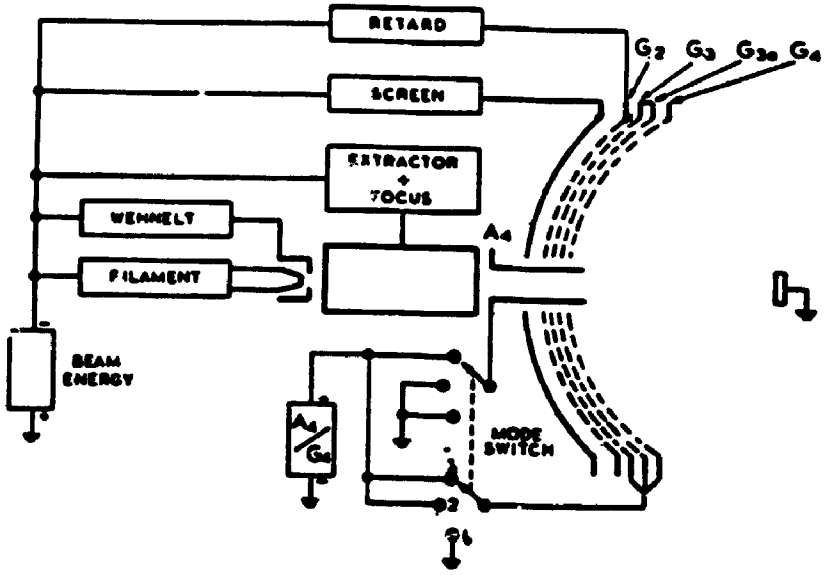
RETARD
SCREEN
EXTRACTOR
+
FOCUS
WEHNELT
FILAMENT
BEAM
ENERGY
MODE
SWITCH
G2
G3
G3a
G4
A4

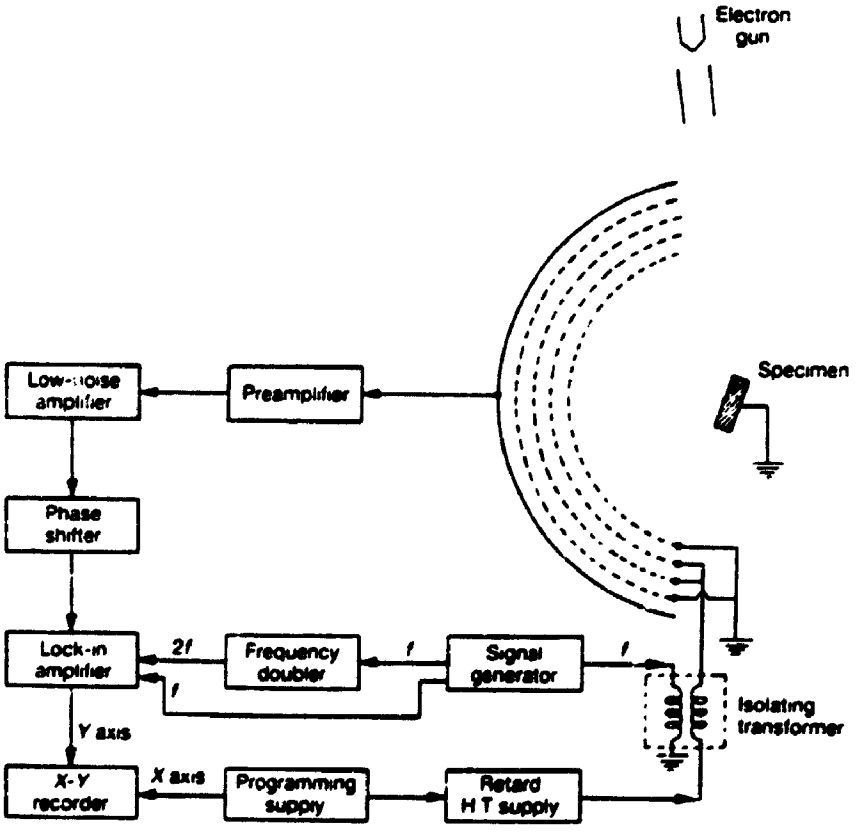
Electron
gun
Specimen
Low-noise
amplifier
Preamplifier
Phase
shifter
Lock-in
amplifier
2f
Frequency
doubler
f
Signal
generator
f
f
Y axis
X-Y
recorder
X axis
Programming
supply
Retard
H T supply
Isolating
transformer

released in this transition. The atom relaxes when the energy is transferred in a non-radiative process to a second electron, which is then ejected. This electron is called an Auger electron and its energy is characteristic of the element.

Platinum, carbon and nitrogen are the three elements that are of interest in this work. The intense Auger lines are Pt(NVV), C(KLL) and N(KLL) lines. The first letter is the original level ionised, the second is the energy level of the electron filling the hole and the third is the level from which the Auger electron leaves. Therefore, the energy used to eject the C(KLL) Auger electron is defined by the K and L levels of the carbon atom. Although large primary energies are used to excite any electrons, the escapes depths of the Auger electrons are small, giving the technique surface specificity.

The electron released is detected using the same LEED optics as a high pass energy filter. The LEED optics consist of 4 grids (see Figure 2.2b). In this figure the optics have an off-axis electron gun. In our work we use the LEED electron gun. The first grid is grounded to provide a field free region between the analyser and the crystal. The second and the third grids are connected together and have the retarding potential applied to them. Electrons with energy higher than e times V, where V is the positive potential applied to the second and third grids, pass through these analyzer grids and also through the fourth grid which is also grounded. The electrons are collected on a solid spherical collector which is the screen. The fourth

grid essentially shields the collector from capacitative coupling with the modulation applied to the retarding grids. A small modulation voltage of 1 V peak to peak at a frequency of 1 KHz is superimposed on the retarding voltage. The collector current is thus modulated at the same frequency. The current is compared in a lock-in-amplifier (a phase sensitive detector) with a reference signal. Amplification of the component of the collector current at 1 KHz (f) gives the energy distribution N(E) of electrons, while amplification of the component at 2f gives the differential distribution, dN(E)/dE.

2.4 Kelvin Probe - Work Function Change Measurements

2.4.1 Kelvin Probe Vibrating Capacitor

The internal work function of a bulk metal is defined as $(E_n - E_{n-1})$, where E_n is the ground state energy with n electrons and E_{n-1} is the ground state energy minus one electron. It is also equal to the negative of the electrochemical potential of the electron. On the surface, the electrons do not have the same electron energy distribution, i.e., the electron distribution does not have a sharp cut off and spills out into the vacuum, creating a surface dipole. The work function may be expressed as:

$$\phi = D - \bar{\mu} \qquad (2.2)$$

where D is the potential produced by the surface dipole and is affected by adsorption, while $\bar{\mu}$ is the potential related to the electronic density of states and remains the same on adsorption.

The change in work function ($\Delta\phi$) can be measured. The measurements can be made very sensitively with changes of 1 mV being readily detectable. For a typical adsorption system of 10^{15} adsorbed particles per cm^2, $\Delta\phi$ is about a volt. Thus the technique can detect 1/1000 of a monolayer. The sign change in $\Delta\phi$ together with a knowledge of the charge on the ad-atom can give information about the relative position of the ad-atom with respect to the surface. For an electronegative ad-atom, such as oxygen, adsorption with its negative charge on top of the surface will cause D and ϕ to increase, as the electrons have to overcome a larger energy barrier. When the ad-atom moves nearer towards the surface, D will become smaller. On diffusing into the metal, the surface dipole may become smaller and $\Delta\phi$ becomes negative. Migration deep into the metal may cause its charge to be screened by conduction electrons and $\Delta\phi$ is zero. Typical screening lengths in metals are very short and thus work function measurements have high surface specificity.

The most important part of the probe is a stainless steel reed with a molybdenum tip. It forms one half of a capacitor, and the platinum crystal forms the other half. This reed is made to vibrate at a frequency of 700 - 800 Hz to form a vibrating capacitor. The current from this vibrating capacitor is:

$$i = \Delta C\,(\phi_s - \phi_r)\omega\cos\omega t \qquad (2.3)$$

where ΔC is the change of capacitance, ω is the frequency of the vibrating reed and $\phi_s - \phi_r = \Delta\phi$ is the contact potential difference and ϕ_s and ϕ_r are work functions of the surface and the reference molybdenum tip respectively. The work function of the

molybdenum tip does not change on adsorption. This is evidenced by the same $\Delta\phi$ in a repeated adsorption after cleaning the crystal.

When a voltage V_a is applied to cancel out this $\Delta\phi$, the current i defined in equation 2.3 goes to zero. Any change in ϕ_s of the sample will result in a change in $\Delta\phi$ or change in V_a. Since ϕ_r is a constant, the applied voltage V_a is a measure of the surface work function ϕ_s. The vibration from the reed is detected by a piezo crystal which feeds a signal into a phase-locked loop. This loop controls the vibration of the reed at a fixed frequency. The current from the vibrating reed (equation 2.3) is amplified, phase sensitively detected, rectified and fed into the feed back loop, which applies a voltage V_a to null the current. A schematic for the electronics is shown in Figure 2.3a.

The reed is mostly made from a stainless steel capillary, except for the molybdenum tip which is spot welded to the stainless steel tube via a piece of tantalum foil. Also a μ-metal piece spot welded approximately 10 mm from the other end, served to couple the driving AC magnetic field to the reed. The reed is driven by an electromagnet made by winding a soft iron rod with 20 turns and 6 layers of 0.010 inch copper wire. There is a metal shield around the reed to shield any fields in the vicinity of the reed. The bias of this shield is controlled and this largely eliminates capacitive coupling to other components in the UHV system.

Figure 2.3a : Schematic for the electronics in vibrating capacitor method (Kelvin probe)*

25 - Shield

13 - Electromagnet

2 - Molybdenum reference tip

1 - Sample, Pt(111)

Figure 2.3b : Construction of the reed in Kelvin Probe.**

25 - Shield

24 - Vibrating reed, frequency = 2ω

13 - Electromagnet, frequency = ω

2 - Molybdenum reference tip is coiled into a loop with an effective area equal to the size of the crystal

1 - Sample, Pt(111)

Notes:

* From lecture notes given by Prof. P.R. Norton, University of Western Ontario (Chem 657).

** From lecture notes given by Prof. P.R. Norton, University of Western Ontario (Chem 657). Pieces for the reed were kindly provided by Dr. K. Griffiths of Interface Science Western.

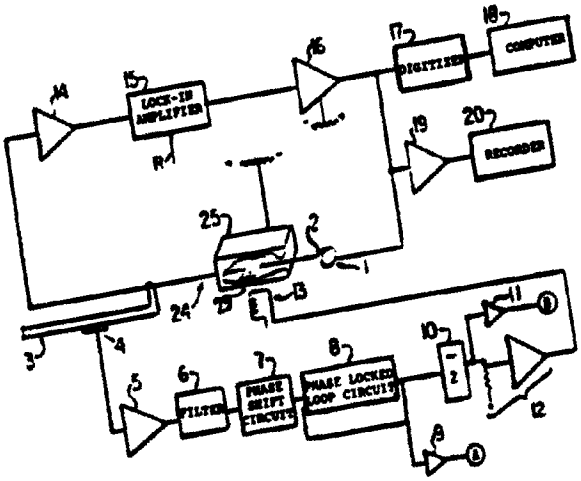

Electronics for measurement of $\Delta\phi$

Electronics for vibration stabilization

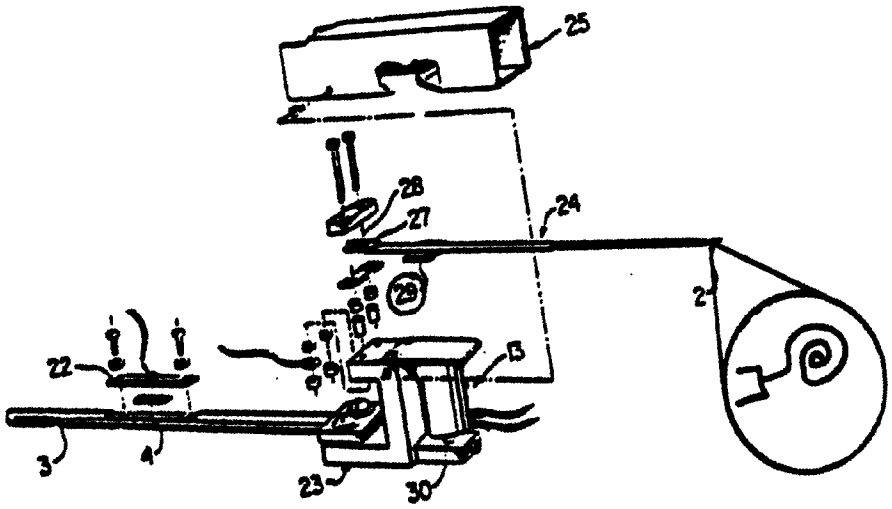

2.4.2 New insights in the design of the Kelvin Probe

Figure 2.3b shows the construction of the reed. The immediate problem in getting the reed to vibrate properly is summarized next. The fundamental frequency of the reed is f_o and its second resonance is several times f_o. The μ metal served to couple the driving AC magnetic field to the reed so that the reed vibrated at its first overtone, with an antinode at the Mo tip and a node positioned about one-third the length of the reed from the tip. A trial and error approach was used together with a stroboscope to study reed vibration. A reed orientation with its first overtone at 760 Hz was constructed as a result of the study.

Although much of the reed construction remains an art, four things important to reed vibration emerged from my study. First, the position of the μ metal relative to the electromagnet is crucial to achieving a strong reed vibration. Second, it is advantageous to make the reed vibrate at a frequency higher than 800 Hz (i.e. lighter reed). This is becausc the reed can be easily made heavier by spot welding, while it is difficult to remove material once it has been welded on. Third, the frequency is best lowered by adding more tantalum foil near the tip of the reed. We now know how much tantalum foil to add to lower the frequency by 25, 50 or 100 Hz, while keeping the reed vibrating strongly. Fourth, it is important when testing the probe on the bench to mount it on the linear translation motion drive (LTM), used on the actual UHV chamber as mechanical coupling affects the reed vibration.

2.5 Fourier Transform Infrared Reflection Absorption Spectroscopy

2.5.1 Fourier Transform Infrared Reflection Absorption Spectroscopy (FT-IRRAS) Theory

The frequency of vibrational modes in molecules are on the order of 10^{13} s^{-1}, which falls in the range of frequencies of infrared radiation. If the bond has a non-zero dipole moment, infrared radiation can be absorbed and a vibrational spectrum of the molecule can be obtained.

For a simple diatomic molecule with mass m_1 and m_2, the natural vibrational frequency of a bond is expressed as:

$$\bar{\nu} = \frac{1}{2\pi c}\sqrt{\frac{k}{\mu}} \tag{2.4}$$

where k is the force constant and μ is the reduced mass, ($\mu = m_1m_2/(m_1 + m_2)$).

When the number of oscillators is small as is the case in a surface experiment, the intensity of the absorption will also be small. Furthermore, if the oscillators are adsorbed on the surface of an opaque metal sample, conventional transmission infrared can no longer be used.

IRRAS is a technique which permits vibrational spectra of adsorbed molecules on metal surfaces to be obtained. In this reflection experiment, only light polarized with the electric field parallel (p light) to the plane of reflection excites the infrared

active modes of the adsorbed molecules on reflection. At all angles of incidence, the electric field perpendicular to the plane of reflection, E_s undergoes a phase change of 180 degrees and the resulting standing wave has a small field. For the p polarization, the resultant amplitude of the incident and reflected electric fields at the surface can be resolved into two components shown in equations[1] below :

$$E_p\| = E_p^i \cos \alpha \{(\sin \theta - r_p \sin (\theta + \delta_p)\} \quad (2.5a)$$

$$E_p\perp = E_p^i \sin \alpha \{(\sin \theta + r_p \sin (\theta + \delta_p)\} \quad (2.5b)$$

where $E_p\|$ is the component parallel to the surface, $E_p\perp$ is the component perpendicular to the surface, $E_p^i \sin \theta$ is the incident electric field and θ is an arbitrary phase, α is the angle of incidence measured with respect to the surface normal, r_p is the reflection coefficient, δ_p is the phase change on reflection. δ_p is nearly zero for small angles of incidence and is 90 at grazing incidence, and 180 at 90 degree incidence. At small angles of incidence, α is nearly zero, and $E_p\perp$ is small. Although cos α is nearly one, $E_p\|$ is small because the incident and reflected waves are in opposite directions and the vector sum is zero. At large angles of incidence, particularly at grazing incidence, there is an enhancement of $E_p\perp$ along the surface normal. The absorbance, proportional to the change in reflectance, upon adsorption to total reflectance from clean surface ($\Delta R/R$) is a maximum when p light is brought in at grazing incidence to the crystal. As the angle of incidence approaches 90°, the ($\Delta R/R$) falls off again.

---

[1]Hayden B.E. in "Vibrational Spectroscopy of Molecules on Surfaces" (Yates J.T.Jr., Madey T.E. eds.) (1987) p.267

As described above, all molecules with a non zero dipole are capable of absorbing infrared radiation. However, when the dipole is *adsorbed* on a metal surface, an image dipole will be set up in the metal. If the dipole lies parallel to the surface, the net dipole moment will be zero, and infrared radiation will not be absorbed. If the dipole lies perpendicular to the surface, there will be an enhancement of the dipole moment and infrared radiation will be absorbed. This establishes the surface dipole selection rule for adsorbates on metal surfaces, which states that only those vibrationally active modes which have a dipole component normal to the surface will be excited. (i.e. absorb radiation).

In FTIR, the infrared light from the source is split at the beam splitter (germanium on KBr). One beam is reflected off a stationary mirror, while the other is reflected off a moving mirror (see Figure 2.4a for the Michelson interferometer). In a Cygnus 100 FTIR machine, all light of different wavelengths from the globar (silicon carbide) source is imaged onto the beam splitter, recombined and detected at the mercury cadmium telluride (MCT) detector. The detector therefore sees a superposition of all this light which is called an interferogram (Figure 2.4b). This interferogram is characterised by a large centre burst when the path difference of each pair of coherent beams is zero and light of all wavelengths interfere constructively.

Figure 2.4a : Michelson Interferometer. *

Figure 2.4b : A typical interferogram of a blackbody-type source detected by the mercury cadmium telluride (MCT) detector. *

Note:

* From P.R. Griffiths and J.A. de Haseth. **Fourier Transform Spectrometry.** Vol. 83 in Chemical Analysis, Wiley, 1986, p. 2 and p. 30.

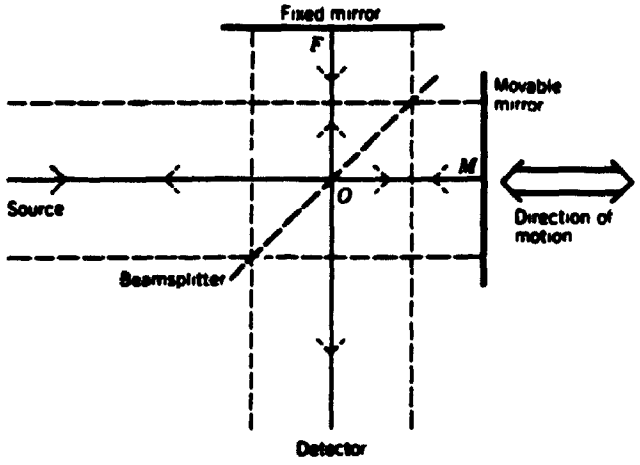
Fixed mirror
F
Movable mirror
M
O
Source
Direction of motion
Beamsplitter
Detector

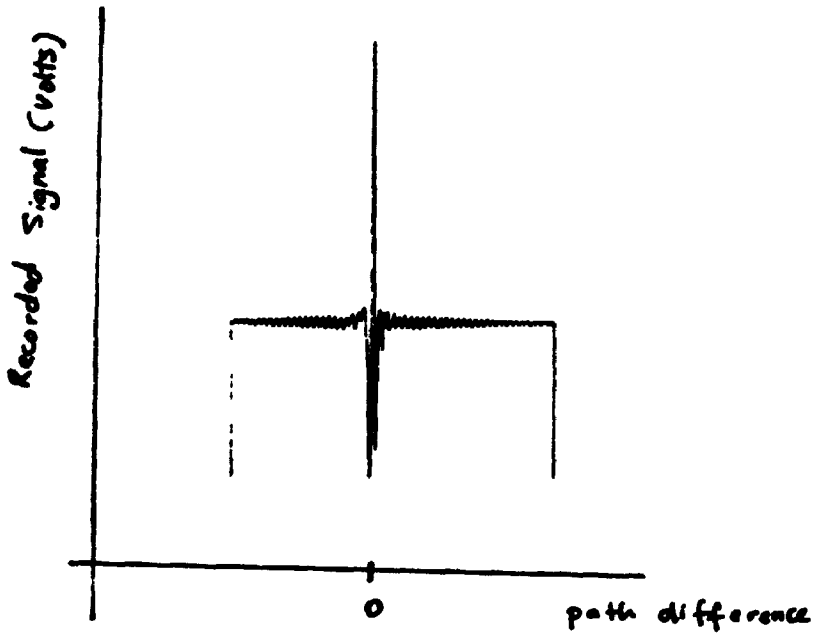
Recorded Signal (volts)
0
path difference

In a single beam FT-IRRAS spectrometer, one beam is reflected off a metal surface at high incidence angle before reaching the MCT detector. A He-Ne laser is also imaged onto the beam splitter. After reflecting off the stationary and moving mirror, the beams are recombined and the sinusoidal output is detected by a photodiode. In this way, the position of the scanning mirror is accurately measured. The computer uses the laser fringes to trigger the analog to digital converter (ADC) at precise intervals.

The digitised interferogram is Fourier transformed to yield a plot of infrared intensity versus the wavenumber. The signal to noise ratio of the spectrum is limited by the signal to noise ratio of the interferogram. This in turn is limited by the dynamic range of the 16 bit ADC convertor. In short the single beam experiment is digitizing noise limited.

2.5.2 Considerations for Optical Design of IRRAS Experiment

The problems we have at hand can be summarized below:

- The light has to be brought to a focus at the crystal.
- The light has to be reflected off the crystal at grazing incidence.
- The optical path length has to be free of CO_2 and H_2O.
- Infrared windows are needed to allow the radiation to pass in and out of the vacuum chamber.
- The infrared window needs to be vacuum sealed. This is provided using O-

rings and differential pumping.

- The focusing elements need to be mounted securely but at the same time they need to be provided with some degrees of freedom .
- In a single beam experiment the s-polarised light is not absorbed and serves only to saturate the detector. The s-polarised light has to be eliminated.
- Thermal radiation from the crystal has also to be excluded.
- All radiation must have the same focusing properties so that each will follow the same optical path.
- The IRRAS experiment has to have a large dynamic range as a small absorbance signal is to be detected against a large background. This is the source of photon noise.
- The infrared radiation is not visible to the human eye and it is therefore difficult to align the optics.
- In the study of chemical reactions we need a probe that will quickly sample the reaction. It should also sample all regions of the infrared region at the same time so that meaningful comparisons can be made.
- In addition, we also need a high throughput in the optical system so that it will be sensitive to small absorbances.

2.5.3 The FTIR-RAS system for investigation of reactions in OMCVD

A FTIR spectrometer was chosen over a dispersive instrument as it offered the multiplex advantage whereby all spectral frequencies can be brought to the crystal

at the same time. Furthermore the scan time is not limited by the scan time of the monochromator. FTIR spectrometers also have a throughput advantage over dispersive instruments as more flux can pass through the interferometer than the monochromator. More photons can thus be obtained from a globar source when an interferometer is used.

The range of frequencies in the mid IR is 3000 - 700 cm^{-1}. Pt-C and Pt-N frequencies are below 700 cm^{-1}. A narrow band MCT detector can be used in the range of 3000 - 700 cm^{-1} for high sensitivity measurements. For measurements below 700 cm^{-1} a bolometer is required for high sensitivity measurements. Furthermore, all the optics have to change from KBr to mylar optics to allow radiation below 700 cm^{-1} to pass through. A further limitation is placed on the mirror speed (v) of the moving mirror in the interferometer. This is because the IR radiation is modulated at a frequency of $f=2v\bar{\nu}$ and the bolometer has poor response at frequencies higher than 400 Hz. This means that the mirror speed has to be slowed down when using a bolometer. This does not work in our favour when we are investigating chemical reactions. With a narrow band MCT, the mirror speed can be set at higher speeds as it has good response at higher Fourier frequencies.

As sensitivity and high mirror speeds are important in our study, we have chosen to restrict ourselves to the mid IR region and use a narrow band MCT for detection of the modulated IR radiation.

As the light has to be brought to the crystal at grazing incidence, the entrance and exit ports on the vacuum chamber were constructed so that they were 160 degrees apart. The light leaves the FTIR spectrometer as a collimated beam and has to be brought to a focus at the crystal. This could be achieved either with a lens or a focusing mirror. A mirror is favoured over a lens as the focusing properties in a lens depends on the wavelength of the light. When a mirror is used the focusing properties are strictly determined by geometrical optics and are not dependent on wavelength. This means that each spectral element may be brought to the same focus at the crystal. The light which is reflected off the crystal has to be brought to a focus at the detector element of the MCT detector. This can be achieved with two off-axis parabolic mirrors. The off-axis parabolic mirror is cut from a section of a large parabolic mirror and seated in a cross sectional area which has been made by cutting an aluminum pipe at an appropriate angle. The mirror is seated securely with beeswax. The mirror and its seat are secured to an optical mount purchased commercially.

In a perfectly collimated light beam, the light can be brought to a sharp focus, regardless of the focal length of the mirror. However, the globar source is not a perfect point source and the IR beam is not perfectly collimated. It has a beam divergence. At the focus the size of the image is then proportional to the product of the beam divergence and the focal length. To produce a very sharp focus would require a focal length of zero. In practice, the desired short focal length is limited

by the size of the vacuum chamber. In our system we have used an off-axis mirror with a 30 cm focal length. Furthermore, if the image has a diameter d at the focus, the image projected on the crystal is an ellipse with a major axis of d/sin (90-α), where α is the angle of incidence. The platinum crystal is thus the optical element limiting throughput in the whole optical system. It has an area of about 1 cm^2. Light was brought in at 80 ° incidence because this is the optimal angle for maximum absorption. This angle is a compromise between the angle of 88° (absorption factor for p-polarization goes through a sharp maximum at this angle) and variation of intensity of reflected light with incidence angle. The light reflected off the crystal was collected by two parabolic mirrors and focused onto the MCT detector (see Figure 2.1). The parabolic mirrors were mounted on optical mounts that provided adjustments for optical alignment. The mirrors and the mounts were in turn seated in a hermetically sealed mirror box, which has an aluminum base and plexiglass walls. The spectrometer and the mirror boxes were purged with air that has been passed through filters that reduce water vapour and carbon dioxide to very low levels. The optical boxes were slipped over the outer diameter of the infrared window mounts to provide a hermetic seal. During optical alignment a He-Ne laser was used to assist in alignment of the optics. When the parabolic mirrors had been aligned with the He-Ne laser, they were also aligned for infrared radiation. This was not true for lenses. This was a further reason for using mirrors instead of lenses. The UHV chamber was sealed off from the dry air purge in the mirror boxes. Potassium chloride (KCl) windows were mounted in the recess of a window mount. A first set

of four bolts compressed the two sets of viton O-rings. One set of one ring was on the dry air face of the KCl window and a second set of two rings was on the vacuum face. The window mount (see Figure 2.5), together with the KCl window was finally mounted on a 4½-inch port on the vacuum chamber. The vacuum seal was provided by compressing the copper gasket with a second set of 4 bolts. The space in between the two sets of O-rings was differentially pumped by a rotary pump. This design for the infrared window mounts using two sets of bolts instead of one set prevented the KCl window from breaking when the bolts were tightened on the copper gasket.

The FTIR spectrometer was seated on a spectrometer table which was supported by three kinematic mounts. The table can be raised and lowered by adjusting the kinematic mounts. When the chamber was to be baked, the spectrometer table was lowered so that it was sitting on its wheels. It could then be wheeled away during bakeout.

The precursor in our investigation is square planar and the molecule has an occluded area of about 44 Å^2. If it were to adsorb with its molecular plane parallel to the surface, it would easily sit on 10 to 12 platinum atoms (see Figure 2.6). Saturation coverages would approximately be 1/12 ML (1.25×10^{14} molecules per cm^2). The number of C≡N oscillators (2 per molecule) would be 2.5×10^{14} oscillators

Figure 2.5 : IR window mounts

Note: ConFlat (Varian trade name for metal-gasketed flanges*)

Window Mount (Retainer ring and $4^1/_2$-inch conFlat)

* see Milleron N. and Wolgast R.C. in "Methods of Experimental Physics", Vacuum Physics and Technology, Vol.14 (1979), chapter 6.

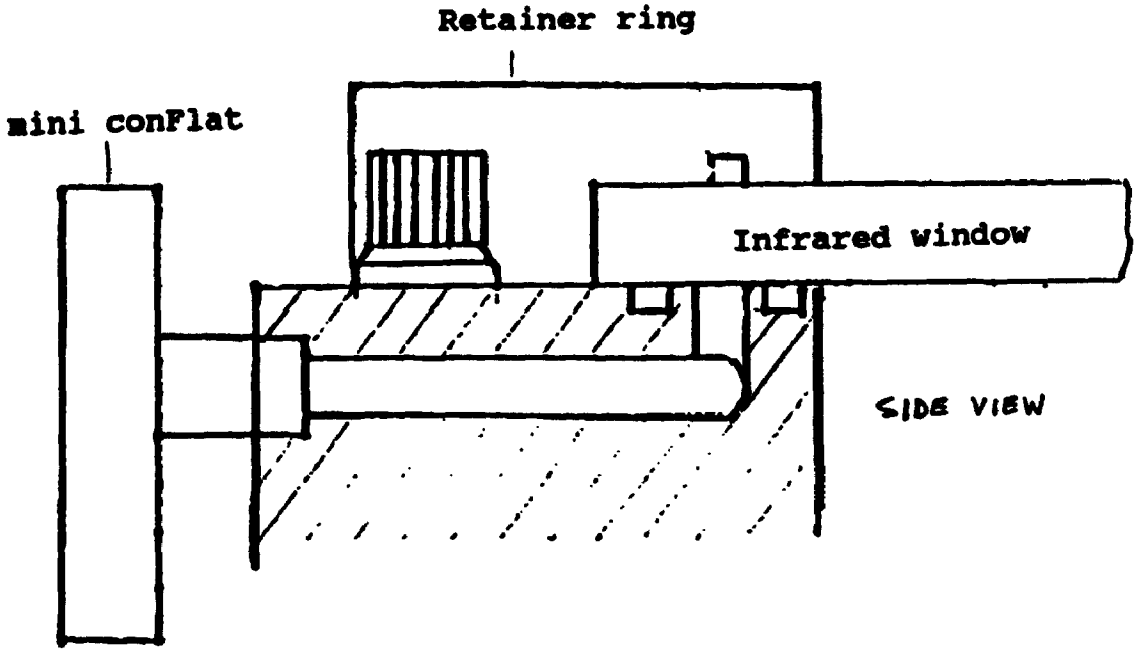
Retainer ring
mini conFlat
Infrared window
SIDE VIEW

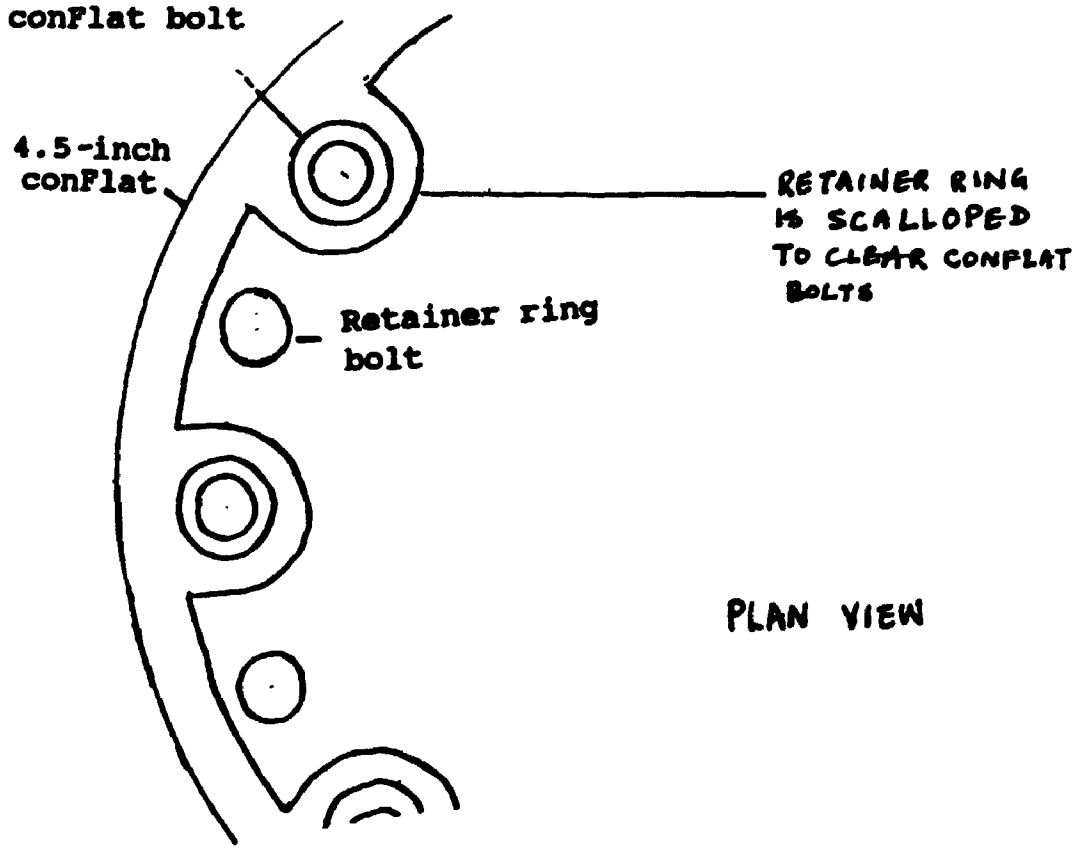
conFlat bolt
4.5-inch conFlat
RETAINER RING IS SCALLOPED TO CLEAR CONFLAT BOLTS
Retainer ring bolt
PLAN VIEW

Figure 2.6 : *cis*-dimethyl platinum diisocyanide/Pt(111)

Pt(111) surface

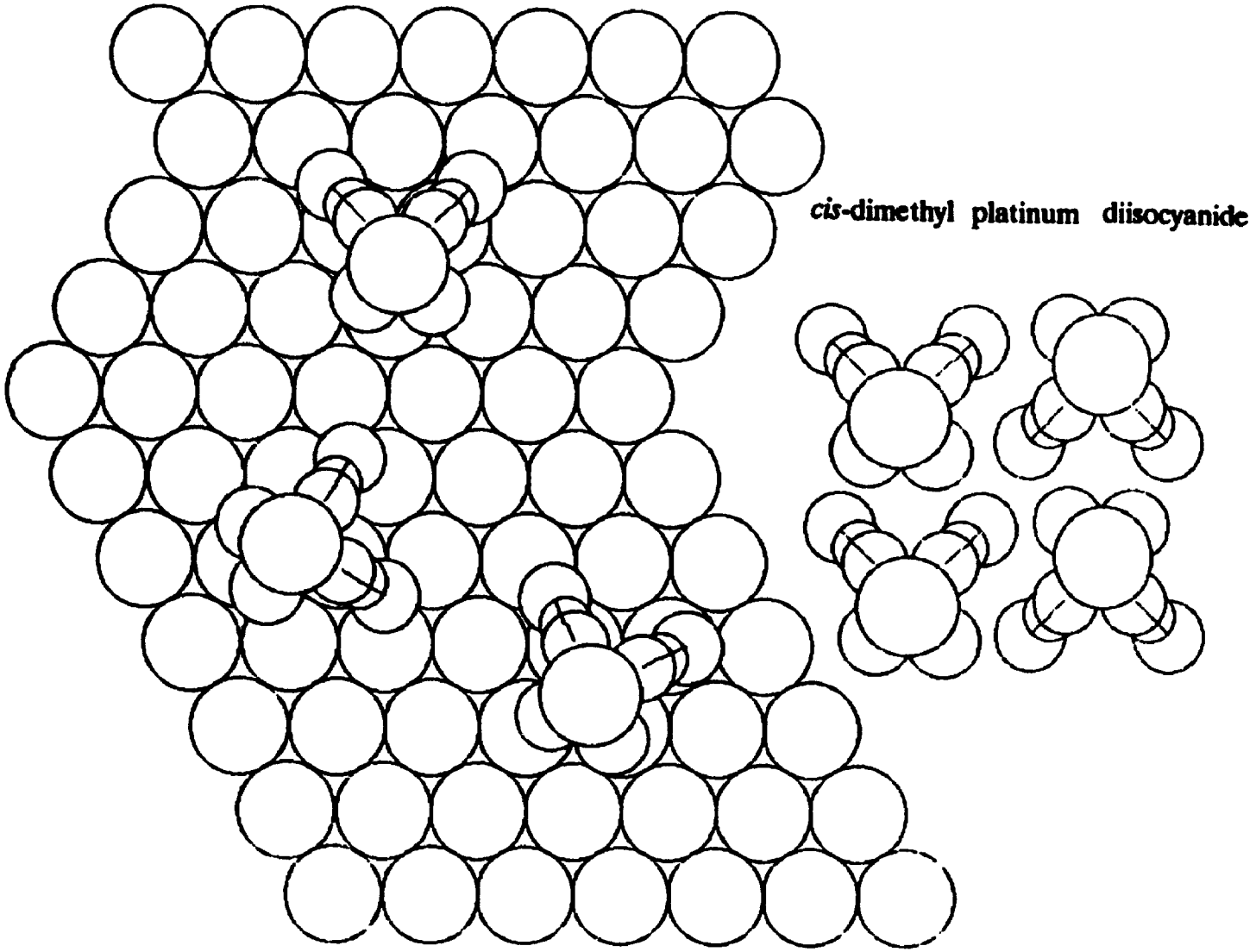

cis-dimethyl platinum diisocyanide

per cm^2. Furthermore, the adsorbate layer may be ordered on Pt(111) and the number of C≡N oscillators might be expected to be smaller than 2.5×10^{14} per cm^2. This made detection of the adsorbed precursor with IRRAS understandably difficult, especially when one remembers the surface selection rule, which allowed the dipole to be detected in IRRAS only if it has a non-zero component perpendicular to the surface.

In general, this translated to longer dosing times or exposures before it could be detected by IRRAS. Over this time, the source intensity, detector sensitivity, changes in concentrations of absorbing gases in the spectrometer and variations in the optical alignment could affect spectral quality. Baseline mismatch from such effects manifested itself by a sloping baseline and undulating baseline in the infrared region from 1500 to 750 cm^{-1}. Variations in optical alignment was identified to be due to the long liquid nitrogen dewar which held the crystal. When it was filled with liquid nitrogen, it appeared that the natural frequency of the probe approached a harmonic of the frequency of the rotation of the turbomolecular pump. When liquid nitrogen was removed, the quality of the baseline greatly improved.

2.6 Temperature Programmed Desorption (TPD)

2.6.1 Theory

In the interaction of an adsorbate molecule with the crystal, the molecule is first adsorbed on the crystal. The interaction of the molecule with the crystal can be studied by desorbing the molecule by heating the crystal. This is the basis of temperature programmed desorption (TPD). In TPD, the crystal is heated at a fixed rate of β K/s. The crystal is usually cooled by filling the probe with liquid nitrogen and the temperature raised by resistively heating the crystal (see below). A mass spectrometer Hiden (HAL 601) is used to detect the multiple desorbing mass fragments.

Let R_d be the rate of desorption, then the rate of desorption of molecules or atoms per unit area is expressed as:

$$R_d = \frac{V}{AkT_g}\left[\frac{d(\Delta P)}{dt} + \frac{\Delta P}{\tau}\right] \tag{2.6}$$

where V is the volume of the chamber, A is the adsorbent area in cm^2, k is the Boltzmann constant, T_g is the gas temperature and ΔP is the pressure rise. τ is the characteristic pumping time, such that $\tau = V/S_p$, where S_p is the pumping speed in the chamber. For very fast pumping, the pumping time approaches zero, and

$$R_d = \frac{V}{AkT_g}\left[\frac{\Delta P}{\tau}\right] \tag{2.7}$$

The rate of desorption is proportional to the pressure rise.

The Redhead equation for the rate of desorption is given by equation (2.8) below:

$$R_d = -\frac{dN}{dt} = \nu^{(n)} N^n \exp(-E_d/kT) \tag{2.8}$$

where N is the coverage (molecules cm^{-2}), $\nu^{(n)}$ is the pre-exponential for the n th order desorption process and E_d is the activation energy for desorption.

If the sample temperature T change linearly with time, then, $T = T_0 + \beta t$ and the peak temperature may be found by differentiating the desorption rate with respect to the temperature and setting the differential to zero.

When $\nu^{(n)}$ and E_d are independent of coverage N, the following statements are true:

- First order desorption peaks are characterized by an asymmetric shape and a peak temperature independent of initial coverage.
- Second order desorption is characterized by a symmetric peak with a peak temperature which decreases with increasing coverage.
- Zero order desorption peak temperature increases as initial coverage increases.

2.6.2 Setup in Temperature Programmed Desorption (TPD) Experiment

To collect as much as possible of the mass desorbed before it is pumped away, the ioniser of the mass spectrometer must be positioned as close to the crystal as possible. This is because the material desorbs with a certain solid angle at the crystal. The further the ioniser is from the crystal, the less it will detect of the desorbed material. Furthermore, the ioniser may pick up material which desorbs from the nickel posts and from the back of crystal. If the ioniser cannot be placed near the crystal, a collecting cone can be placed with its aperture close to the crystal. This cone will selectively collect only masses desorbing from the crystal and exclude material desorbing from the nickel supports. The mass spectrometer used in this way usually has to be differentially pumped so that the mass makes only one pass through the ioniser. This reduces the noise level in the TPD spectra. In cases where an additional pump is not available, the exit hole can be placed close to the main pump which is pumping the chamber.

In the OMCVD chamber, laser induced desorption (LID) experiments are planned in the future, so the ioniser is placed far away from the crystal. This is to enable accurate measurement of the time of flight of the desorbing fragment after the firing of the laser pulse. The requirements for TPD and LID are thus orthogonal.

The whole mass spectrometer sits in an enclosed cylinder which is differentially pumped by a titanium sublimator pump equipped with liquid nitrogen cooling. At the end of this cylinder (crystal end) a 6.3 cm hole is drilled so that a 6.3 cm O-ring sits in a groove at the circumference of the hole. A collecting cone with large O.D. 6.3 cm is slide-fitted into this hole. The cone is made of pyrex. The small aperture of the cone facing the crystal has a diameter of about . cm. The distance of the aperture to the crystal may be changed by sliding the cone towards or away from the crystal. Since infrared light is absorbed by pyrex, FTIR-RAS experiments cannot be done when the cone is very close to the crystal. In our setup, a compromise is reached which allows us to conduct FTIR-RAS with the collecting cone pulled away from the crystal, out of the path of the IR radiation which is reflected from off the crystal. In this geometrical arrangement, we can collect the masses desorbed from the crystal; however caution needs to be exercised in the assignment of TPD peaks since material desorbing from the nickel posts may show up in the TPD spectra. Although the mass spectrometer is a 600 amu instrument, detection of masses greater than 300 amu from a flashed crystal is difficult. This is because the transmission of mass fragments through the quadrupole begins to fall for masses greater than 300 amu. At 600 amu the transmission has fallen to half of what it was at masses less than 300 amu. This makes the detection of platinum-containing masses difficult. Furthermore, the mass spectrum of the organometallic complex (molecular mass of 307) obtained with a magnetic sector machine cannot be compared to a mass spectrum of the complex obtained with a quadrupole mass spectrometer.

2.6.3 Differential Pumping For TPD

Differential pumping ensures that the mass fragments make one pass through the ioniser. This arrangement improves the noise level in a typical TPD spectrum. The mass spectrometer was totally isolated from the main chamber by a stainless steel cylinder. There was a hole in the centre of the collecting cone to allow molecules to travel to the ioniser of the mass spectrometer. The dimension of the hole was such that the ioniser could see the solid angle of the crystal. A tee nipple was positioned so that a titanium sublimator pump (TSP) could be placed sitting on the tee. A fine mesh spot welded to the inside of the tee prevented any titanium flakes from falling onto the optics of the mass spectrometer. A brace supported the total weight of the tee, mass spectrometer, and sublimator pump.

2.7 Platinum (111) Crystal

The Pt(111) surface was obtained by orientation of a single crystal and platinum boule. A two circle goniometer set up to do Laue X-ray back reflection is used to aid in the orientation of the crystal. The crystal is mounted onto a goniometer head, which in turn is attached to one circle of the goniometer. The crystal can thus be moved about two orthogonal axes.

The boule was mounted onto the goniometer and the measured diffraction angles and symmetries were compared to standard tables and maps. The (111) plane was then orientated by moving the boule by the approximate number of degrees along the two orthogonal circles of the goniometer. A Laue X-ray photograph is taken to ensure correct orientation of the (111) plane. Part of the goniometer carrying the boule could be removed while preserving the proper orientation for cutting with a diamond saw. An elliptical cut was made along the (111) plane and the slice was mounted onto a polishing jig and the cut face was polished with diamond paste, down to 10 μm, and etched in strong acid solution (30 ml HNO_3 + 10 ml H_2SO_4 + 10 ml o-H_3PO_4 + 50 ml CH_3COOH).

The entire polishing jig was mounted in the goniometer to establish orientation of the surface to within 0.5° of the (111) plane by further adjustments. Diamond grit paper was mechanically run over the cut face to align it with the (111) plane. The surface was further polished down to 1 μm grade with diamond paste in a mechanical polisher and fine-polished in a vibrating polishing machine using 0.06 μm alumina/water slurry.

A platinum ribbon (0.20 mm thick by 1mm wide by 20 mm long) was spot welded to the back of the Pt(111) crystal. The platinum ribbon carrying the crystal is in turn spot welded to two nickel posts, held in a probe dewar. The crystal is cooled by filling the probe dewar with liquid nitrogen. The temperature of the crystal

can be raised by resistively heating the crystal. The temperature of the sample was measured by a K-type chromel alumel thermocouple spot welded to the back side of the crystal. The sample temperature was controlled by a temperature programme and slave power supply.

The cleaning procedure for the crystal starts with sputtering of the platinum surface using argon ion bombardment. The chamber is backfilled with argon to a pressure of 1×10^{-5} torr. The argon is ionized and a 2 keV 2 μA Ar^+ ion beam is focused onto the crystal by the ion gun. The sputtering removes silicon and other impurities that cannot be removed chemically. The crystal is then annealed in oxygen pressure of 1×10^{-6} torr at 700 °C to remove carbon. The crystal is then flashed at a temperature of 1000 °C to restore crystal order after ion bombardment.

2.8 Organometallic Doser

Figure 2.7 shows a multiplexer flange with five $1^1/_3$ inch ports carrying the doser tube, inconel heater wire, thermocouple and rotary shutter (flag). This whole assembly is mounted on a linear translation motion drive (LTM), which allows the doser to be brought close to the crystal during dosing and also allows it to be moved away from the crystal during IRRAS measurements.

The doser tube is mounted on a flange which is 84° away from the mass spectrometer, so that the complex can be specularly reflected off the crystal into the ioniser of the mass spectrometer. The microcapillary array preferentially doses the

Figure 2.7 : Organometallic doser equipped with microcapillary array and with rotary shutter. The doser tube is heated with inconel heater wires and temperature is read with type K thermocouple.

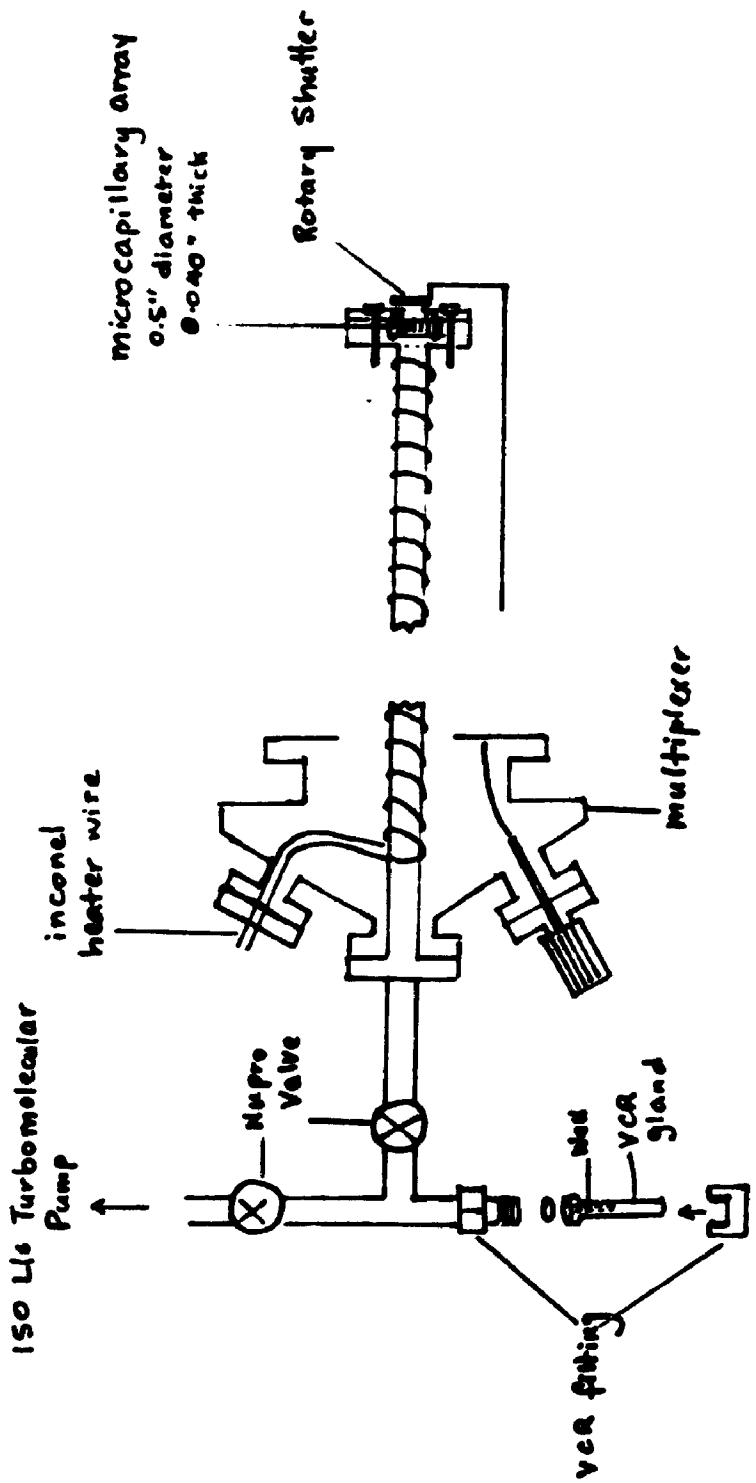
Microcapillary array
0.5" diameter
0.040" thick
Rotary Shutter
inconel
heater wire
multiplexer
ISO Lit Turbomolecular
Pump
Nupro
Valve
VCR
gland
VCR fitting

crystal while not dosing other parts of the apparatus. There is a LEED shield which shields the LEED optics from the dosing gas. This arrangement minimises background contamination of the chamber by these large organometallic molecules. In our present arrangement it is difficult to detect the precursor using the quadrupole mass spectrometer in the background residual gases, as the concentration is very low. To detect the precursor coming out of the end of the capillary array may require relocating either the mass spectrometer or the doser so that there is a line of sight from the doser to the mass spectrometer.

The doser reservoir is cleaned with methanol and completely baked for 24 hours between mounting of HPt, DPt and D'Pt (organometallic precursors). Adsorption of $D_{12}Pt$ on a Pt(111) surface passivated by heating in acetylene demonstrates that there is no CH/CD exchange in the doser. The doser reservoir was heated to 100 °C with heating tape and wrapped with aluminum foil to minimize heat loss.

A VCR[2] blind gland (purchased commercially) was drilled to allow a thin walled pyrex vial to be inserted in the well. The precursor was put in the vial which was in turn inserted in the VCR well. The VCR gland was attached to the rest of the doser via a copper gasket, which provided the seal. The precursor in the vial was heated to 100 °C to sublime it. "Unused" precursor vapour could be pumped away

[2] trade name for metal gasket face seal fittings.

by the turbomolecular pump which pumped the manifold. Fresh precursor could then be sublimed and immediately introduced into the ultra high vacuum chamber along the doser tube, through the capillary array and beamed towards the crystal. This arrangement minimized the interaction of the precursor with the heated stainless steel walls.

During dosing, the doser tube (heated to 120 °C) is brought to within 20 mm of the crystal. Precursor vapour was pumped away by the turbomolecular pump which pumped the gas manifold and fresh precursor was sublimed. The shutter was opened, followed quickly by opening of the Nupro valve. The precursor was then allowed to travel from the heated reservoir (100 °C) down the heated doser tube (120 °C), through the microcapillary array and beamed towards the crystal.

Dosing was interrupted by closing the exit of the capillary array by placing the rotary shutter in front of it. The Nupro valve was valved off and precursor vapour remaining in the tube was pumped away without dosing the crystal.

The next three chapters present the experimental results.

CHAPTER 3

REACTIONS OF *cis*-$(CH_3)_2Pt(MeNC)_2$ IN AN INFRARED GAS CELL

3.1 Introduction

Chapter 1 described how $(CH_3)_2Pt(MeNC)_2$ can been used as a volatile organometallic precursor for organometallic chemical vapour deposition (OMCVD) of platinum thin films. Chemical vapour deposition involving the Pt(II) precursor, cis-dimethyl platinum diisocyanide has already been described in Section 1.3. The main findings were:

- With UV radiation, the CVD was enhanced and the decomposition temperature could be lowered (to 150 °C), compared to 250 °C without UV radiation .
- In the presence of H_2, the CVD decomposition temperature would be lowered to 100 - 150 °C from 250 °C.
- In the decomposition of HPt, the rate of film growth is 100 Å /min at 250°C.
- The platinum film conductance is $(1.4 - 3.0)\times10^4$ mho cm^{-1} compared to 9.4×10^4 mho cm^{-1} for 99.8% pure Pt.
- In the presence of H_2 , films deposited have crystallite size of 500 Å compared to 2000 Å when H_2 is absent.

- The XPS study of film composition showed 34% C impurity when H_2 was not present. This could be reduced to 4% when H_2 flow rate was 40 ml min^{-1} .
- The SIMS study of DPt showed high counts of deuterium signal. Its intensity paralleled that of the platinum signal over the whole profile. Both signals fell when the underlying silicon signal grew in intensity.
- The following intensity ratios for m/e =13 and 14 were obtained using the SIMS :

$$I_{13} / I_{14} = 26 \quad \text{for platinum films using HPt}$$

$$I_{13} / I_{14} = 5 \quad \text{for platinum films using DPt}$$

The above result indicates that the carbon impurity comes from the methyl platinum groups.

This chapter studies the mechanism of the decomposition of the precursor in a gas cell, using transmission infrared spectroscopy as a probe. 2 mg of precursor was completely sublimed in a closed infrared cell with no pumping. The precursor was decomposed at 300 °C and infrared gas phase spectra were obtained during the course of the decomposition. It was pointed out in Section 1.1.2 that the pressure in the CVD is an important variable which determines the extent of the gas phase reactions and surface reactions in the reactor. In view of this, it was appropriate to measure the vapour pressure of the precursor.

3.2 Experimental

An infrared cell (Figure 3.1a) was constructed of pyrex glass. Potassium chloride (KCl) windows were attached to both ends of the pyrex cell and sealed by viton O-rings. The cell had an internal volume of 76 ml. The whole assembly was held in a stainless steel support with four threaded rods which allowed the assembly to be tightly clamped together using eight nuts. The infrared cell had an inlet for introducing the hydrogen and an outlet for pumping the cell down to 1×10^{-3} torr with a rotary pump. The pressure was measured using a Pirani gauge. The seals were found to be satisfactory for these experiments. The cell was heated with heating tape and the temperature was measured with an iron-constantan thermocouple. The heated gas cell was placed in the sample compartment between the Michelson interferometer and detector because radiation emitted from the hot cell was unmodulated and not observed in the interferogram.

The precursors, $(CH_3)_2Pt(MeNC)_2$, [HPt] or $(CD_3)_2Pt(MeNC)_2$, [DPt] were dissolved in benzene and the solution was withdrawn from the stock solution and introduced into the infrared cell using a mohr pipette so that two milligrams of the HPt or DPt was used in all experiments. After the HPt or DPt was introduced, the cell was sealed and pumped down with a rotary pump to a base pressure of 1×10^{-3} torr to remove the solvent. The hydrogen was not introduced directly into the cell but into a side arm valve C at one end (Figure 3.1b). The side arm was attached to hydrogen vacuum line into which hydrogen could be introduced. The whole system

Figure 3.1a : Infrared gas cell for gas phase studies

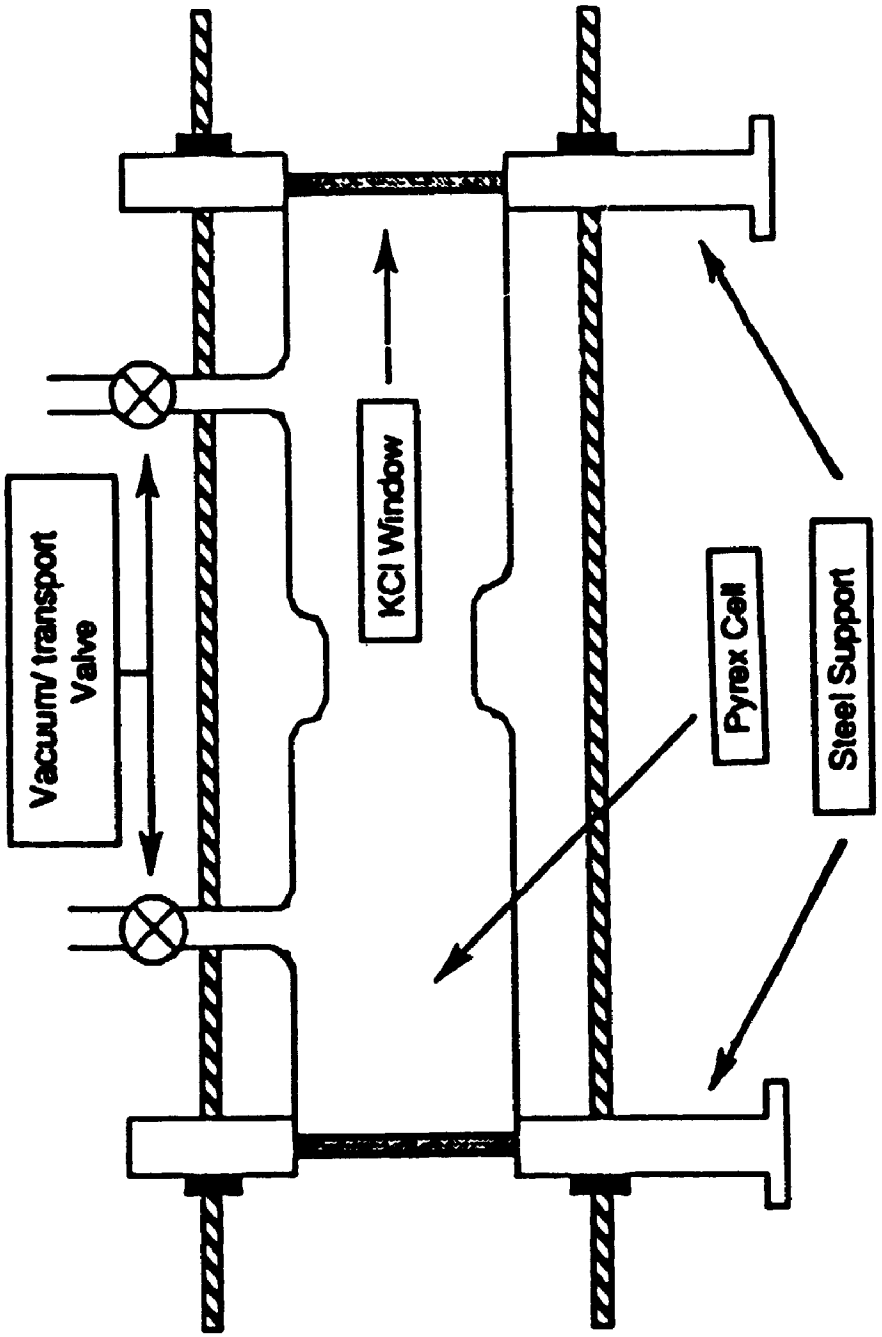
Vacuum/ transport Valve
KCl Window
Pyrex Cell
Steel Support

Figure 3.1b : Infrared gas cell and vacuum line for the introduction of H_2 gas.

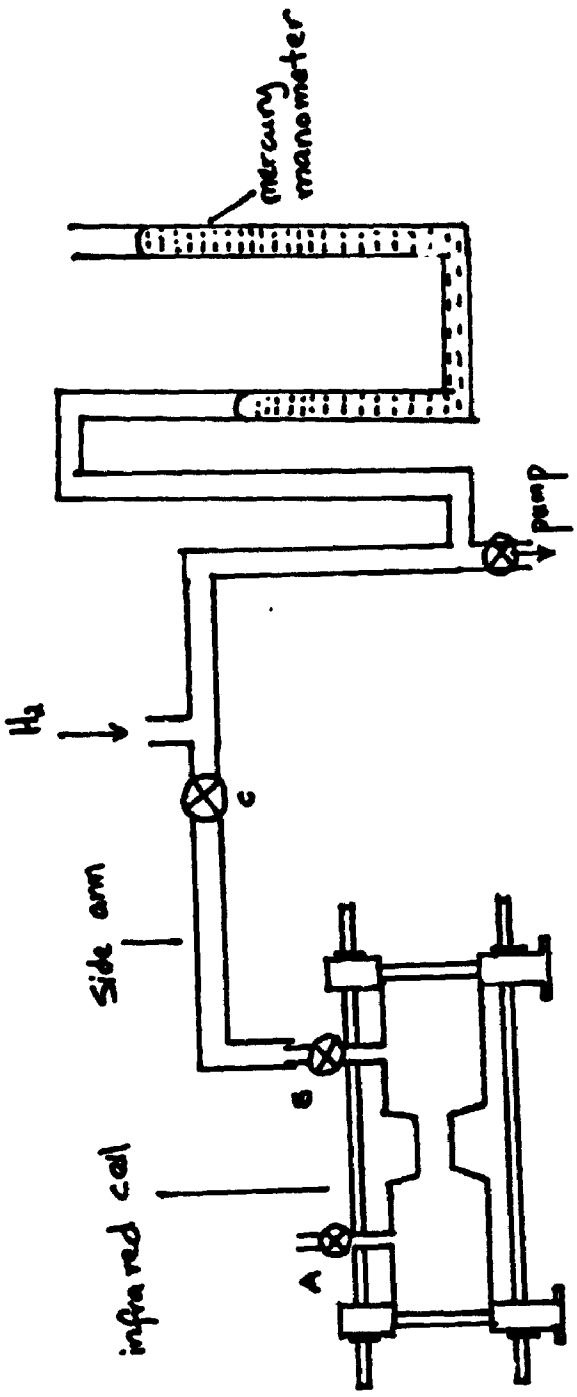
mercury manometer
pump
H_2
c
side arm
b
infrared cell
A

from valve B to the pump was evacuated before leaking in hydrogen. The hydrogen was then allowed to leak in up to valve B and the pressure of the hydrogen measured with the mercury manometer. When the required hydrogen pressure was reached, valve C was closed and the IR cell and the side arm was disconnected from the hydrogen vacuum line. The IR cell was seated in the cell compartment of the FTIR spectrometer and heated to 300 °C, followed by introduction of hydrogen into the gas cell. Infrared spectra were recorded at regular intervals of 10 minutes to follow the course of the decomposition.

3.3 Vapour Characterization

In the experiments to determine the vapour pressure curve, the infrared cell was heated slowly to maintain solid-vapour or liquid-vapour equilibrium in the enclosed cell. Infrared spectra were taken at regular intervals during the slow heating process; absorbance spectra were obtained at 4 cm^{-1} resolution and 320 scans. It took about 2.5 hours to reach a temperature of 234 °C. The average heating rate was 0.026 K/s. There was no evidence of peaks due to thermal decomposition of the precursor in the above temperature range. The absorbance of the most intense peak at 2216 cm^{-1} (due to $\nu(C\equiv N)$, as described earlier) was recorded for each spectrum over a range of cell temperatures from room temperature to 234 °C.

The plot of $[\ln A_{2216}]$ vs $1000/T(K^{-1})$ is shown in Figure 3.2. Assuming that pressure is proportional to the absorbance A, the graph could be recognised as a

Figure 3.2: Plot of lnA_{2216} vs 1000/T (K^{-1}).

(Clausius-Clapeyron Plot)

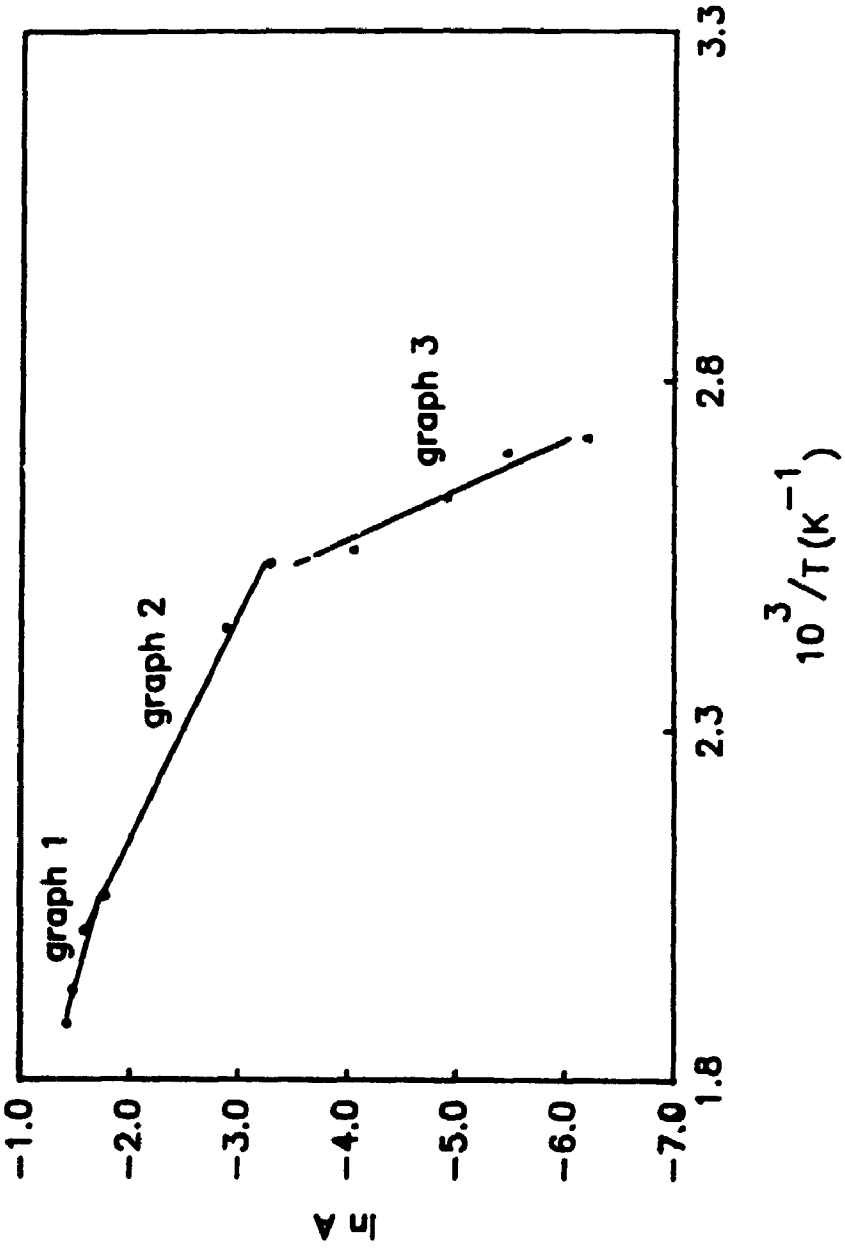
graph 1
graph 2
graph 3
-1.0
-2.0
-3.0
-4.0
-5.0
-6.0
-7.0
1.8
2.3
2.8
3.3
$10^3/T(K^{-1})$
$\ln A$

modified Clausius-Clapeyron plot. Three straight line graphs of regression order 1 could be fitted to the data points as shown in Figure 3.2. The intersection of Graphs 1 and 2 defines the saturation temperature T_s at 488 K at which all the organometallic precursor has gone into the gas phase. The absorbance A_s corresponding to T_s was found from the plot to be 0.186. Using the ideal gas law equation, the pressure P_s corresponding to T_s is 2.6 torr. The gradient of graph 3 was found to be -14.4. Using the relationship $P_T = P_0 e^{-\alpha t}$, where T is the temperature, and t is the difference of the reciprocal of the temperatures and $-\alpha$ is the gradient of the Clausius Clapeyron plot, in the region of gas solid equilibrium, the value of $2.303 \log A_s$ at room temperature was -15.3. By proportionality the vapour pressure at room temperature is 3.3×10^{-6} torr. The intersection of Graphs 2 and 3 defines the triple point of the precursor at 117 °C. Graphs 1, 2 and 3 were electronically digitized using sigma scan. The electronically digitized values from graphs 2 and 3 were converted to pressure in torr. The pressure versus temperature curve is shown in Figure 3.3.

3.3.1 Product and Labelling Studies

Spectrum 1 in Figure 3.4 is an IR gas phase spectrum of CH_4. The two strong peaks are at 3017 and 1305 cm^{-1}, which are the ν(C-H) stretch and $\delta(CH_3)$ deformation modes. Spectrum 2 shows a CH_3D IR gas phase spectrum. Strong peaks are observed at 3017, 2200, 1300 and 1155 cm^{-1}, which respectively, are the ν(C-H), ν(C-D), $\delta(CH_3)$ symmetrical bending mode and (C-D) bending mode.

Figure 3.3 : Vapour pressure curve for *cis*-dimethyl platinum diisocyanide

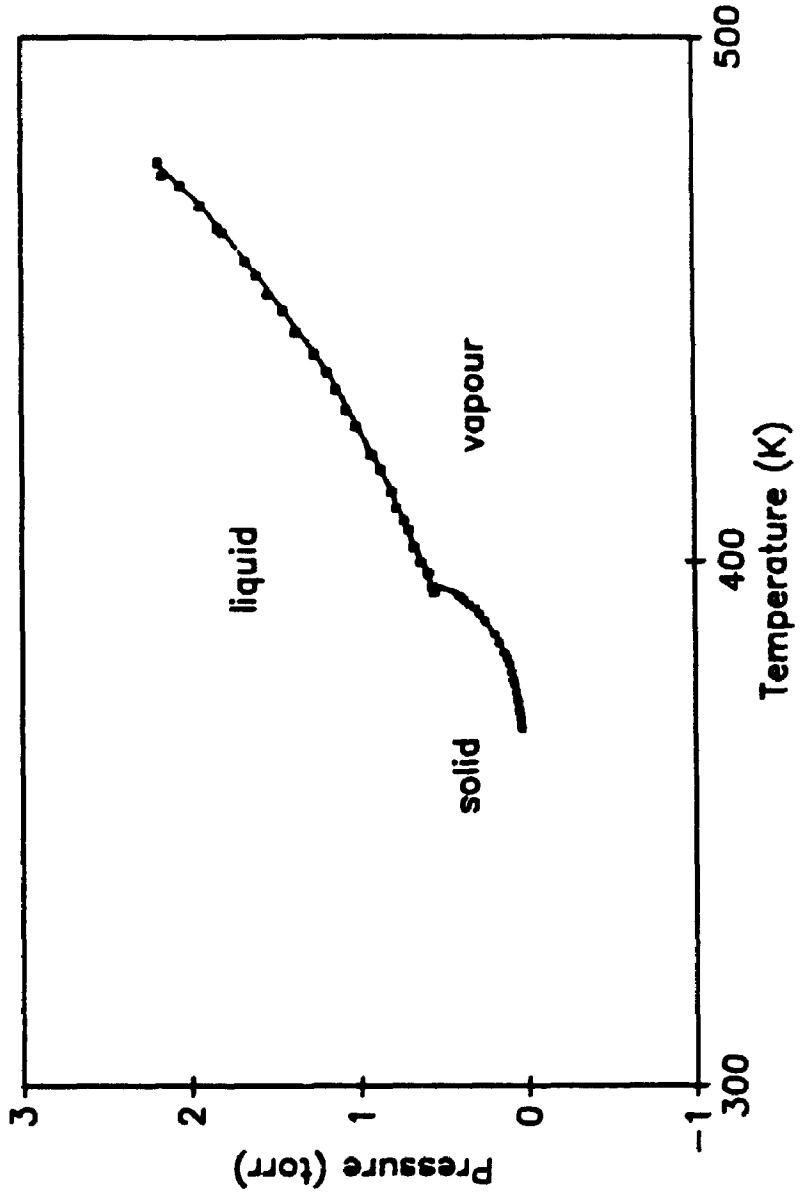
Pressure (torr)
3
2
1
0
−1
300
400
500
Temperature (K)
liquid
vapour
solid

Figure 3.4 : FTIR spectra of methane-deuterium isotopic studies

(320 scans, 4 cm^{-1} resolution).

Spectrum 1 : CH_4 at 25 °C.

Spectrum 2 : CH_3D at 25 °C.

Spectrum 3 : CD_3H at 25 °C.

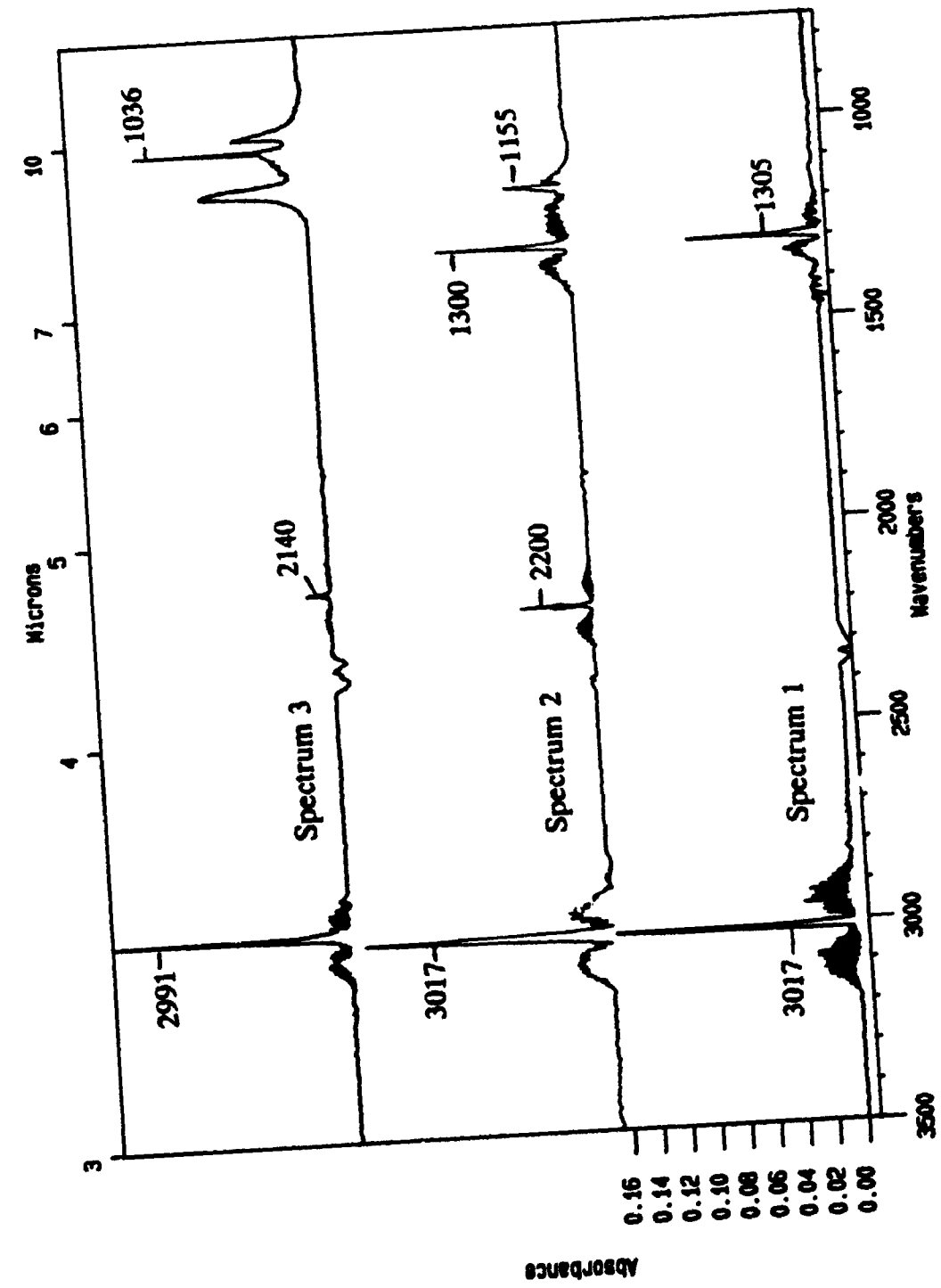
Microns
3
4
5
6
7
10
Spectrum 3
Spectrum 2
Spectrum 1
2991
2140
1036
3017
2200
1300
1155
3017
1305
Absorbance
0.16
0.14
0.12
0.10
0.08
0.06
0.04
0.02
0.00
3500
3000
2500
2000
1500
1000
Wavenumbers

Spectrum 3 in Figure 3.4 is a CD_3H IR gas phase spectrum. Strong peaks are observed at 2991, 2140 and 1036 cm^{-1}, which correspond respectively to ν(C-H), ν(C-D) and CD_3 bending modes. The band at 1130 cm^{-1} is assigned to an impurity. CD_4 IR gas phase spectrum has strong peaks at 2259 and 996 cm^{-1}, which are the ν(C-D) and C-D bending mode respectively. [1]

Spectrum 1 in Figure 3.5 is a MeNC gas phase IR spectrum and Spectrum 2 is a gas phase IR spectrum of decomposed MeNC. A library search [2] showed that this is the IR spectrum of acetonitrile.

In the gas phase spectrum of HPt are the peaks at around 2200 cm^{-1}, the asymmetric and symmetric stretches of the CN group. There is a triplet of C-H stretches due to the methyl nitrogen and methyl platinum groups. Spectrum 1 in Figure 3.6 is an IR spectrum of HPt decomposition at 307 °C. Two peaks at 3017 and 1305 cm^{-1} not present in the gas phase spectrum of the HPt are the gaseous products of decomposition assigned to the vibrational modes of methane (CH_4). When the cell is evacuated by the rotary pump, the peaks at 3017 and 1305 cm^{-1} are no longer present in the spectrum. The PQR branches of the peak at 3017 cm^{-1} are clearly observed. Spectrum 2 in Figure 3.6 is a decomposition IR spectrum of DPt

---

[1] see Wilmshurst, J.K. and H.J. Bernstein, **Can. J. Chem.**, 35 (1957), 226.

[2] Pouchert C.J., "The Aldrich library of FT-IR spectra - vapour phase" (Edition 1), Vol.3 (1989).

Figure 3.5 : FTIR spectra of methyl isocyanide decomposition.

(320 scans, 4 cm^{-1} resolution)

Spectrum 1 : CH_3NC at 25 °C.

Spectrum 2 : Decomposed MeNC at 307 °C.

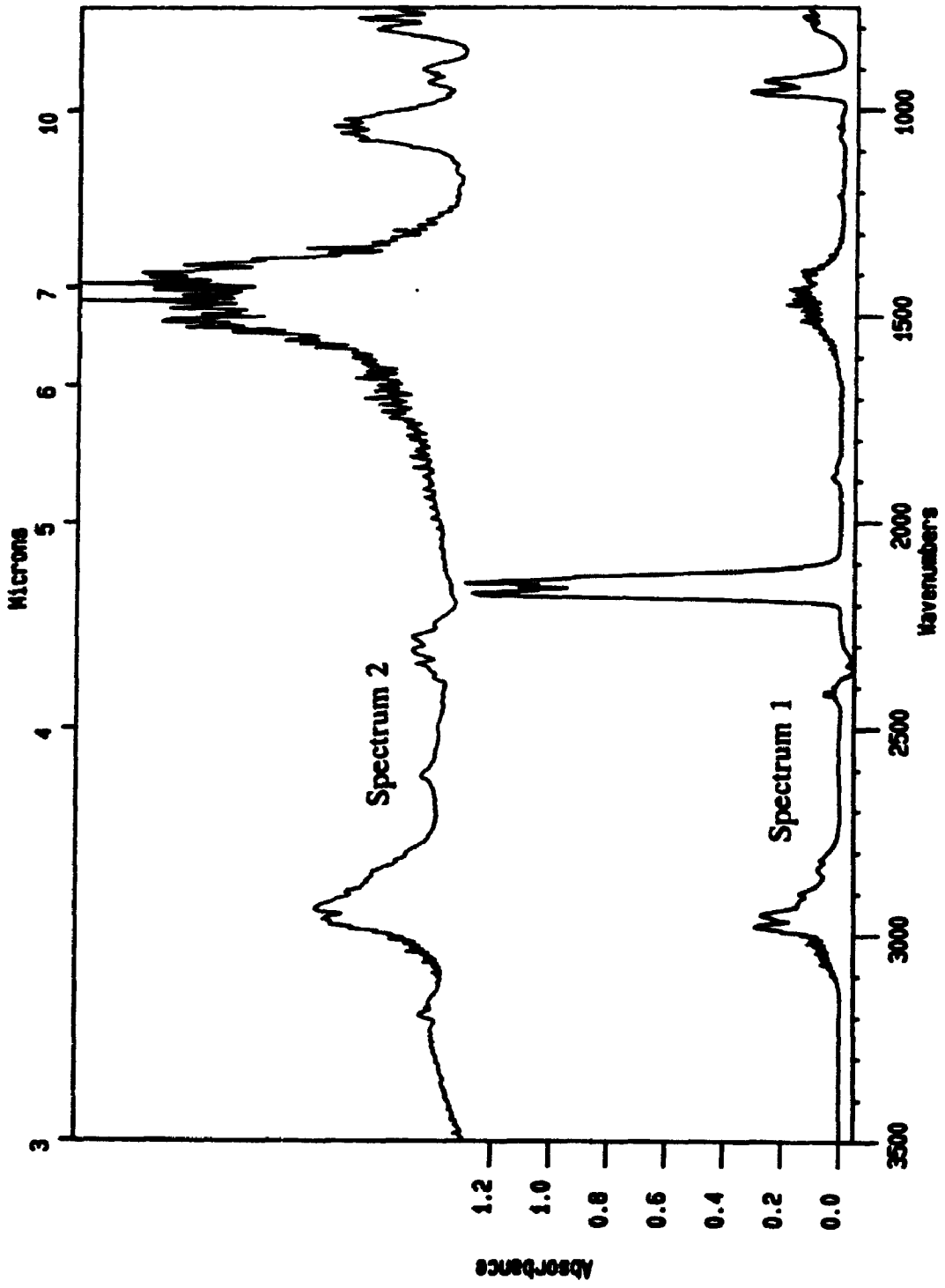
Microns
3
4
5
6
7
10
Spectrum 2
Spectrum 1
Absorbance
0.0
0.2
0.4
0.6
0.8
1.0
1.2
Wavenumbers
3500
3000
2500
2000
1500
1000

Figure 3.6 : FTIR spectra of the decomposition of *cis*-dimethyl platinum diisocyanide in the presence of hydrogen -- deuterium isotopic studies.

(320 scans, 4 cm^{-1} resolution)

Spectrum 1 : HPt at 307 °C.

Spectrum 2 : DPt at 307 °C.

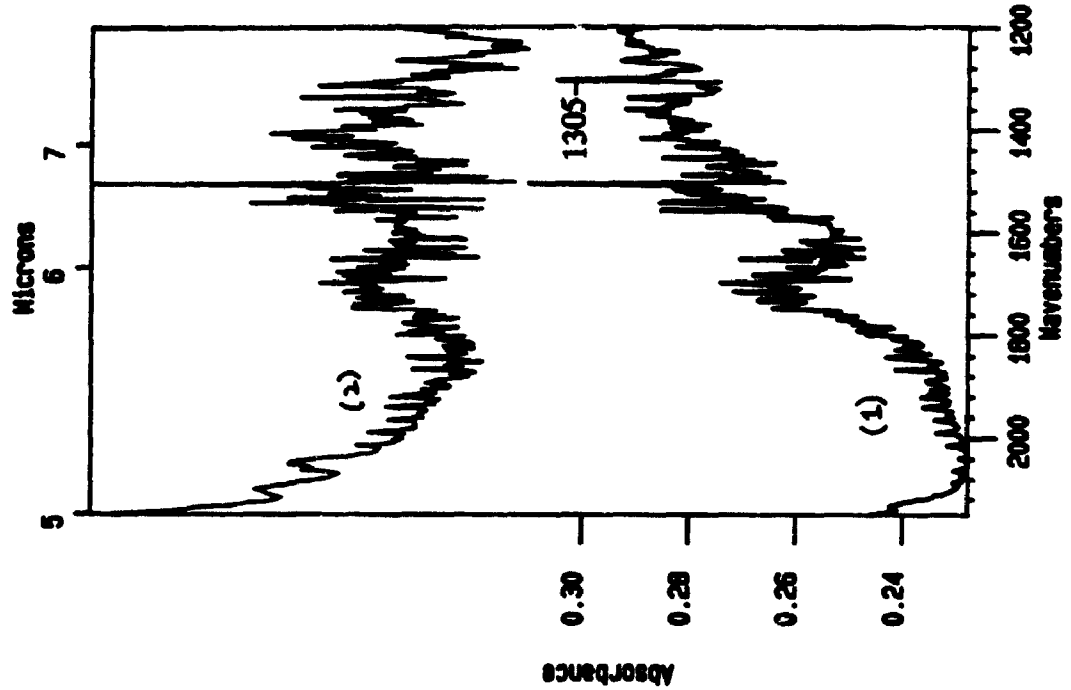
Microns
5
6
7
(2)
1305
(1)
2000
1800
1600
1400
1200
Wavenumbers
0.30
0.28
0.26
0.24
Absorbance

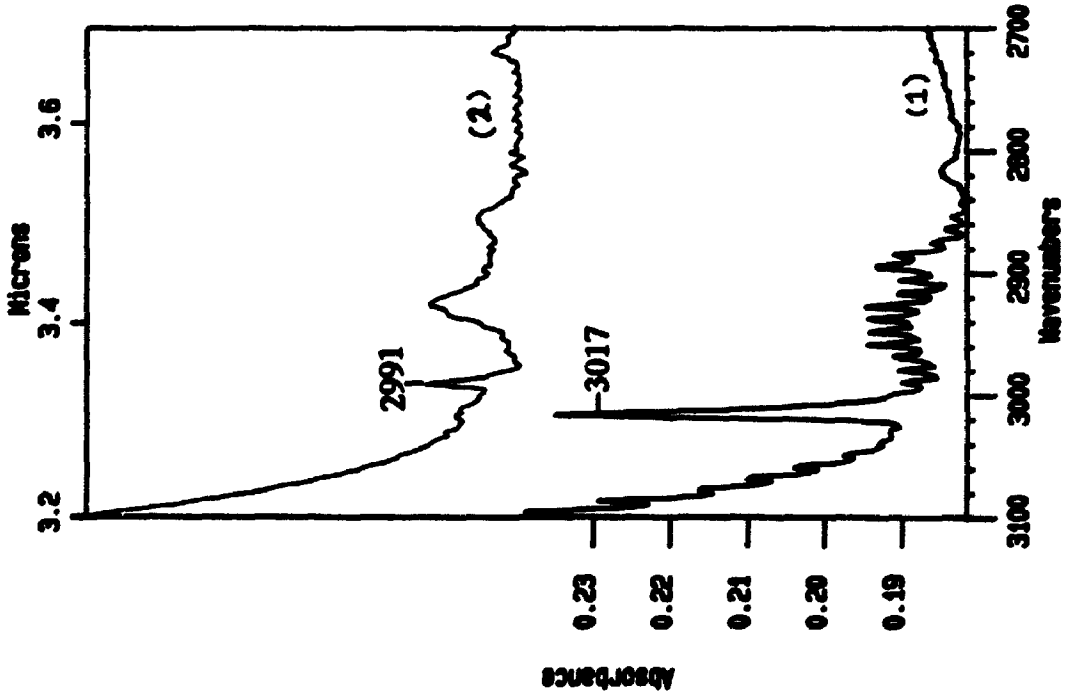
Microns
3.2
3.4
3.6
2991
(2)
3017
(1)
3100
3000
2900
2800
2700
Wavenumbers
0.23
0.22
0.21
0.20
0.19
Absorbance

cis-$(CD_3)_2Pt(CNMe)_2$. The peak at 3017 cm^{-1} is not observed. Instead, a peak at 2991 cm^{-1} is observed. This is assigned to the ν(C-H) stretch of CD_3H. This implies that the methane produced is from the methyl platinum rather than the methyl nitrogen on the methyl isocyanide ligand. Similar decomposition of D'Pt *cis*-$(CH_3)_2Pt(CNCD_3)_2$, only gave CH_4 (band at 3017 cm^{-1}) and no CD_3H. In addition, no CH_3D was observed. Analysis of the rotational fine structure can differentiate between CH_3D and CH_4. Furthermore, there is a ν(C-D) stretch in CH_3D. This shows that the extra atom is not from the methyl on the ligand, MeNC.

Spectrum 1 in Figure 3.7 is a co-decomposition IR spectrum of HPt and H_2. The peaks 3017 and 1305 cm^{-1} are again assigned to methane. Additional peaks are observed at 3300, 961 and 930 cm^{-1}. On pumping out the volatile products from the gas cell, the bands at 3017, 1305, 3300, 961 and 930 cm^{-1} are removed.

Spectrum 2 in Figure 3.7 shows the decomposition of HPt and D_2. The peaks at 3017 and 1305 cm^{-1} are assigned to the ν(C-H) stretch and $\delta(CH_3)$ deformation of CH_3D. The peak at 3300 cm^{-1} has been shifted to 2780 cm^{-1}. The peaks at 961 and 930 cm^{-1} are no longer observed and presumably have been shifted down to 738 and 715 cm^{-1} by D-substitution, which is beyond our detection limit. These bands must therefore be due to vibrations in product molecules from the hydrogenation by H_2.

Spectrum 3 in Figure 3.7 shows the codecomposition of DPt and D_2.

Figure 3.7 : FTIR spectra of the decomposition of *cis*-dimethyl platinum diisocyanide in the presence of hydrogen -- deuterium isotopic studies.

(320 scans, 4 cm^{-1} resolution)

Spectrum 1 : HPt/H_2 at 307 °C.

Spectrum 2 : HPt/D_2 at 307 °C.

Spectrum 3 : DPt/D_2 at 307 °C.

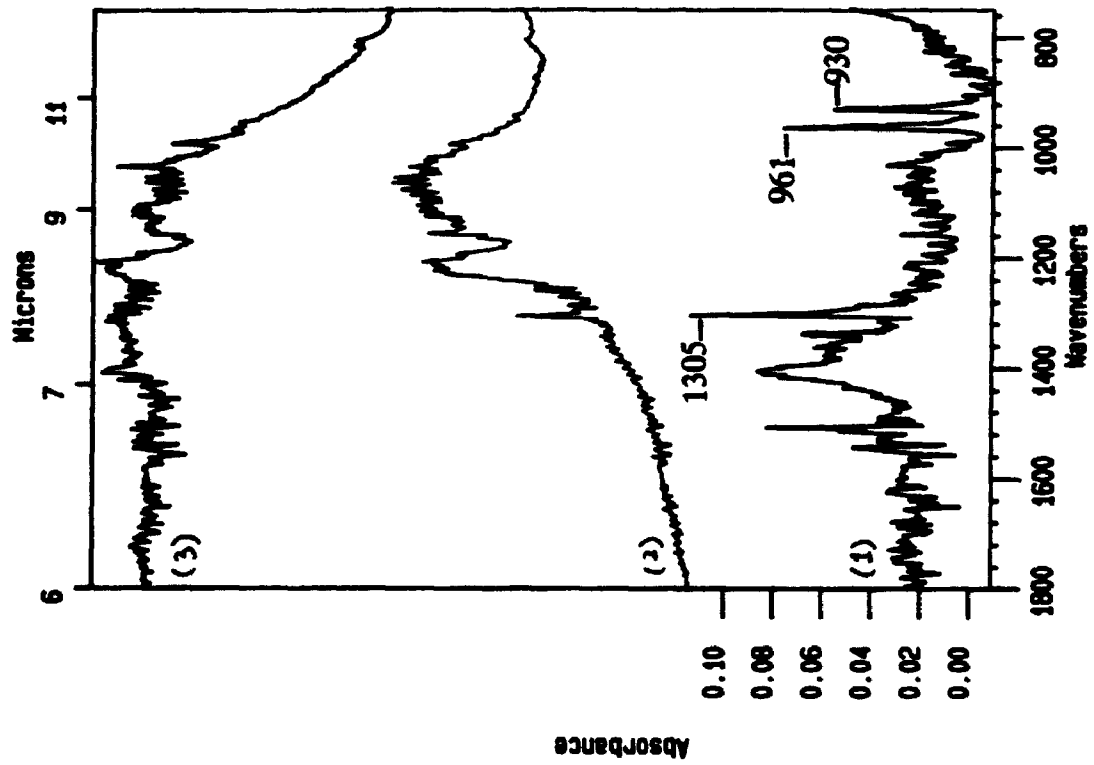
Microns
6
7
9
11
(3)
(2)
(1)
1305
961
930
Wavenumbers
1800
1600
1400
1200
1000
800
Absorbance
0.10
0.08
0.06
0.04
0.02
0.00

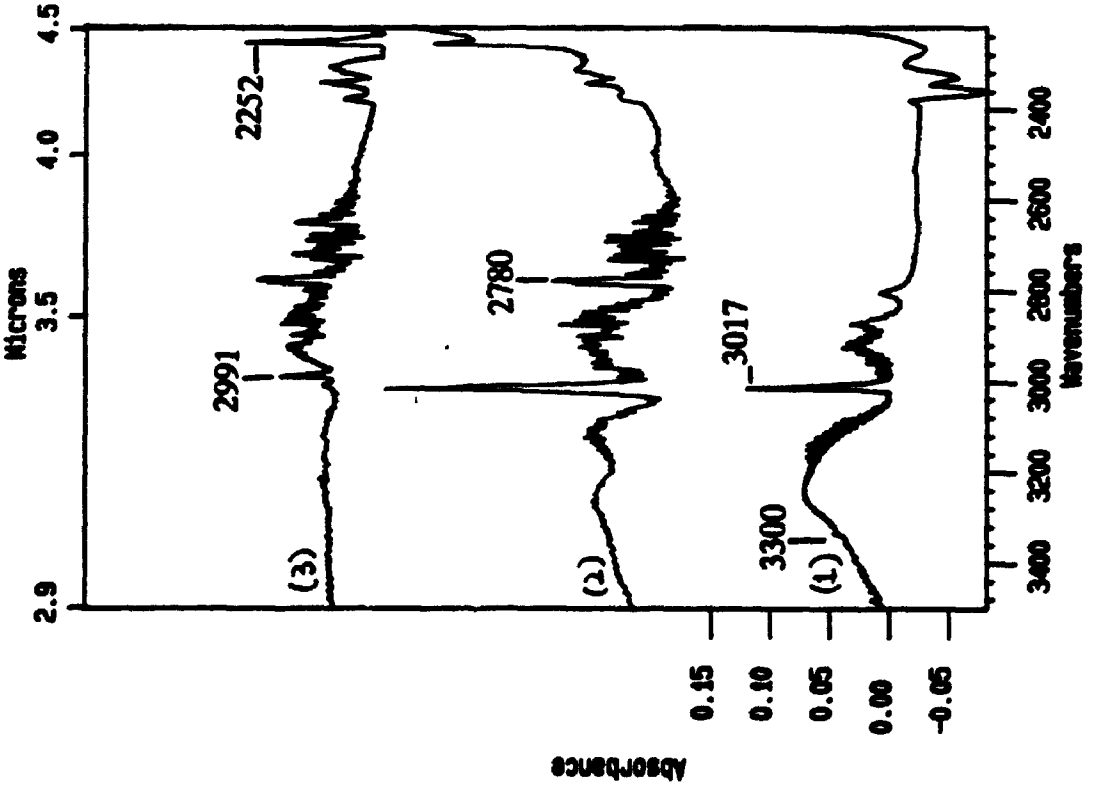
Microns
2.9
3.5
4.0
4.5
(3)
(2)
(1)
2991
2252
2780
3017
3300
Wavenumbers
3400
3200
3000
2800
2600
2400
Absorbance
0.15
0.10
0.05
0.00
-0.05

Peaks due to volatile products are at 2991 and 2252 cm^{-1}, which are assigned to ν(C-H) and ν(C-D) in CD_3H and CD_4 respectively. Obviously, there is some H_2 introduced with the D_2. This result shows that the methane produced in HPt and H_2 co-decomposition comes from the methyl platinum group. The peak at 2780 cm^{-1} was not shifted when HPt was replaced with DPt (compare Spectrum 2 and 3 of Figure 3.7). This band is thus assigned to a reaction product of D_2 and the MeNC ligand. It is assigned to a ν(N-D) stretch.

3.3.2 Kinetic Study

The kinetics of CVD from *cis*-[$PtMe_2(MeNC)_3$] were studied by monitoring the appearance of the ν(C-H) stretch of methane at 3017 or via the reduction of the ν(CN) stretch of the complex at 2216 cm^{-1}. Figure 3.8 shows the decomposition profile of HPt over time. The analysis is qualitative and only apparent rate constants are reported.

a. Decomposition of HPt

Figure 3.9a plots $-ln\ (A_\infty - A_t)$ against time t, where A_t is the absorbance of the ν(C-H) stretch of methane. Figure 3.9b plots $-ln\ C_t$ against time, where C_t is the absorbance of ν(CN) stretch of the HPt at 2217 cm^{-1}. Both plots could be fitted with a straight line graph with good agreement for the first order rate constant, k

Figure 3.8 : HPt decomposition profile over time at 307 °C.

Spectrum 1 : 0 min at 307 °C.

Spectrum 2 : 25 mins at 307 °C.

Spectrum 3 : 90 mins at 307 °C.

Spectrum 4 : gas cell cooled to 25 °C, at the end of the experiment.

Note: The number to the left of each spectrum accompanied by a "×", are the factors by which the displayed spectrum should be multiplied to compare with spectrum 1.

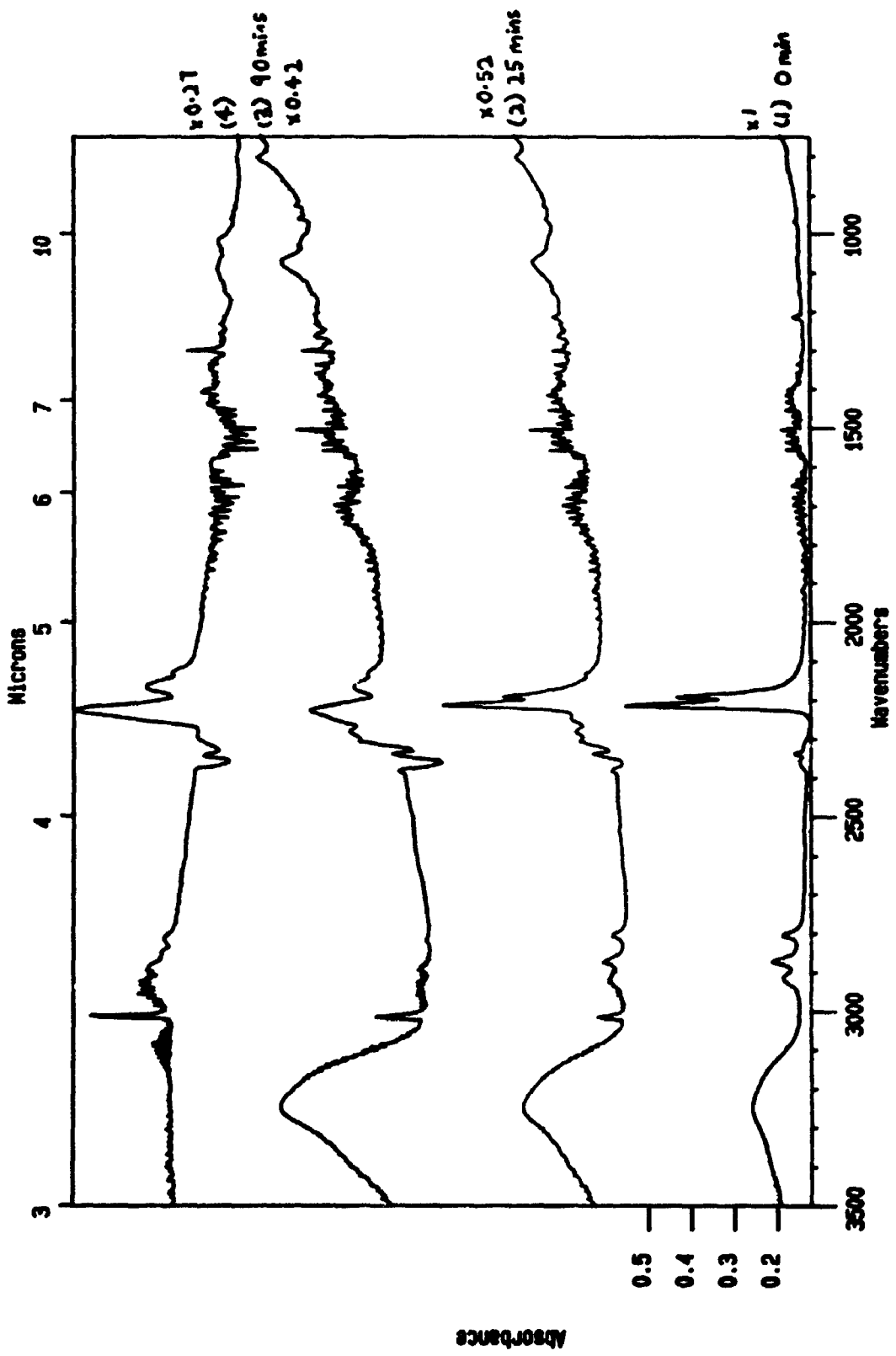
x0.27
(4)
(2) 90 mins
x0.42
x0.52
(2) 25 mins
x1
(1) 0 min
Microns
3
4
5
6
7
10
Wavenumbers
3500
3000
2500
2000
1500
1000
Absorbance
0.5
0.4
0.3
0.2

Figure 3.9a : Plot of *-ln* (A_∞ - A_t) versus time (minutes) during the decomposition of HPt at 307 °C , where A_t is the absorbance at 3017 cm^{-1} due to evolved methane at

time t.

Figure 3.9b: Plot of *-ln* C_t versus time (minutes) during decomposition of HPt at 307 °C, where C_t is the absorbance at 2217 cm^{-1} due to the C≡N stretch in remaining complex (HPt).

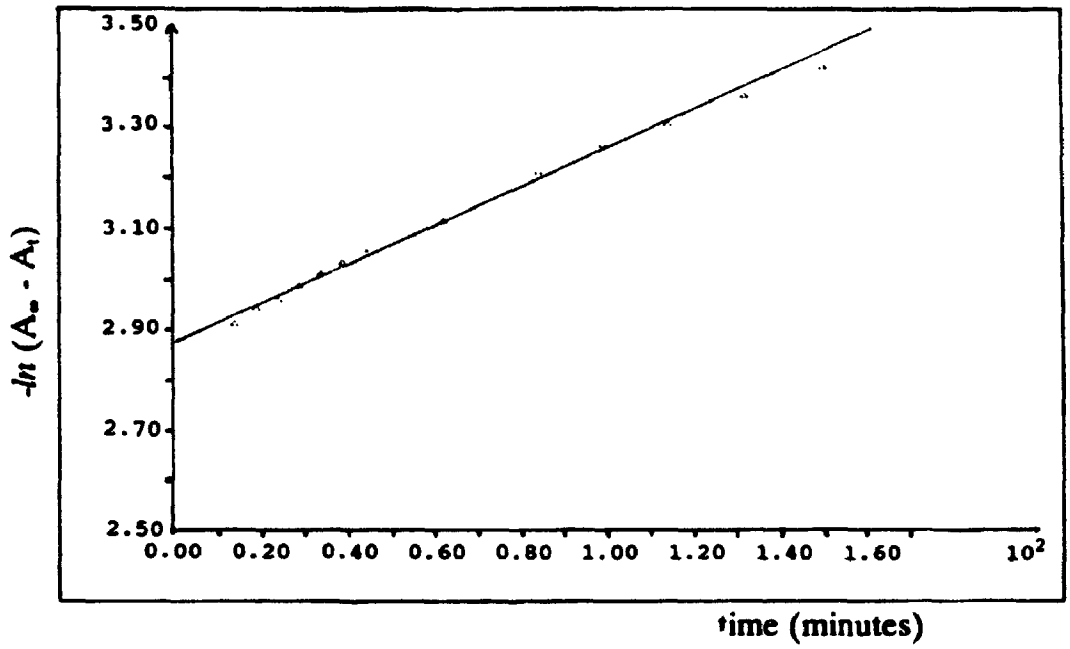
3.50
3.30
3.10
2.90
2.70
2.50
-ln (A∞ - At)
0.00 0.20 0.40 0.60 0.80 1.00 1.20 1.40 1.60 10²
time (minutes)

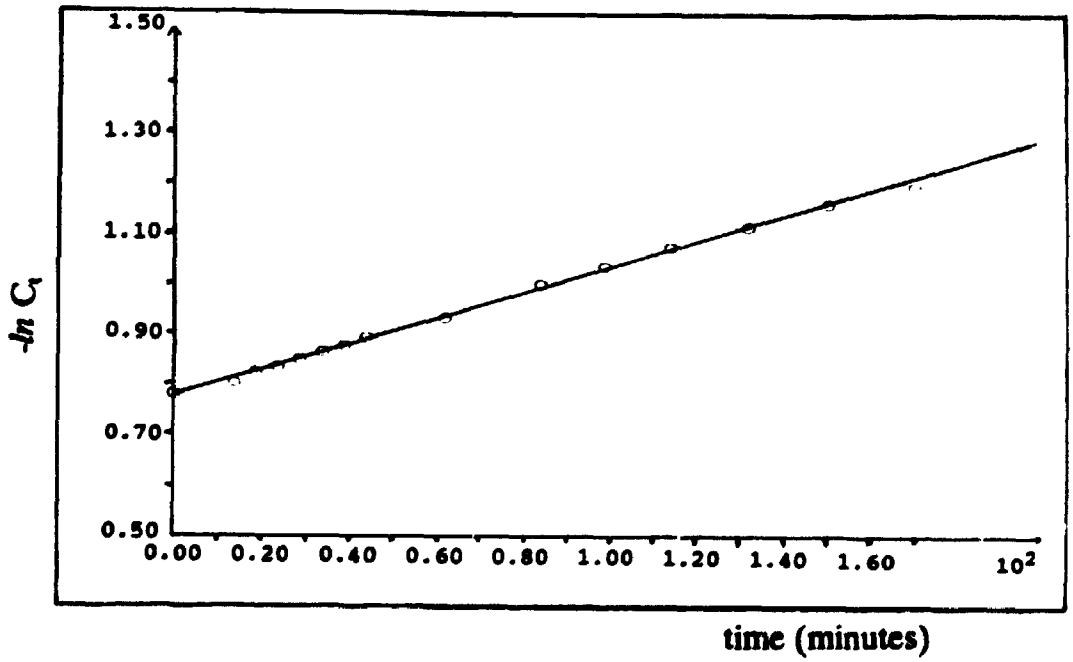
1.50
1.30
1.10
0.90
0.70
0.50
-ln Ct
0.00 0.20 0.40 0.60 0.80 1.00 1.20 1.40 1.60 10²
time (minutes)

(k = 3.8×10^{-3} min^{-1} and 2.6×10^{-3} min^{-1} [3]in Figures 3.9a and 3.9b respectively).

b. Decomposition of HPt and DPt

6.5×10^{-6} moles of HPt and DPt were decomposed together and the bands at 3017 and 2991 cm^{-1} were monitored. Figure 3.10 plots $-ln[(A_\infty - A_t) / A_\infty]$ against time t, using the absorbance at 3017 cm^{-1}, the ν(C-H) stretch in methane at 2291 cm^{-1} and the ν(C-H) stretch in CD_3H. The k_H/k_D obtained was 1.35 showing a kinetic isotope effect. This result shows that the rate determining step must involve the methyl platinum group.

c. Co-Decomposition of HPt and free MeNC where $P_{MeNC} / P_{HPt} = 0.54$

6.5×10^{-6} moles of the HPt was decomposed with free MeNC where the pressure ratio of MeNC to HPt was 0.54. Methane was produced and the kinetics monitored by following the growth of the ν(C-H) band of methane. Figure 3.11 shows a plot of -log $(A_\infty - A_t)$ against time t, where A_t is again the absorbance of the ν(C-H) stretch of methane. The reaction rate is shown in the first part of the reaction which corresponds to the retardation of decomposition because of added MeNC. The second part shows an increase in the rate of methane produced, and this occurs when MeNC isomerizes to CH_3CN (see also Figure 3.5). At higher pressures of MeNC, the initial rate of production of methane was too slow to be monitored by FTIR.

---

[3] The ν(CN) stretch at 2216 cm^{-1} from the complex occurs near the CN stretch from the polymeric material which is formed. This may account for the discrepancy in the values of the rate constant.

Figure 3.10 : Plot of $-ln[(A_\infty - A_t) / A_\infty]$ versus time (minutes) during the decomposition of HPt and DPt at 307 °C , where A_t is the absorbance either at 3017 cm^{-1} due to CH_4 or at 2990 cm^{-1} due to CD_3H.

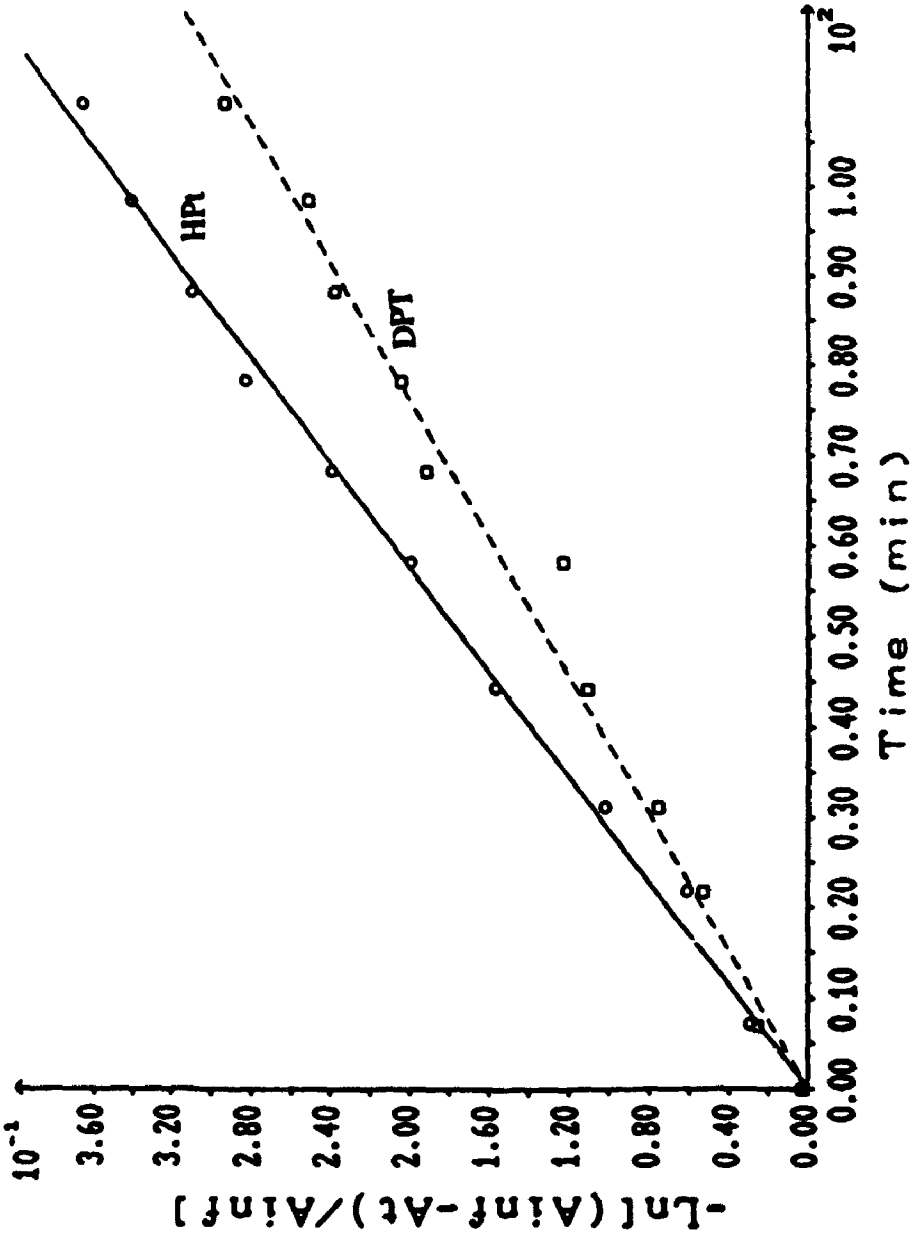
HPt
DPT
-Ln[(Ainf-At)/Ainf]
Time (min)
10^{-1}
10^{2}
0.00
0.40
0.80
1.20
1.60
2.00
2.40
2.80
3.20
3.60
0.00
0.10
0.20
0.30
0.40
0.50
0.60
0.70
0.80
0.90
1.00

Figure 3.11 : Plot of -log (A_∞ - A_t) versus time (minutes) during the codecomposition of HPt and MeNC at 307 °C.

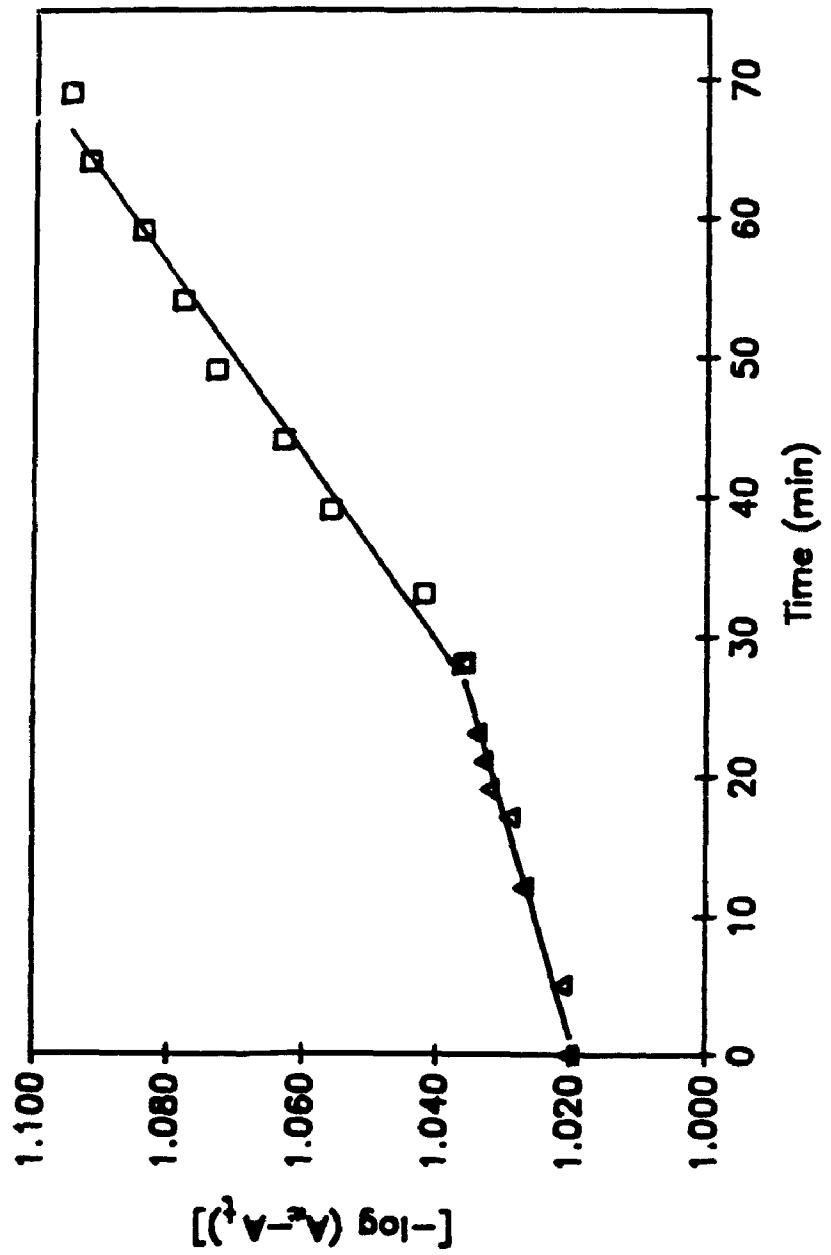
1.100
1.080
1.060
1.040
1.020
1.000
[−log (A∞−At)]
0
10
20
30
40
50
60
70
Time (min)

d. Co-Decomposition of HPt and H_2

Figure 3.12 shows a typical decomposition of *cis*-dimethyl platinum diisocyanide in the presence of H_2 over time. When 6.5×10^{-6} moles of HPt was decomposed with hydrogen gas at about 100 torr, methane evolution was accelerated.

Figure 3.13 is plot of $\sqrt{[(A_\infty - A_t) / A_\infty]}$ against time t, where A_t is the absorbance of the ν(C-H) stretch of methane for different hydrogen pressures. The gradient is $-k'/[\sqrt{(2A_\infty)}]$, where $k' = k[H_2]$. The plot can be fitted with a straight line graph for each of the different hydrogen pressure used. This shows that the order of reaction with respect to the complex is 0.5, in contrast to 1 when HPt was decomposed alone.

3.4 Discussion

3.4.1 Decomposition of *cis*-dimethyl platinum diisocyanide

a. In the absence of hydrogen

The decomposition of the precursor yields methane as a gaseous product. The methane is produced from combination of the methyl platinum group with a hydrogen atom, since DPt decomposition gave only CD_3H and no CH_4. The absence of any CH_4 implies that the methyl group on the ligand is not involved in the evolution of methane. The hydrogen atom is not obtained from the methyl on the ligand and probably arises from the cell walls or residual hydrogen which is not pumped away. The decomposition involves initial ligand loss in an equilibrium step.

Figure 3.12 : HPt and H_2 codecomposition profile over time at 307 °C.

Spectrum 1 : 0 min at 307 °C.

Spectrum 2 : 30 mins at 307 °C.

Spectrum 3 : 67 mins at 307 °C.

Spectrum 4 : 98 mins at 307 °C.

Spectrum 5 : 140 mins at 307 °C.

Spectrum 6 : gas cell cooled to 25 °C, at the end of the experiment.

Note: The number to the left of each spectrum accompanied by a ×, are the factors by which the displayed spectrum should be multiplied to compare with spectrum 1.

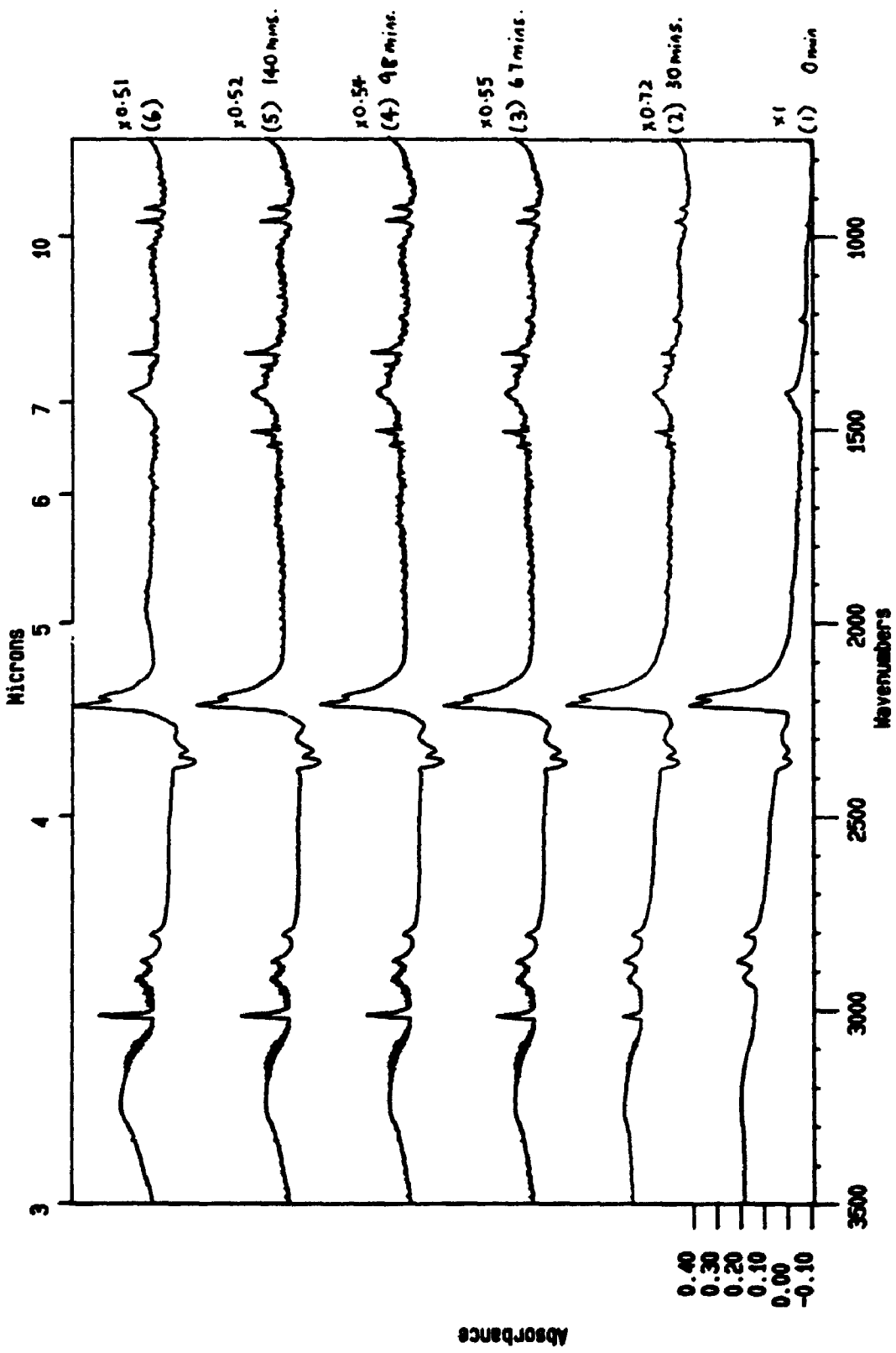
x0.51
(6)
x0.52
(5) 140 mins.
x0.54
(4) 98 mins.
x0.55
(3) 67 mins.
x0.72
(2) 30 mins.
x1
(1) 0 min
Microns
3
4
5
6
7
10
Wavenumbers
3500
3000
2500
2000
1500
1000
Absorbance
0.40
0.30
0.20
0.10
0.00
-0.10

Figure 3.13 : Plot of $\sqrt{[(A_\infty - A_t) / A_\infty]}$ versus time (minutes) during the codecomposition of HPt and H_2 at 307 °C, at the following pressures of H_2 -- (a) 99 torr, (b) 132 torr, (c) 198 torr and (d) 264 torr, and where A_t is the absorbance at 3017 cm^{-1} due to CH_4.

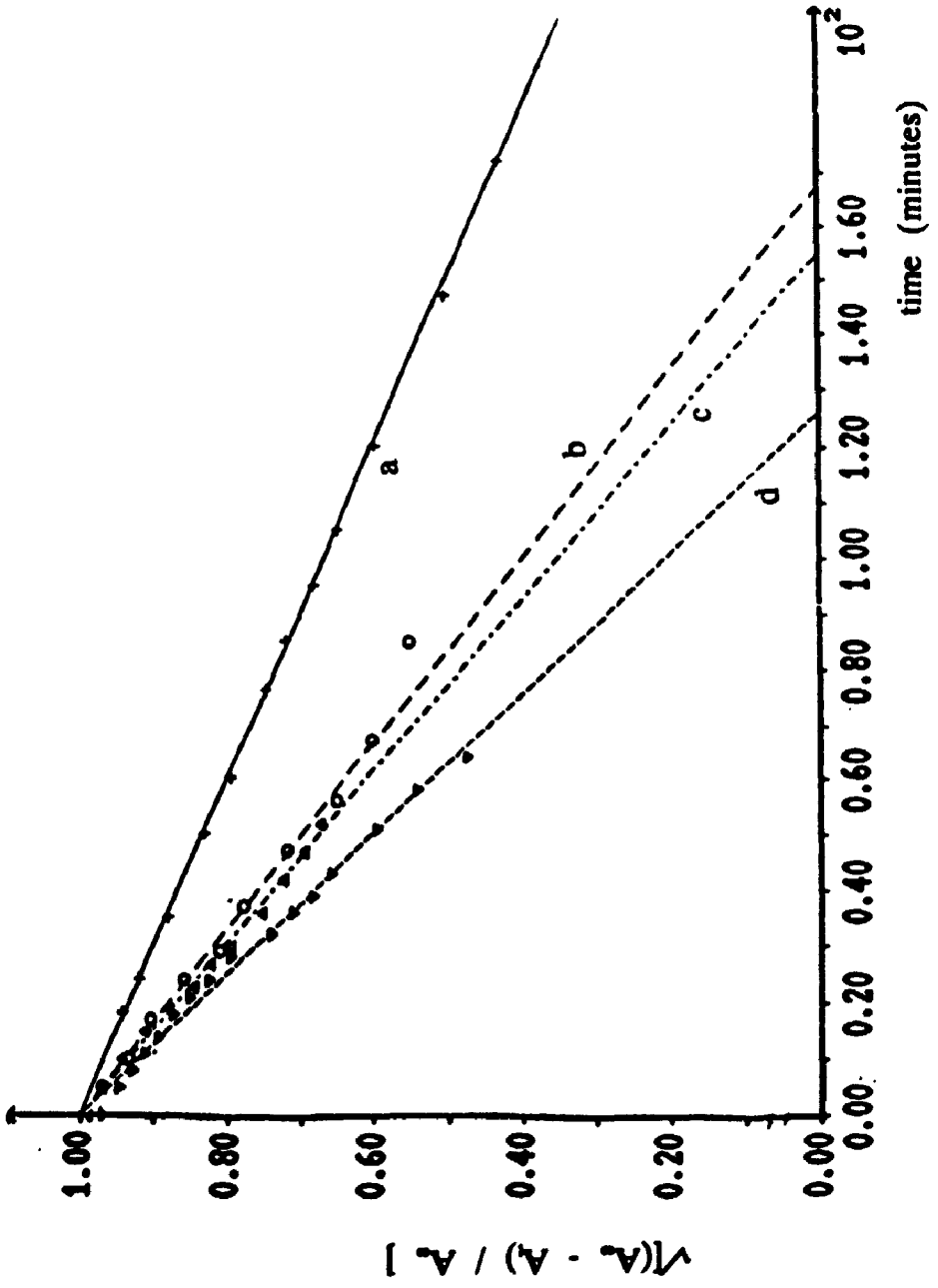
√[(A∞ - A) / A∞]
1.00
0.80
0.60
0.40
0.20
0.00
0.00
0.20
0.40
0.60
0.80
1.00
1.20
1.40
1.60
10²
time (minutes)
a
b
c
d

The ligand polymerizes to give a polymer with CN stretch frequencies of 2232 and 2172 cm^{-1}. No acetonitrile was detected in the decomposition of HPt, although free MeNC decomposition does give acetonitrile. This is largely due to the small amount of methyl isocyanide from HPt decomposition. In a separate experiment, HPt was decomposed in a hot wall reactor and the volatile products quickly pumped out and condensed on a highly polished platinum (111) surface at 110 K. Infrared light from an FTIR instrument was reflected off the platinum surface in a FTIR-RAS experiment. A multilayer CH_3NC on Pt(111) FTIR-RAS spectrum was observed. Thus the CH_3NC was detected before it isomerized to CH_3CN.

The kinetics of decomposition was shown to be first order with respect to the complex. It has been shown that the first step involves reversible loss of the methyl isocyanide ligand.

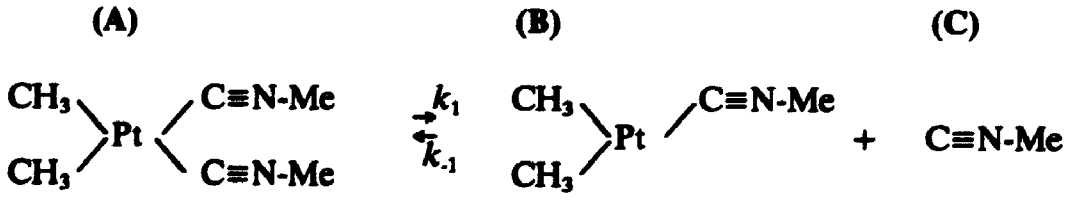

Assuming that methane is formed from the irreversible decomposition of molecule (B) in a rate determining step, then,

$$\frac{d[CH_4]}{dt} = k[B] \qquad (3.1)$$

where [B] is the concentration of (B).

Since,

$$K = \frac{[B][C]}{[A]} \qquad (3.2)$$

where [A] and [C] are the concentration of (A) and (C) respectively and K is the equilibrium constant in the reversible step.

This implies that:

$$\frac{d[CH_4]}{dt} = \frac{kK[A]}{[C]} \qquad (3.3)$$

Equation (3.3) shows that the rate is first order with respect to the complex if the concentration of methyl isocyanide is constant. Since methyl isocyanide is formed from the decomposition of HPt and then polymerizes and isomerizes, this is not an unreasonable assumption. It is interesting that by the application of gas phase kinetics to the present form of the mechanistic scheme, one can derive an order of reaction equal to one, which is in agreement with the experimentally measured rate order.

b. In the presence of hydrogen -- the role of hydrogen

In co-decomposition with hydrogen, methane is again produced from the combination of the methyl platinum and the added hydrogen as co-decomposition of DPt and D_2 gives only CD_4 and some CD_3H but no CH_3D or CH_4 (3017 cm^{-1} band is absent). The ligand still polymerizes as evidenced by the C≡N stretches at 2232

and 2172 cm^{-1} which were still present when the cell was evacuated. However, additional peaks at 3300, 1600, 961 and 930 cm^{-1} from a volatile product (not methane) were also detected. The bands at 961 and 930 cm^{-1} show P,Q,R branches with rotational fine structure. These bands at 961 and 930 cm^{-1} were also observed when the free MeNC was co-decomposed with HPt.

The reaction of free MeNC and H_2 yields dimethyl amine - $(CH_3)_2NH$. [4] However, dimethyl amine is not detected in the co-decomposition of CH_3NC and H_2, at 570 K in our reactor. In contrast, we detected two infrared bands at 961 and 930 cm^{-1}, which were absent in the infrared spectrum of dimethyl amine [5]. We postulate that the H_2 must have added to CH_3CN rather than CH_3NC. This postulate is consistent with the isomerization of CH_3NC at the high temperature of 570 K.

Comparison of the bands at 961, 930, 3300 and 1600 cm^{-1} with the IR spectrum of NH_3 [6] provided a match. The rotational spacings about the two Q branches at 930 and 961 cm^{-1} matched those in ammonia and was equal to 20 cm^{-1}. Ammonia was formed by hydrogenation by H_2 gas because when HPt was codecomposed with D_2, the peaks at 3300, 1600, 961 and 930 were shifted to lower energy. It was concluded that in the decomposition of HPt with H_2 gas, MeNC ligand

---

[4] see Ugi Ivar (ed)., **Isonitrile Chemistry**, Academic Press, New York, 1971, p. 80.

[5] Supra footnote 2, chapter 3.

[6] Supra footnote 2, chapter 3.

was lost from the complex. After CH_3NC isomerized to CH_3CN, H_2 reacted with CH_3CN. Subsequent reactions gave NH_3 as a product.

The rate of methane evolution was accelerated in the presence of hydrogen. The kinetics of decomposition became more complex and the order of reaction with respect to the complex changed from one (in the absence of hydrogen) to half (in the presence of hydrogen. Furthermore, the order with respect to hydrogen was 0.85. The ½ order of reaction with respect to the complex could not be arrived using simple gas phase kinetic analysis.

The increased rate of methane evolution in the presence of hydrogen almost certainly points to a catalytic effect. A platinum film is deposited as a result of the decomposition of *cis*-dimethyl platinum diisocyanide. It was difficult to observe an induction period in our experiments. However, codecomposition of HPt with H_2 over a preformed platinum film (i.e. a platinum film from a previous decomposition) showed an increase in the rate of evolution of methane over a codecomposition without the preformed platinum film. Hence there is evidence for a heterogenous component in the reaction mechanism.

The surface reactions could be due to H_2 or CH_3NC interaction with the platinum surface or even a combination of the above. Considering the explosive isomerization of CH_3NC to CH_3CN under the reaction conditions, the interaction of

CH_3CN with the platinum surface could be important.

Christmann et al.[7] had investigated the hydrogen interaction with Pt(111) and showed that hydrogen adsorbs dissociatively on Pt(111). There are two adsorption states -- β_1 and β_2, with peak temperatures of about 223 and 325 K respectively. H_2 is formed on desorption. It is therefore reasonable to consider H_2 adsorption on the growing platinum surface in our experiments. The growing platinum film would present a highly reactive surface (recall that codecomposition of HPt and H_2 yields highly pure Pt films).

Szilágyi [8] provided evidence for hydrogenation reactions when CH_3CN and H_2 were coadsorbed on a Pt/SiO_2 supported catalyst at 300 K. Both gases were introduced at pressures of about 0.3 torr. He provided a possible reaction scheme where CH_3CN adsorbed in an η^2(C,N) configuration with the carbon and nitrogen atom each bonded to a platinum atom. Hydrogenation of the η^2(C,N) gave a hydrogenated species where the carbon atom nearest the nitrogen atom was doubly bonded to two platinum atoms and the nitrogen atom itself had been hydrogenated to give a primary amine.

With the above background information, it is possible that the methyl

---

[7] K. Christmann, G. Ertl and T. Pignet. **Surf. Sci.** 54, (1976), 365 - 392.

[8] Szilágyi, T. **Appl. Surf. Sci.**, 35, (1988), 1, 19.

isocyanide released in the initial reversible equilibrium step in HPt decomposition isomerized to CH_3CN (acetonitrile), which subsequently adsorbed in an η^2(C,N) configuration. H_2 adsorption on the platinum surface possibly provided the hydrogen atoms for the hydrogenation of acetonitrile to give the absorbed amine species, which subsequently decomposes to give NH_3. Indeed, NH_3 has been observed as a product from the codecomposition of HPt and H_2. The methyl platinum groups may easily pick up the hydrogen atom on the platinum surface to give methane. This provides a satisfactory explanation for the observation of CD_3H when DPt was codecomposed with H_2 in the infrared gas cell.

The reaction mechanism discussed above strongly points to the catalytic role of the platinum surface. The rate of evolution of methane from the codecomposition of *cis*-dimethyl platinum diisocyanide and hydrogen may be limited by the surface coverage of hydrogen atoms on the platinum surface. A complete description of the kinetics must therefore include this heterogenous component.

3.4.2 Structure of Transition State in HPt Decomposition

Transition state theory assumes that there is an equilibrium between reactant and the transition state, which undergoes decomposition to products. We have already shown that methane is produced in the decomposition of HPt. Moreover, methane is produced from the combination of a methyl platinum group and hydrogen atom.

Focusing only on the methyl platinum group, we consider our reactants and transition state as shown below:

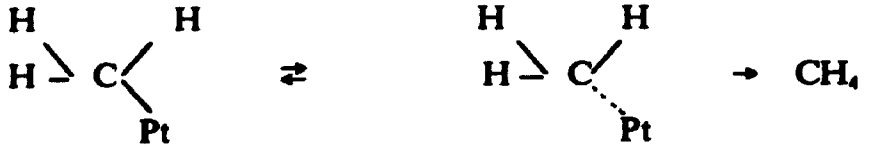

reactant transition state product

From transition state theory,

$$rate = w\left(\frac{kT}{h}\right)\left(\frac{Q^*}{Q_A}\right) e^{-E_0^\circ/RT} C_A \qquad (3.4)$$

where w is the transmission coefficient, and Q is the total partition function (equal to $q_{trans}q_{rot}q_{vib}$) and the asterisk denotes the transition state. The kinetic isotope effect can thus be expressed as a ratio of partition functions:

$$\frac{k}{k_i} = KIE = \frac{Q^*}{Q_A} \Big/ \frac{Q^{*i}}{Q_A^i} \qquad (3.5)$$

where the i denotes the isotopically labelled molecule.

Following (Gates, Russell and Yates) [9] , we assume :

$$Q^* = Q^{*i} \qquad (3.6)$$

so that,

Further assuming that transitional and rotational partition functions are equal for Q_A^i

---

[9] See S. M. Gates, J. N. Russell Jr. and J. T. Yates, Jr. **Surf. Sci.**, 146 (1984), 199-210.

$$KIE = \frac{Q_A^i}{Q_A} \qquad (3.7)$$

and Q_A, then,

$$KIE = \frac{Q_{vib}^i}{Q_{vib}} \qquad (3.8)$$

For the Pt-C carbon, ν(Pt-CH_3) stretch is around 650 cm^{-1}.

The reduced mass for (CH_3-Pt) is given by:

$$\mu_1 = \frac{195 \times 15}{195 + 15} = \frac{2925}{210} \qquad (3.9)$$

And the reduced mass for (CD_3-Pt) is given by:

$$\mu_2 = \frac{195 \times 18}{195 + 18} = \frac{3510}{213} \qquad (3.10)$$

Therefore,

$$\sqrt{\mu_2 \times \frac{1}{\mu_1}} = 1.087 = \frac{\nu_1}{\nu_2} \qquad (3.11)$$

Given that we know $\nu_1 = 650\ cm^{-1}$, then $\nu_2 = 600\ cm^{-1}$.

Again following (GRY),

$$KIE \approx \exp\left[\frac{a}{2T}(\omega - \omega^i)\right] \qquad (3.12)$$

where $a = hc/k$, T is the temperature in Kelvin, ω and ω^i are the observed vibrational frequencies of a single mode of the Pt-C bond.

Considering only the Pt-C stretch,

$$KIE = \exp\left[\frac{a}{2T}(650-600)\right] = 1.064 \qquad (3.13)$$

Thus a *KIE* of 6.4% is expected from the cleavage of the Pt-CH_3 bond to form methane.

However, we observe a *KIE* of 1.35 when the hydrogens on the methyl platinum group were replaced with deuterium atoms. This kinetic isotope effect definitely does not arise from the change of the Pt-C bond. Some other site in the system is stretched or distorted in the transition state. This type of *KIE* is thus called a secondary kinetic isotope effect. Using equation (3.12), the *KIE* for (C-H) stretch yields a value of 3.0. Proceeding similarly, *KIE* = 1.40 for CH_3 deformations, using ω_H = 1305 cm^{-1} (from CH_4) , ω_B = 1036 cm^{-1} (from CD_3H) and the decomposition temperature T = 580 K. This calculated value of *KIE* is very close to the experimental observed *KIE* of 1.35. It is therefore concluded that the CD_3 methyl group is distorted in the transition state. The structure of the transition state may not be represented as:

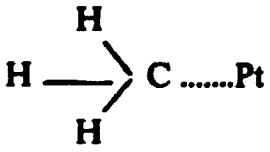

methyl group not distorted during Pt-C bond cleavage.

but could possibly be represented as:

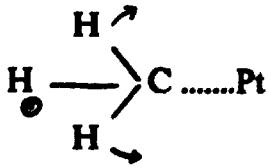

methyl group distorted or deformed during Pt-C bond cleavage.
the arrows emphasize the distortions in the methyl group.

3.5 Conclusion

The decomposition mechanism of *cis*-dimethyl platinum diisocyanide has7 been studied using FTIR. Isotope labelling studies and kinetic measurements were made. The complex loses methyl isocyanide in an initial reversible equilibrium step. Methane is the main volatile hydrocarbon product and is formed from the combination of a methyl platinum group and a hydrogen atom (from the cell wall).

The decomposition of *cis*-dimethyl platinum diisocyanide in the presence of hydrogen was more complex. Methane was formed again, by the combination of the methyl platinum group and a hydrogen atom from the added hydrogen gas. Ammonia was also identified as another volatile product. Ammonia appears to be formed from the hydrogenation of acetonitrile (acetonitrile was obtained from the isomerization of methyl isocyanide). The kinetics became more complex when H_2 was added. Surface reactions of the H_2 and CH_3CN with the platinum surface may be responsible for the complex kinetics.

CHAPTER 4

INTERACTION OF ACETONITRILE WITH PLATINUM(111)

4.1 Introduction

From our earlier studies of the decomposition of HPt in Chapter 3, it was shown that the evolution of methane was retarded in the presence of free methyl isocyanide. The methane arose exclusively from the methyl platinum group and so the first step in the decomposition of HPt involved a loss of the methyl isocyanide coordinated to the platinum atom in a reversible step.

Methyl isocyanide has a structural isomer, acetonitrile which is thermodynamically more stable and under the reaction conditions used in our gas phase work, methyl isocyanide isomerizes to acetonitrile.

The interaction of HPt with the growing platinum film is obviously an important aspect of the chemical vapour deposition of platinum using HPt as a precursor. However, considering what has been learned from the decomposition studies of HPt in Chapter 3 and the intended study of the interaction of HPt with Pt(111) described in Chapter 5, it was appropriate to learn more of the interaction of methyl isocyanide and acetonitrile with Pt(111). In this chapter, results of the

interaction of acetonitrile and Pt(111) are presented, and the methyl isocyanide interaction with Pt(111) is presented in Section 5.4.1 in the next chapter.

Acetonitrile has a β carbon and β hydrogens. Recently, β-hydrogen (hydrogen bonded to the carbon in a β position from the aluminum atom) in triisobutylaluminum have been shown to participate in its chemical decomposition.[1] Furthermore, there is evidence in the organometallic literature of agostic bonding (where no bonds are broken) involving the participation of carbon-hydrogen bonds as ligands. [2]

While we were particularly interested to look for the interaction of the C-H bond with Pt(111) in the CH_3CN/Pt(111) system, this system is interesting in itself. In the process of the investigations, we have also unveiled more properties of this system. CH_3CN has a nitrogen lone pair which may cause the molecule to bond end-on (terminally on metal surfaces). Most known organometallic complexes involving acetonitrile bond end-on. In addition, it has π electrons, which may cause it to bond side-on to the metal atom (parallel to the metal surface).

This system has also been studied by Sexton and Avery [3], using high resolution

---

[1] B. E. Bent, R. G. Nuzzo and L. H. Dubois, **J. Am. Chem. Soc.**, 111, 1989, 1634.

[2] M. Brookhart and M. L. Green, **J Organometall. Chem.**, 250, 1983, 395.

[3] B. A. Sexton and N. R. Avery, **Surf. Sci.**, 129, 1983, 21.

electron energy loss vibrational spectroscopy (HREELS), X-ray photoelectron spectroscopy (XPS), temperature programmed desorption (TPD) and work function change ($\Delta\phi$) measurements. They prepared the monolayer by annealing to 180 K to remove the multilayer. Their HREELS data showed a band at 1615 cm^{-1} which they ascribed to the ν(C=N) stretch. The XPS data showed the C 1s and N 1s binding energies at 284.6 and 397.2 eV respectively for this monolayer, large shifts (2.3 and 2.9) to lower binding energies from 286.9 and 400.1 eV for weakly adsorbed acetonitrile. This was consistent with the band at 1615 cm^{-1} (ν(C=N)) observed in HREELS. They proposed that the CN triple bond rehybridised to a double bond with both C and N atoms of the CN group bonded to the surface. They denoted this monolayer species, an η^2(C,N) state. [4] The CN bond had a significant contribution from impact scattering. Thus while establishing the η^2(C,N) state, it was not possible to determine from the HREELS data whether the CN bond axis was completely parallel to the surface or is slightly inclined. The desorption temperature for this monolayer was reported as 210 K.

Our investigations have proved fruitful in elucidating further properties of the η^2(C,N) state not previously reported. This state has intermolecular screening of each CH_3CN by other coadsorbed CH_3CN molecules. Similar effects have been seen in other coadsorption systems. [5] There is also evidence from IRRAS which favours a

---

[4] Supra footnote 3, chapter 4.

[5] H. Moritz and H. Lüth, **Vacuum**, 41, 1-3, 1990, 63.

parallel orientation. We provide evidence that the β-hydrogen in an unannealed CH_3CN submonolayer (prepared by adsorbing CH_3CN on Pt(111)), with desorption temperature 240 K, is involved in chemisorption. This observation has implications for the mechanism of dehydrogenation in the decomposition of *cis*-dimethyl platinum diisocyanide on clean platinum(111). Finally, we identify an adsorbed species with a CN dipole having a component perpendicular to the surface in an annealed submonolayer (prepared by annealing a multilayer). Both terminally and bridge bonded species are detected.

4.2 Experimental

The experiments were conducted in the previously described ultra high vacuum system equipped with temperature programmed desorption (TPD), work function measurements ($\Delta\phi$) and infrared reflection absorption spectroscopy (IRRAS). Base pressures of 1×10^{-10} torr were easily obtained. Acetonitrile was obtained commercially (BDH). It was subjected to several freeze-pump-thaw cycles before use. The Pt(111) crystal was cleaned by argon ion bombardment, annealing in 2×10^{-6} torr of oxygen at 1125 K and a high temperature flash in vacuum. The surface cleanliness and order were checked with Auger and LEED. Crystal dosing was achieved by backfilling the chamber. Exposures were reported in Langmuirs, L, where 1 L = 10^{-6} torr seconds, with uncorrected ion gauge readings.

Typical FTIR-RAS experiments employed 500 scans with a resolution of 8 cm^{-1}; noise levels were about 1×10^{-4} absorbance units (absorbance = $\log_{10}I/I_o$) at 3000

cm^{-1} where the globar source emissivity has a minimum and 5×10^{-5} absorbance units elsewhere. IRRAS is a single beam technique and a clean 110 K Pt(111) surface was used as reference.

Work function ($\Delta\phi$) measurements were made with a Kelvin probe of our own design. The end of this probe has a stainless steel reed with a molybdenum tip vibrating at 760 Hz. The reed could be positioned about 1mm above the crystal to form a vibrating capacitor. This vibration could be tracked using a phase-locked-loop. The current from the the vibrating capacitor goes into a lock-in-amplifier. The voltage applied to null the capacitor current measured the work function change.

TPD spectra was obtained with a differentially pumped 600 amu Hiden Analytical quadrupole mass spectrometer. The heating rate was 4 K/s.

4.3 Results

4.3.1 Temperature Programmed Desorption, TPD

Figure 4.1 presents TPD spectra of acetonitrile on Pt(111). The TPD spectra are all for mass 41, the molecular mass of acetonitrile. Spectrum 1 (1.6 L) shows only one peak at 220 K. With smaller exposures, the desorption temperature moves up (1 L = 230 K). From a qualitative analysis of the integrated area, this peak saturates at 1.6 L exposure. Spectrum 2 (5 L) shows two peaks. One has a

Figure 4.1 : TPD of CH_3CN on Pt(111) - coverage studies.

Spectrum 1 : 1.6 Langmuir exposure

Spectrum 2 : 5 Langmuir exposure

(Adsorption temperature = 110 K,

Ion mass = 41, Heating rate = 4 K/s).

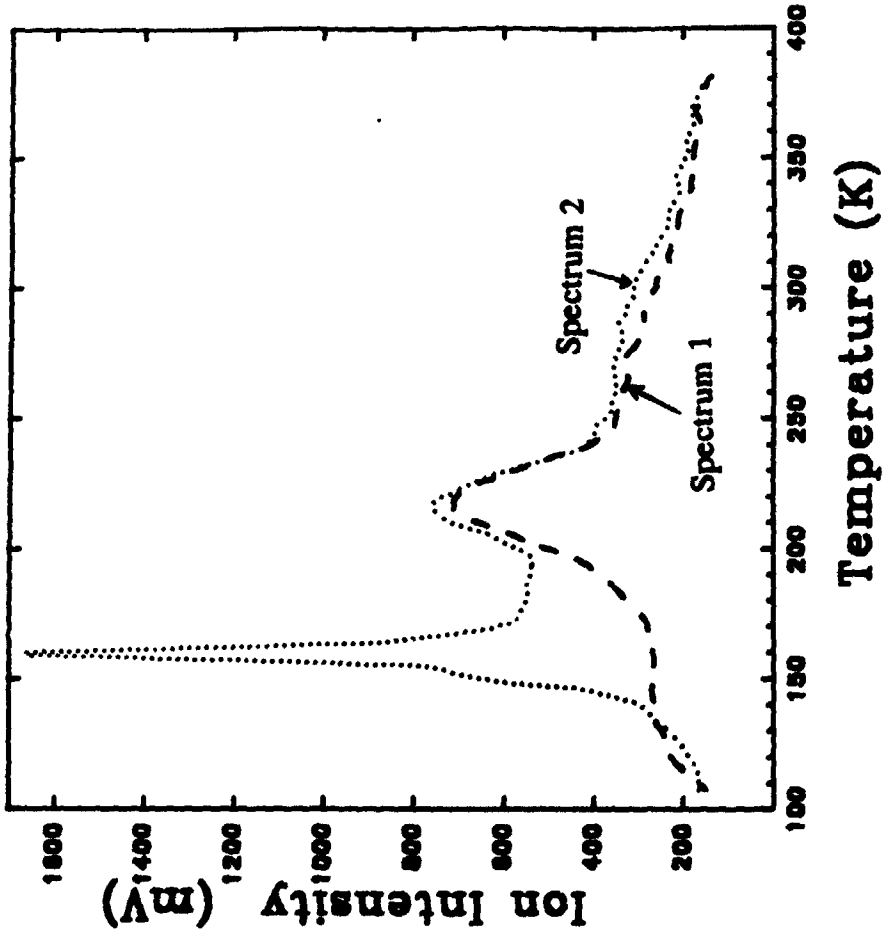
Ion Intensity (mV)
1800
1400
1200
1000
800
600
400
200
Temperature (K)
100
150
200
250
300
350
400
Spectrum 2
Spectrum 1

desorption temperature of 160 K and the higher temperature peak desorbs at a temperature of 220 K. With still higher exposures, the maximum of the low temperature peak shifts to 155 K. This peak is assigned as multilayer CH_3CN. The 220 K peak is therefore assigned to desorption of monolayer CH_3CN from Pt(111). No dissociation or reaction products were detected in TPD. Desorption of CH_3CN is molecular from the multilayer and monolayer coverages on Pt(111).

4.3.2 Work function change, $\Delta\phi$

Figure 4.2 presents the work function change as a function of acetonitrile exposure. Crystal temperature during deposition was 110 K. At about 2 Langmuirs, $\Delta\phi$ reaches a "plateau" value of -1.4 volts before the work function further decreases to a second limiting value of -1.5 volts at 4 Langmuirs. Concurrently, in TPD, a 4 Langmuir exposure shows the multilayer just beginning to grow. Thus the first plateau value of -1.4 volts is ascribed to the monolayer of acetonitrile and the multilayer is assigned a $\Delta\phi$ of -1.5 volts. When a multilayer of CH_3CN was annealed from 100 K to 600 K, the work function begins to rise at 145 K, reaches a saturation at 180 K before starting to rise again at 210 K, the desorption temperature of the monolayer. The steep rise eventually levels out and returns to a value close to that for the clean crystal. This agrees with the temperature desorption $\Delta\phi$ result obtained by Sexton and Avery. [6]

---

[6] Supra footnote 3, chapter 4.

Figure 4.2 : Work function change of CH_3CN on Pt(111) as exposure is increased

Monolayer saturates at -1.4 volts, multilayer at -1.5 V.

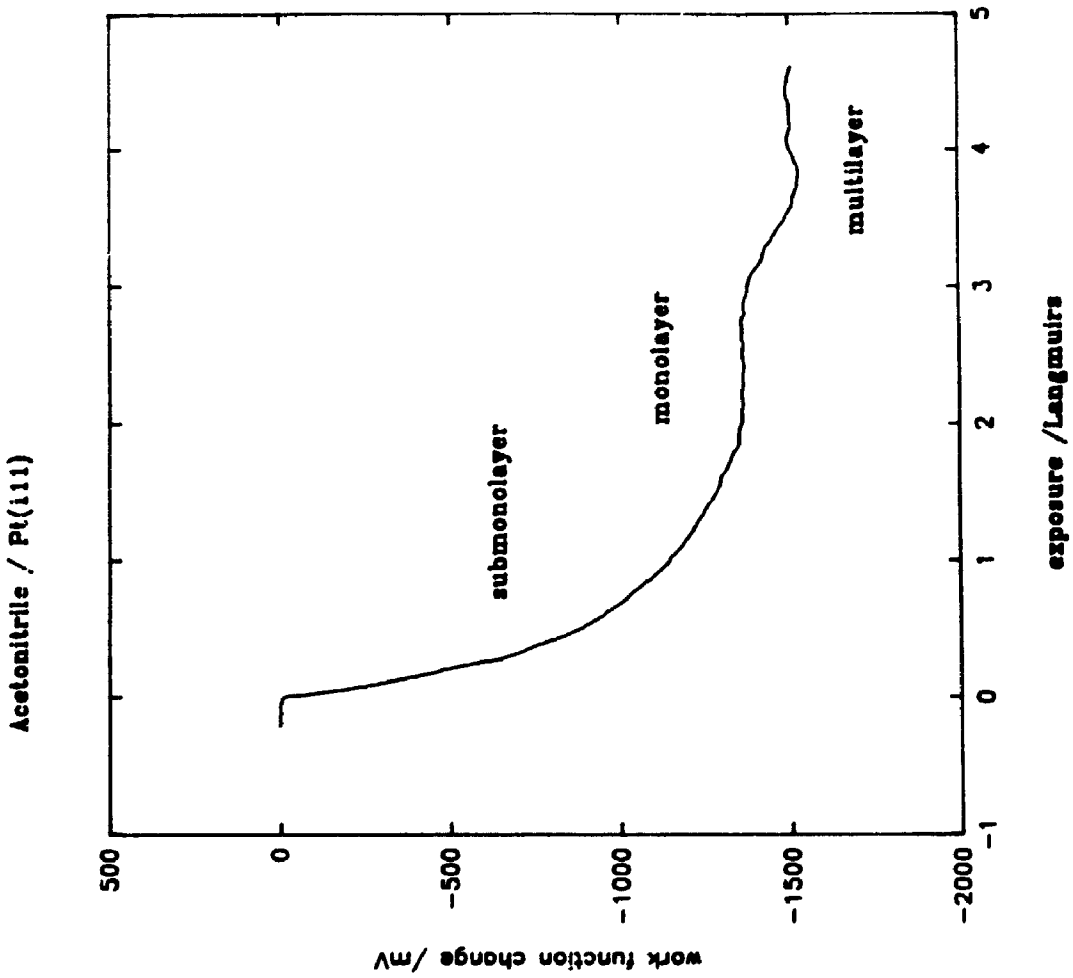
Acetonitrile / Pt(111)
work function change /mV
exposure /Langmuirs
submonolayer
monolayer
multilayer
500
0
-500
-1000
-1500
-2000
-1
0
1
2
3
4
5

4.3.3 Fourier Transform Infrared Reflection Absorption Spectroscopy, FTIR-RAS

Figure 4.3 shows FTIR-RAS data at 110 K for CH_3CN exposures of 0.5, 3, and 20 L. The 20 L FTIR-RAS (Figure 4.3, spectrum 3) is the CH_3CN multilayer on Pt(111) and is in good agreement with the gas phase spectrum. The major infrared bands appear in Table 4.1.

In their vibrational studies using HREELS, Sexton and Avery measured the spectrum of a monolayer prepared by annealing a multilayer film to 180 K. The desorption temperature of the monolayer was 210 K. [7] Using FTIR-RAS we have studied the submonolayer prepared by dosing the crystal with 0.5 L exposure ("unannealed" submonolayer; Figure 4.3, spectrum 1). The desorption temperature of the unannealed submonolayer is 230 K.

In the infrared spectra of submonolayer CH_3CN, the C≡N and C=N stretches (2200 and 1615 cm^{-1}, respectively) were below our detection limit of 5×10^{-5} absorbance units. As FTIR-RAS spectroscopy only measures a dynamic dipole moment which has a component normal to the surface, this implies the CN bond axis lies parallel to the surface. The asymmetric and symmetric C-H stretches occur at 2975 and 2910 cm^{-1}. The latter has a stronger intensity. These peaks show a 30 cm^{-1} red shift from the multilayer values. The band at 1038 cm^{-1} is assigned to a CH_3 rock and

---

[7] Supra footnote 3, chapter 4.

Figure 4.3 : FTIR-RAS of CH_3CN on Pt(111) - adsorption studies at 110 K.

(500 scans and 8 cm^{-1} resolution).

Spectrum 1 : Unannealed submonolayer (0.5 L). Absorbance scale shown for this spectrum; relative sensitivity = 1.

Spectrum 2 : Unannealed monolayer (3 L)

Spectrum 3 : Multilayer (20 L)

Note: The number to the left of each spectrum accompanied by a *, are the factors by which the displayed spectrum should be multiplied to compare with spectrum 1.

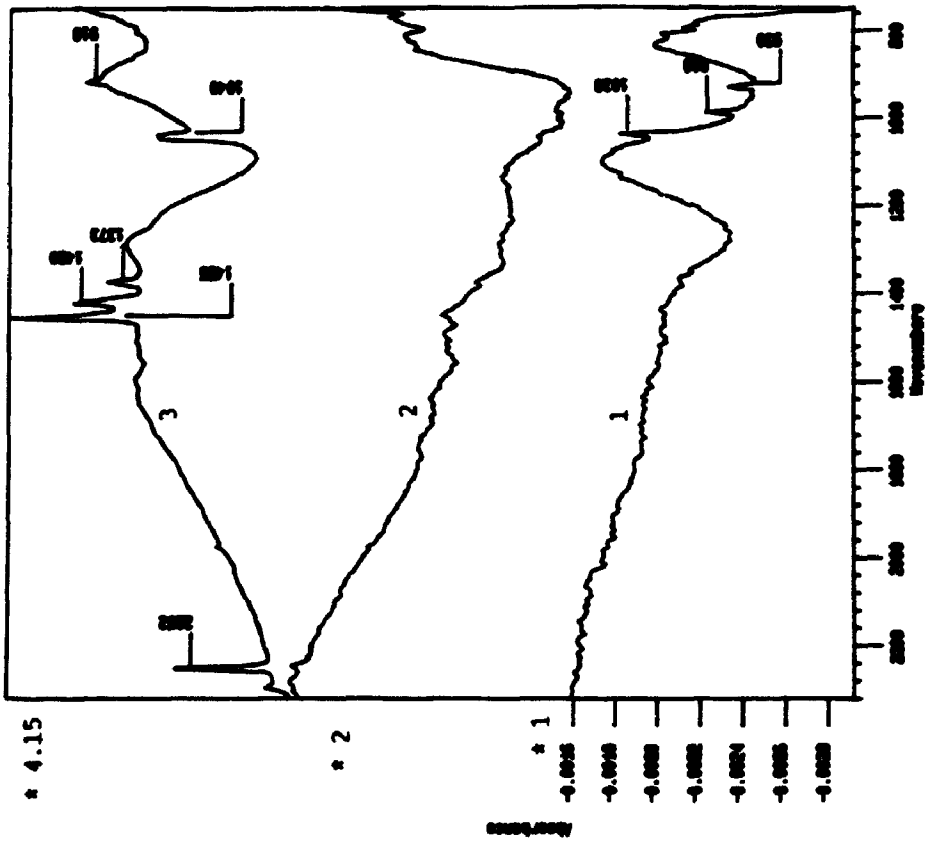
* 4.15
* 2
* 1
3
2
1

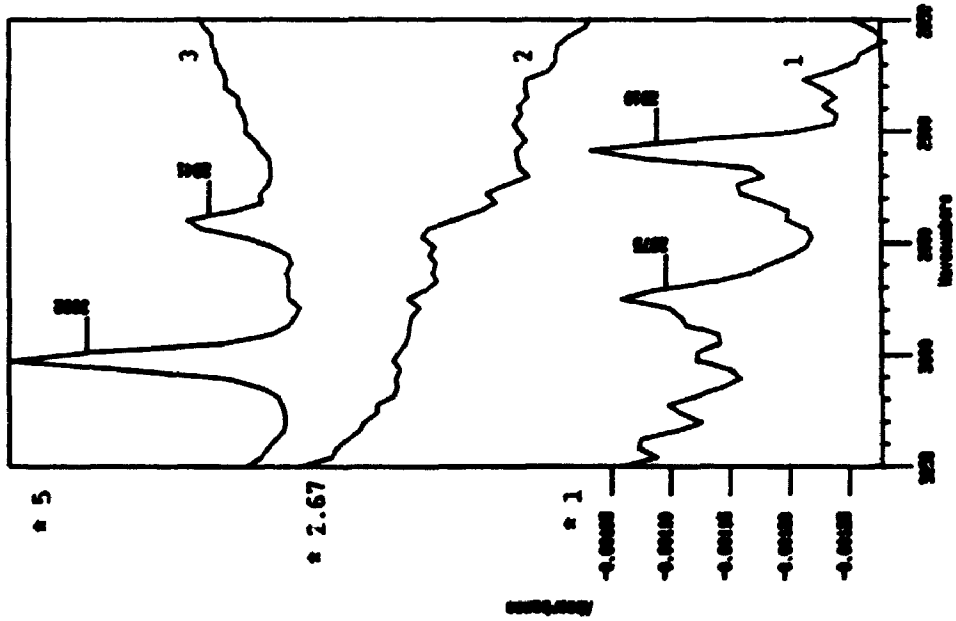
* 5
* 2.67
* 1
3
2
1

Table 4.1

Infrared frequencies of CH_3CN on Pt(111)

	Vapour (IR)	Multilayer FTIRRAS	Monolayer HREELS	Unannealed sub-monolayer FTIRRAS	Annealed sub-monolayer FTIRRAS
$\nu_{as}(CH)$	3009	3002	3005	2975	
$\nu_s(CH)$	2954	2941	2960	2910	
$\nu(CN)$	2268	2252	1615		2236, 1820
$\delta_{as}(CH_3)$	1454	1455, 1420	1435		
$\delta_s(CH_3)$	1389	1373	1375		
$\rho_r(CH_3)$	1041	1040	1060	1038	
$\nu(C\text{-}C)$	920	918	950	930	
Not Assigned				988	

the band at 930 cm^{-1} is the C-C stretch. Surprisingly, the $\delta(CH_3)$ bands lie below our detection limit. There is a new band at 988 cm^{-1} which is not present in the multilayer spectrum. It is unlikely that this is due to the Pt-C or Pt-N stretches as these modes lie below 500 cm^{-1}, beyond the limit of our narrow band MCT detector. The assignments of the FTIR-RAS infrared bands in the submonolayer to the various vibrational modes were based on the multilayer and gas phase spectra because the band positions in the submonolayer spectra occur near those in the multilayer spectra.

The 3 L FTIR-RAS spectrum ("unannealed" monolayer; Figure 4.3, spectrum 2) shows a decrease in the infrared intensity of the bands at 2975, 2910, 1038, 988 and 930 cm^{-1} present in the unannealed submonolayer. The $\nu(C{=}N)$ stretches were again below the detection limit for the monolayer while the $\nu(C{\equiv}N)$ stretch is beginning to be observed. With exposures larger than 5 L, the multilayer peaks described previously grow in. This is consistent with our previous TPD assignment of multilayer formation with exposures of greater than 4 Langmuirs.

Sexton and Avery reported spectral resolution of 50 cm^{-1} or more for their HREELS data. The HREELS spectrum in the $\delta(CH_3)$ infrared band region of the multilayer only showed a single peak at 1430 cm^{-1}. [8] However, the FTIR-RAS spectrum of the multilayer (Figure 4.3, spectrum 3) described here clearly shows that

[8] Supra footnote 3, chapter 4.

the degeneracy of the $\delta_{as}(CH_3)$ bends in the gas phase have been lifted in the adsorbed phase. This may be due to some intermolecular interaction in the multilayer at

110 K.

Figure 4.4 shows FTIR-RAS spectra of different coverages obtained by step-wise annealing of a multilayer film. As before, the multilayer FTIR-RAS (Figure 4.4, spectrum 1) was obtained by dosing the crystal at 110 K. On annealing past the desorption temperature (160 K) of the multilayer to 163 K (Figure 4.4, spectrum 2), the C≡N stretch, and the CH_3 bends all decrease below detection limit. The C-C stretch and CH_3 rock have diminished intensity. The C-H stretches appear to be an overlap of two sets of stretches, making it difficult to observe.

Subsequently, the crystal was annealed to near the desorption temperature of the monolayer and held for 1 minute at 213 K to allow some of the monolayer acetonitrile to desorb ("annealed" submonolayer). The temperature was reset to 110 K for FTIR-RAS measurement (Figure 4.4, spectrum 3). Surprisingly, we observed an infrared band in the C≡N stretch region at 2236 cm^{-1}, red shifted from the multilayer value by 17 cm^{-1}. In addition, we observe another band at 1920 cm^{-1}. On further annealing to 223 K (Figure 4.4, spectrum 4), the spectrum basically remained unchanged and the CH_3 rock and C-C stretch were no longer detected. This new adsorbed species must certainly have a C≡N dipole moment with a non zero normal

Figure 4.4: FTIR-RAS of CH_3CN on Pt(111) --desorption studies

(500 scans and 8 cm^{-1} resolution)

Spectrum 1 : Multilayer (110 K)

Spectrum 2 : Annealed monolayer (163 K)

Spectrum 3 : Annealed submonolayer (213 K)

Spectrum 4 : Annealed submonolayer (223 K). Absorbance scale shown for this spectrum; relative sensitivity = 1.

Note: The numbers to the left of each figure panel accompanied by a *, are the factors by which each spectrum (in order from the bottom of the figure) should be multiplied to compare with spectrum 4.

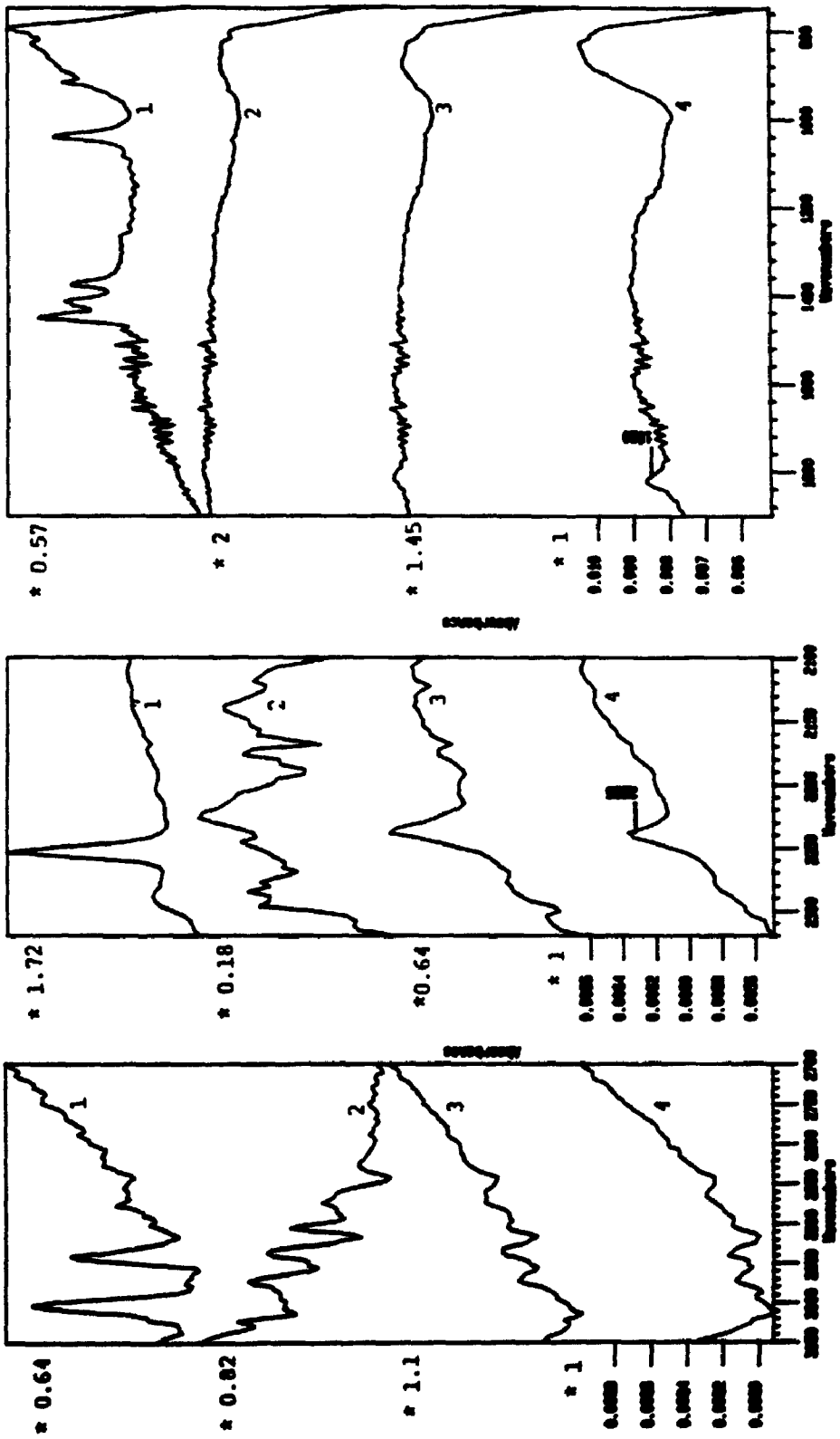
* 0.57
* 2
* 1.45
* 1
* 1.72
* 0.18
*0.64
* 1
* 0.64
* 0.82
* 1.1
* 1
1
2
3
4

component to the surface. The CH stretches are again poorly resolved and the spectra do not permit detailed interpretation.

4.4 Discussion

The unannealed submonolayer has been shown to exhibit interesting FTIR-RAS features. The red shift of 30 cm^{-1} for the C-H stretches plus the absence of any infrared bands in the CH_3 bend region indicates that the methyl group is not a freely vibrating entity. The interaction of acetonitrile with the Pt(111) surface for this layer must therefore extend beyond the CN group, and appears to involve the methyl group as well.

HREELS data for the annealed monolayer on Pt(111) show the asymmetric and symmetric C-H stretches to be in agreement with the gas phase values as are the CH_3 bends. The major feature in the HREELS data is the appearance of ν(C=N) stretch which is assigned to a C=N lying parallel to the surface in an η^2(C,N) structure. The methyl group in this η^2(C,N) structure appears to be freely vibrating as the band positions for the ν_{as}(C-H), ν_s(C-H) and $\delta(CH_3)$ agree with those in the gas phase. It is unfortunate that the infrared bands in the unannealed CH_3CN monolayer have reduced intensity. The C-H stretches are hardly detectable.

The unannealed submonolayer appears to be adsorbed with the CN axis parallel to the surface. However, its methyl group seems to be involved in

chemisorption as well. We therefore distinguish this state as an η^{2*}(C,N) structure, where the * refers to the involvement of the methyl group in chemisorption.

The acetonitrile molecule has an α and β carbon, where α and β denote successive positions away from the nitrogen atom. The hydrogen atom attached to the β carbon denoted as a β-hydrogen has been shown to participate in chemical reactions. In the surface reactions of triisobutylaluminum with Al(111), the β-hydrogen coordinates to the empty orbitals of the aluminum surface, resulting in a β-hydride elimination. [9]

We have no evidence of decomposition of CH_3CN in TPD experiments and propose that the β-hydrogen is involved in agostic bonding to the metal surface. Agostic bonding (where no bonds are broken) is found in reactions in organometallic chemistry. [10] The electron pair on the C-H bond coordinates to a site on the metal atom. The bonding results in a longer C-H bond distance. The stronger the interaction the more red shifted the stretches will be. 400 to 500 cm^{-1} shifts have been reported in organometallic complexes. This may in part explain the 30 cm^{-1} red shift of the C-H stretches in our FTIR-RAS experiments. Furthermore the same interaction will remove the CH_3 bends and only a CH_2 scissor mode would be expected. However, the scissor mode is not observed and may mean that two or all

[9] Supra footnote 1, chapter 4.

[10] Supra footnote 2, chapter 4.

three β-hydrogens may be involved. The observation of the $\rho_r CH_3$ rock at 1038 cm^{-1} and the ν(C-C) single bond stretch at 930 cm^{-1} in FTIR-RAS plus the absence of decomposition products in TPD provides further support for the idea that the methyl group still stays singly bonded to the C≡N group during π bonding via the CN group and agostic bonding via the electron pair of the C-H group.

The HREELS of the annealed monolayer shows the C-H stretches and CH_3 bends in good agreement with those in the gas phase infrared spectrum. In the light of the discussion on the unannealed submonolayer, it appears that the β-hydrogen is relieved of its participation in chemisorption when the submonolayer becomes a monolayer. This displacement of the agostic hydrogen from its agostic site by another donor group is not unexpected in organometallic chemistry.[11] The η^{2*}(C,N) clearly will bond to more sites per molecule than the η^2(C,N), as the β hydrogens agostically bond to the surface. When more acetonitrile is adsorbed on the surface, the β-hydrogen may be displaced from their bonding site on the surface by the CN donor group and the methyl group recovers as a fully vibrating entity.

The FTIR-RAS of the 1.5, 2 and 3 Langmuir exposures show a decrease in the infrared band intensities of all bands in the unannealed submonolayer (0.5 L). This observation is counter intuitive as closer packing of the acetonitrile molecules should result in an increase of the perpendicular component of the dipole and hence

---

[11] Supra footnote 2, chapter 4.

larger intensities in a FTIR-RAS spectrum. The decrease in intensities is probably due to a screening of the dynamic dipoles as coverage is increased. Moritz and Lüth have shown in their coadsorption system of CO/CH_3CN on Pt(111) that the coadsorbed acetonitrile is able to screen the strong dynamic dipole of CO because of polarization effects. [12] They showed that the CO was not removed by coadsorption of CH_3CN as the CO signal could be recovered by annealing the crystal to 300 K to desorb the acetonitrile.

Our FTIR-RAS adsorption studies of acetonitrile on Pt(111) are consistent with Lüth's conclusions. However, it appears that each acetonitrile molecule can screen the dipoles in neighbouring acetonitrile molecules. Avery and Matheson have also attributed the absence of a ν(C-N) and CNC bending band in a related molecule, methyl isocyanide monolayer to a reduction in the dynamic dipole moment caused by polarization effects. [13] It is also noted that no $\nu(C\equiv N)$ or $\nu(C=N)$ stretches could be observed in the unannealed CH_3CN monolayer. This is consistent with CN bond lying parallel to the surface in the monolayer.

The FTIR-RAS result for an unannealed monolayer (2 and 3 Langmuir) is consistent with the HREELS data. [14] This is because in HREELS, vibrations can

---

[12] Supra footnote 4, chapter 4.

[13] N.R. Avery and T. W. Matheson. **Surf. Sci.**, 143, (1984), 110.

[14] Supra footnote 3, chapter 4.

be observed due to impact scattering whereas FTIR-RAS only measures the normal component of a dynamic dipole moment.

Warming a multilayer to 213 K (desorption temperature of monolayer is 210 K) and holding this temperature for one minute, gave an annealed submonolayer with quite different FTIR-RAS features from that obtained directly with a 0.5 L exposure (unannealed submonolayer). Further warming to 223 K for one minute, did not change the spectrum. The interesting features are bands at 2236 and at 1820 cm^{-1}. By analogy with CO adsorption on Pt(111), we believe they represent terminal and bridge bonded (CN) species, respectively. Both terminally and bridge bonded methyl isocyanide, CH_3NC, have been observed by Avery and Matheson. [15] However, the high activation barrier for isomerization of CH_3CN to CH_3NC makes the formation of terminally and bridge bonded CH_3NC unlikely in the present experiment. Further, methyl isocyanide does not desorb molecularly [16] ,in contrast to our present findings on CH_3CN. We conclude that these infrared bands represent terminal and bridge bonded CH_3CN, bonded to the surface through the N atom. The carbon atom in the terminally bonded species is sp hybridized with the CH stretches vibrating symmetrically about the molecular axis, which is also the symmetry axis. The carbon in the bridged species is sp^2 hybridized and the CH stretches are vibrating about the symmetry plane, formed by CCN atoms. This may partly explain the poorly resolved

---

[15] Supra footnote 13, chapter 4.

[16] Supra footnote 13, chapter 4.

CH stretches in the 2800 to 3000 cm^{-1} region.

To summarize, on initial adsorption, there are few acetonitrile molecules with few donor CN groups, allowing agostic bonding to occur and each molecule adopts an η^{2*}(C,N) bonding configuration. With the addition of more acetonitrile, there are more CN donor groups, and the β-hydrogen is relieved of its participation in chemisorption. The acetonitrile then adopts the η^2(C,N) structure in the monolayer. With higher exposures the multilayer grows in. As the crystal is annealed, the multilayer is removed and the η^2(C,N) monolayer is left. On further annealing the CH_3CN adopts both terminal- and bridged- nitrogen bonding configurations. Molecular acetonitrile is recovered upon desorption. TPD data show a shift of the peak temperature for the monolayer to lower temperature with increased coverage. The monolayer peak shapes are symmetrical. In the light of the discussion regarding agostic bonding and terminally and bridged bonded CH_3CN, it appears that the desorption may be a first order process in acetonitrile with an activation energy which varies with coverage.

4.5 Conclusions

In studying the interaction of acetonitrile with Pt(111), we have used temperature programmed desorption, work function measurements and infrared reflection absorption spectroscopy. We have shown that the η^2(C,N) state can have intermolecular screening of its dynamic dipole moments, resulting in a reduction in

the intensities of the infrared band intensities. However, the major findings of this work pertain to the submonolayer of acetonitrile on Pt(111). The properties of the submonolayer have been shown to depend on how the submonolayer was prepared. In an "unannealed" submonolayer, the layer adopts an η^{2*}(C,N) bonding configuration, where the CN vector lies parallel to the surface and the β-hydrogens are also involved in chemisorption. In an "annealed" submonolayer, the layer adopts a different bonding configuration, with both terminal and bridge bonded CH_3CN on the surface.

CHAPTER 5

INTERACTION OF *CIS*-DIMETHYL PLATINUM DIISOCYANIDE WITH PLATINUM (111) AND PLATINUM (111)-C SURFACES

5.1 Introduction

The pressure in the chemical vapour deposition reactor may be varied over a few orders of magnitude. At high pressures, the chemical decomposition reactions are probably a combination of molecule-molecule and molecule-surface interactions. In contrast, under ultra high vacuum conditions the important reactions are the molecule-surface interactions.

Deposition of platinum on a substrate using HPt will involve the interaction of HPt with the surface of the substrate. However, after the first layer of platinum atoms have been deposited on the substrate, the flux of HPt will interact with a platinum surface.

The platinum film deposited from the decomposition of the organometallic precursor could be amorphous, microcrystalline or polycrystalline in structure. Grain sizes of 500 - 2000 Å have been observed, with carbon impurity from 4 - 34 atom %. [1] In brief, it is very poorly characterised. To simplify the problem, a Pt(111) surface

[1] N. H. Dryden, R. Kumar, E. Ou, M. Rashill, S. Roy, P. R. Norton, R. J. Puddephatt and J. D. Scott, **Chem. Mater.**, 3 (1991), 677 - 685.

was chosen. A Pt(111) surface is a well ordered surface (bulk platinum has a face centered cubic (f.c.c.) structure). Pt(111) can also be easily cleaned by sputtering and heating in oxygen, followed by heating in vacuum. Furthermore there are no known surface reconstructions for this surface.

This chapter studies the interaction of *cis*-dimethyl platinum diisocyanide with Pt(111). In chapter 1, it was shown that carbon was left behind in the platinum films from the decomposition of *cis*-dimethyl platinum diisocyanide. Hence, in this chapter we focus on the molecule-surface interactions and how they change as a highly reactive Pt(111) is gradually passivated by deliberate incorporation of carbon onto the surface. Indeed the interactions were found to change as the surface reactivity was gradually turned off. However, carbon contamination did not immediately passivate the surface and monolayer adsorption was found for a surface with some surface carbon. In contrast, dissociative chemisorption was observed on a highly reactive clean Pt(111) surface.

It is also demonstrated that the complex could be successfully transported from its reservoir, down the doser tube, out through the microcapillary array and onto the crystal surface without suffering prior decomposition in the doser.

To facilitate the assignment of infrared bands in the FTIR-RAS study of the precursor, CH_3NC and adsorption on Pt(111) was also studied. CH_3CN adsorption

on Pt(111) was uescribed in chapter 4.

5.2 Experimental

The experiments were conducted in an ultra high vacuum chamber. The crystal was an 8×14 mm Pt(111) crystal approximately 3 mm thick. X-ray Laue methods were used to orientate the (111) plane and the crystal was cut from the boule and polished accordingly. A chromel alumel thermocouple was spot welded to the back surface (unpolished) of the crystal for measurement of its temperature.

The main techniques used in this investigation were Fourier transform infrared reflection absorption spectroscopy (FTIR-RAS), temperature programmed desorption (TPD) and measurement of work function changes ($\Delta\phi$).

The FTIR-RAS experiment typically used 500 scans and a resolution of 8 cm^{-1}. The present method is a single beam technique, so a single beam spectrum of the clean crystal is first recorded, followed by acquisition of a single beam spectrum of the adsorbed molecule on the surface. Accordingly, when studying the interaction of HPt with Pt(111) surface with surface carbon, the absorbance spectrum is referenced to a single beam spectrum of the Pt(111) surface with surface carbon. Signal to noise was about 1×10^{-4} absorbance units for 500 scans (0.01 %). It took about 2 to 3 minutes to record a spectrum.

The TPD experiment involved ramping the crystal temperature at a fixed heating rate of 7 K/s and multiplexing the mass spectrometer to collect the mass fragments desorbing from the crystal.

The work function change was measured using a homebuilt Kelvin probe. Briefly this is a vibrating capacitor, with the crystal forming one plate of the capacitor. The voltage applied to null the current is a measure of the work function change.

The *cis*-$(CH_3)_2Pt(CNMe)_2$ precursor HPt and its deuterated analogues DPt, D'Pt and $D_{12}Pt$ were synthesized in Prof. R.J. Puddephatt's laboratory and sublimed twice in a vacuum line before being loaded into the reservoir. The complex was heated to sublimed it from the solid state into the gas phase. Each time before dosing the crystal, the vapour of the precursor was pumped out through a 150 l/s turbomolecular pump for 30 seconds so that only *freshly* sublimed precursor was beamed onto the crystal. Exposures were reported in Langmuir, using uncorrected ion gauge pressures which measure the total residual pressure in the chamber. The complex is introduced into the chamber via a microcapillary array, which preferentially doses the crystal without dosing the other parts of the chamber. While this arrangement reduces contamination of the chamber by the organometallic precursor, we have a poor estimate of the actual exposure and coverage of the complex on the surface. In future, serious quantitative work may be done with the

aid of an oscillating quartz microbalance. This device may be placed in front of the capillary array and the mass increase may be monitored by following the decrease in the frequency of the quartz microbalance. The number of molecules actually deposited onto the crystal may be accurately determined.

From the vapour pressure curve, it is estimated that the precursor vapour pressure at 100 °C is about 0.046 torr. This reservoir temperature is maintained at 100 °C to avoid decomposition of the complex. Contamination from residual gas in the doser is shown in the calculation below. The pressure of the residual gases can be found from the combined gas law in equation (5.1),

$$\frac{P_1V}{T_1} = \frac{P_2V}{T_2} \qquad (5.1)$$

where P_1 is the base pressure at 370 K; P_2 is the base pressure at 300 K in the reservoir and gas manifold, which is equal to 1×10^{-7} torr and V is the volume of the reservoir and gas manifold. Then, the contamination of the complex due to the residual gases is,

$$(1.23\times10^{-7})/0.046 \times 100\% = 2.68\times10^{-4}\ \%$$

Methyl isocyanide was also synthesized in Prof. Puddephatt's laboratory and freezed-pumped-thawed three times before use. When not in use it was stored in a refrigerator. The methyl isocyanide was introduced into the chamber by backfilling

in these experiments. Exposures are reported in Langmuirs, using uncorrected ion gauge readings.

The crystal was cleaned by argon sputtering, followed by heating in oxygen at 1×10^{-6} torr of oxygen at 1123 K for half hour. This was followed with further heating in 7×10^{-7} torr oxygen at 1375 K for a further half hour. This was followed by a high temperature flash to 1375 K. Surface cleanliness was checked with Auger spectroscopy.

The Pt(111) surface was passivated by heating in acetylene, at a pressure of 5×10^{-6} torr, at 800 °C for 2 hours, hereafter referred to as Pt(111)-C(ΔC_2H_2). The graphitic rings were observed with LEED and the Pt(111) substrate spots were not observed.

5.3 Results:

5.3.1 Coverage Studies of CH_3NC on Pt(111)

a. Adsorption - FTIR-RAS

Figure 5.1 shows FTIR-RAS spectra of CH_3NC/Pt(111) in the spectral ranges of 3100 - 2800, 2300 - 2120, 1900 - 1650, 1520 - 1370. Spectra 1 to 3 in this figure show FTIR-RAS spectra of CH_3NC with increasing coverage. Spectrum 1 shows a 0.45 L exposure of methyl isocyanide. A band at 2234 cm^{-1} is observed with very weak C-H stretch intensities at 3000 cm^{-1}. The band 2234 cm^{-1} is assigned to a C≡N

Figure 5.1 : FTIR-RAS spectra of CH_3NC/Pt(111) in the spectral ranges of 3100 - 2800, 2300 - 2120, 1900 - 1650, 1520 - 1370 cm^{-1}.

Spectrum 1 : 0.45 L CH_3NC/Pt(111), T_{ads} = 110 K

Spectrum 2 : 0.75 L CH_3NC/Pt(111), T_{ads} = 110 K

Spectrum 3 : 7.7 L CH_3NC/Pt(111), T_{ads} = 110 K

Note: The number to the side of each spectrum accompanied by a "×", are the factors by which the displayed spectrum should be multiplied to compare with spectrum 1.

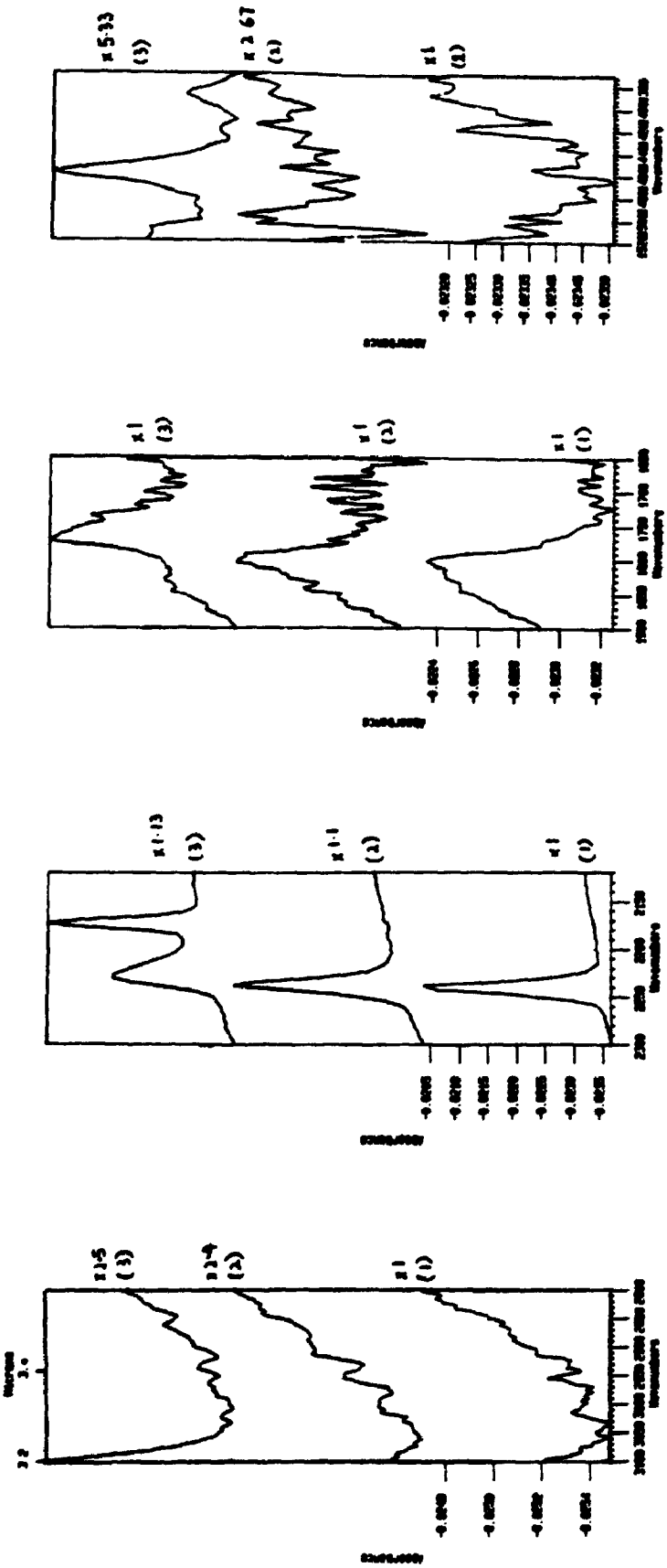

stretching frequency. Spectrum 2 shows a 0.75 L exposure and the CH_3 deformations are now observed at 1300 cm^{-1}. In addition, a band at around 1800 cm^{-1} is observed. Increasing the exposure to 1.7 L , we observe another $\nu(C\equiv N)$ stretch at 2160 cm^{-1} beginning to grow in. This band grows in with coverage and cannot be saturated while the first band is already saturated at 0.5 L. The band at 2234 cm^{-1} is assigned to a C≡N stretch of a methyl isocyanide ligand terminally bonded to the platinum surface. Similarly, the band at 1800 cm^{-1} which also saturates at 0.5 L exposure, is assigned to a bridged bonded methyl isocyanide on Pt(111). Spectrum 3 shows a 7.7 L exposure. The intensities of the CN stretches due to the terminal and bridged bonded species are clearly saturated, whereas the C≡N stretch (2160 cm^{-1}), methyl deformation (1400 cm^{-1}) and C-N stretch (900 cm^{-1} , not displayed) have increased with coverage. The increase in intensities of all these bands is due to the growth of multilayer CH_3NC on platinum (111).

5.3.2 Coverage Studies of *cis*-dimethyl platinum diisocyanide on passivated Pt(111) surface

a. Adsorption - FTIR-RAS

Figure 5.2 shows FTIR-RAS of *cis*-dimethyl platinum diisocyanide on a passivated surface in the spectral ranges of 3020 -2750, 2250 - 2000, 1850 - 1000, and 930 - 830 cm^{-1}.

Spectrum 1 shows a 2.5 L exposure of HPt/Pt(111)-C(ΔC_2H_2). The CN

Figure 5.2 : FTIR-RAS of *cis*-dimethyl platinum diisocyanide on a passivated surface in the spectral ranges of 3020 -2750, 2250 - 2000, 1850 - 1000, and 930 - 830 cm^{-1}. (T_{ads} = 110 K)

Spectrum 1 : 2.5 L HPt/Pt(111)-C(ΔC_2H_2).

Spectrum 2 : 4.5 L HPt/Pt(111)-C(ΔC_2H_2).

Spectrum 3 : 7 L HPt/Pt(111)-p(2×2)-O.

Spectrum 4 : 7.2 L HPt/Pt(111)-C(ΔC_2H_2).

Spectrum 5 : 4.5 L D'Pt/Pt(111)-C(ΔC_2H_2).

Note: The number to the side of each spectrum accompanied by a "×", are the factors by which the displayed spectrum should be multiplied to compare with spectrum 1.

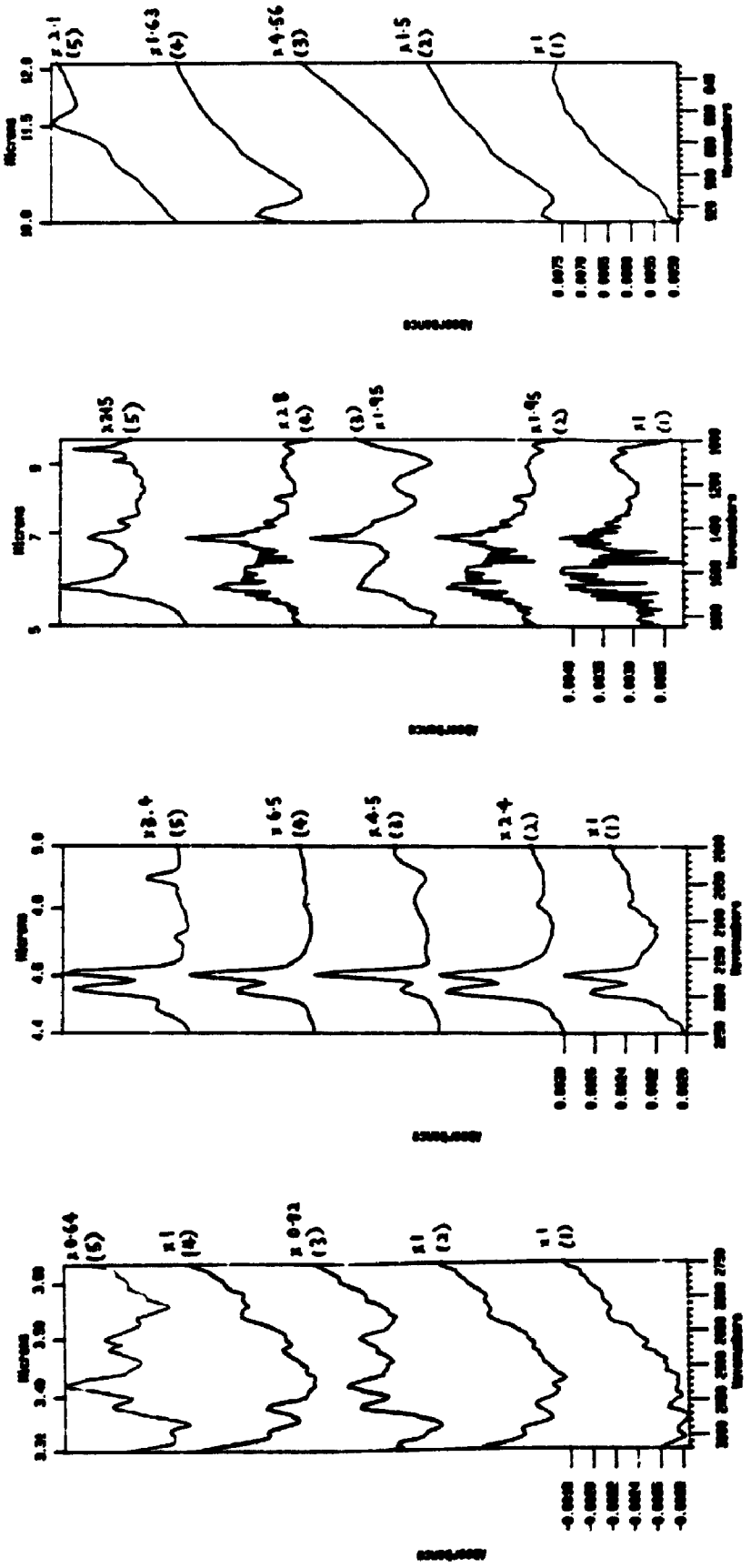

doublet is clearly seen and agrees well with the gas phase values. There is a slight decrease in energy to 2190 and 2170 cm^{-1} respectively for the asymmetric and symmetric C≡N stretches. The separation of 20 cm^{-1} is consistent with that in the gas phase.

Spectrum 2 shows a 4.5 L exposure of HPt/Pt(111)-C(ΔC_2H_2); a C-H rock at 1050 cm^{-1} , a symmetric and asymmetric CH_3 deformation is seen at 1300 and 1450 cm^{-1} respectively. Furthermore, a peak at 1650 cm^{-1} is observed which was not observed in the gas phase spectrum. As the surface is fully passivated this peak could only arise from weak interaction of the complex with the graphitic surface. This is in contrast to the bridged CH_3NC on Pt(111) (band occurs at 1800 cm^{-1}). The C-H stretches are observed, though they do not resemble the C-H stretch triplet in the gas phase spectra.

Pt(111)-p(2×2)-O was prepared by cooling the Pt(111) crystal to 110 K in O_2 at 6.4×10^{-7} torr. The HPt, organometallic complex was subsequently condensed on top of the oxygen layer. The FTIR-RAS spectrum of 7 L HPt using the reflectance from Pt(111)-p(2×2)-O as reference is shown in Spectrum 3.

The C-H triplet stretch is observed with the 2 lower energy peaks 66 cm^{-1} apart as compared to 68 cm^{-1} in the gas phase spectrum, while the higher energy pair of peaks is 35 cm^{-1} apart compared to 43 cm^{-1}. The C-H triplet stretch is however

blue shifted by 40 cm^{-1}. The separation of $\nu_{as}(C\equiv N)$ and $\nu_{s}(C\equiv N)$ stretches of the C≡N doublet in the multilayer HPt on Pt(111)-p(2×2)-O is the same as that in the gas phase spectrum and equal to 20 cm^{-1}. The CH_3 bend at 1451 (1423 in gas IR) cm^{-1} and the C-N stretch at 925 cm^{-1} (973 cm^{-1} in gas IR) are clearly visible.

Spectrum 4 is a 7.2 L HPt/Pt(111)-C(ΔC_2H_2) and the C-N stretch at 925 cm^{-1} is clearly observed.

Spectrum 5 shows a 4.5 L exposure of $(CH_3)_2Pt(CD_3NC)_2$, (D'Pt) on Pt(111)-C(ΔC_2H_2). The six hydrogens on the ligand have been deuterated. New peaks at 2115, 1100, 1060 and 865 cm^{-1} are observed. The band at 1300 cm^{-1} is no longer observed. The band at 2115 cm^{-1} and 865 cm^{-1} are assigned to the ν(C-D) stretch and C-D rock respectively. The band at 1100 cm^{-1} is assigned to a asymmetric CD_3 ligand deformations. The band at 1060 cm^{-1} is assigned to the symmetric CD_3 ligand deformation.

b. After Annealing - FTIR-RAS

When the multilayer D'Pt on Pt(111)-C(ΔC_2H_2) was annealed to 180 K, all of the infrared bands observed at 110 K were reduced beyond detection. Further anneal to high temperatures did not change the spectra. This is consistent with the TPD data described below.

c. Adsorption - TPD

TPD spectra of increasing exposures of HPt on Pt(111)-C(ΔC_2H_2) were obtained. The m/e 15, 27 and 41 were observed at about 150 K. Figure 5.3 is a 0.7 L exposure of HPt on Pt(111)-C(ΔC_2H_2). No high temperature desorption peak was observed. Figure 5.4 shows a TPD of multilayer HPt on Pt(111)-C(ΔC_2H_2) for masses 207 and 292. Other signals that were multiplexed were 195, 199, 207, 250, 251, 235, 236, 293, 277 and 278. No desorption of these masses was detected. The multiplier voltage was 2200 volts. However only m/e 207 was detected at about 190 K. Even so, the signal to noise was extremely poor. The difficulty of detecting these high masses is due to fragmentation, the poorer transmission of high mass fragments in a quadrupole instrument and the very low effective pressure in a TPD experiment. In addition to these factors, the stainless steel snout enclosing the mass spectrometer probably behaves like a pump and the HPt is adsorbed on the surface where it suffers decomposition with subsequent deposition of platinum on the walls of the stainless steel snout.

Figure 5.3 : TPD of 0.7 L exposure of HPt on Pt(111)-C(ΔC_2H_2).

Multilpier Voltage is 1800 V

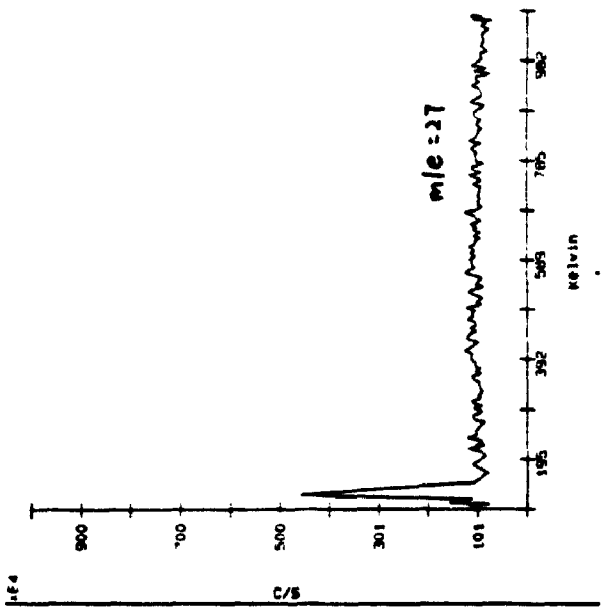
m/e = 27
C/S
Kelvin

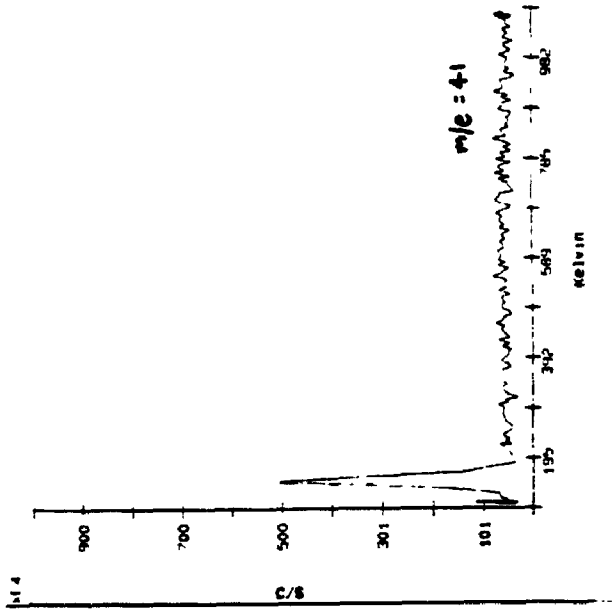
m/e = 41
C/S
Kelvin

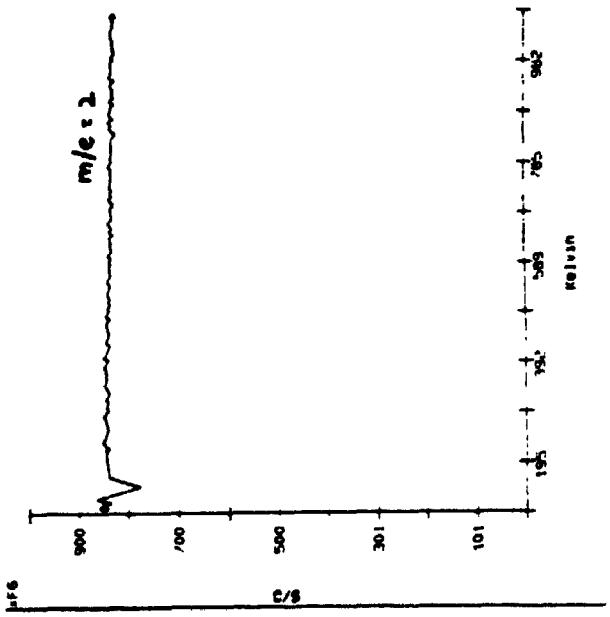
m/e = 2
C/S
Kelvin

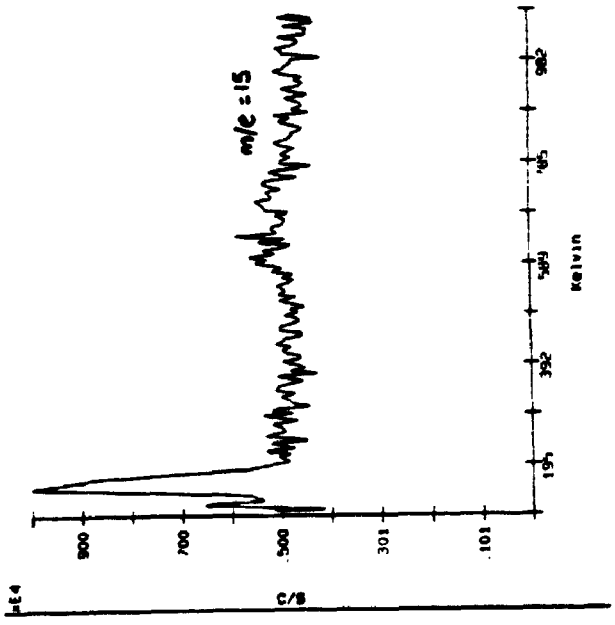
m/e = 15
C/S
Kelvin

Figure 5.4 · TPD of multilayer HPt on Pt(111)-C(ΔC_2H_2) for high masses.

m/e = 207 corresponds to a Pt-C fragment.

m/e = 292 is the largest mass frequent detected with a magnetic sector instrument (MAT 8320).

Multiplier Voltage is 2200 V

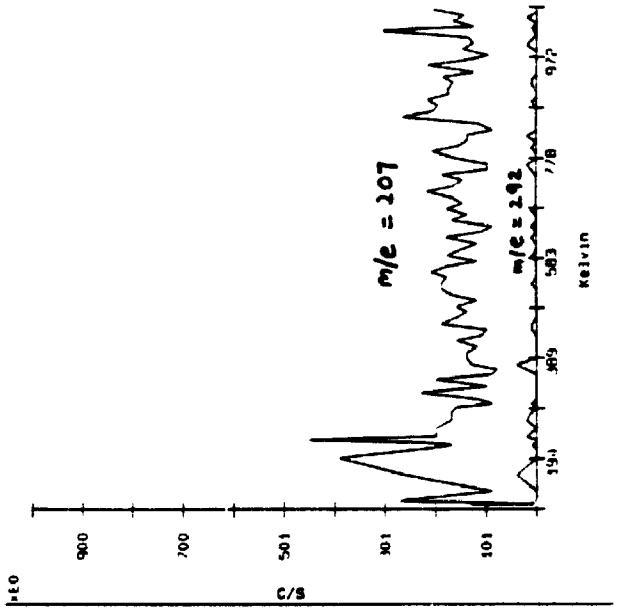
m/e = 207
m/e = 292
C/S
Kelvin

5.3.3 Coverage Studies of HPt interaction with Clean Pt(111)

a. Adsorption at 110 K - $\Delta\phi$

The $\Delta\phi$ change showed a negative change with a saturation value of at least 1 volt. When the reservoir was not pumped, $\Delta\phi$ reached saturation in a shorter time as expected. In all cases, the $\Delta\phi$ reached 95 % of its change at 0.2 L using the uncorrected ion gauge readings. Figure 5.5 shows the $\Delta\phi$ change on adsorption of HPt on Pt(111).

b. Adsorption at 110 K - FTIR-RAS

Figure 5.6 shows FTIR-RAS of *cis*-dimethyl platinum diisocyanide on Pt(111). Spectrum 1 shows a 0.26 L exposure of HPt on Pt(111). There is a band at 2234 cm^{-1}. Spectrum 2 shows a 0.6 L exposure of DPt. We observe again the 2234 cm^{-1} band. Based on the FTIR-RAS work on CH_3NC the peak at 2234 cm^{-1} is assigned to the $\nu(C\equiv N)$ in terminally bonded CH_3NC on Pt(111). The C-H stretches are very weak in intensity. Spectrum 3 shows a 1.17 L exposure of DPt/Pt(111). Again we observe the 2234 cm^{-1} band, which is assigned to terminal CH_3NC on Pt(111). Two new peaks at higher energy than the 2234 cm^{-1} band, appear at 2190 and 2170 cm^{-1} and are assigned to the $\nu_{as}(C\equiv N)$ and $\nu_s(C\equiv N)$ stretches (C≡N doublet) in the multilayer respectively. This assignment is based on a comparison with HPt adsorption on Pt(111)-C(ΔC_2H_2) (see discussion in Section 5.3.2a). No ν(C-D) stretch at around 2150 - 2000 cm^{-1} were observed in contrast to D'Pt/Pt(111)-C(ΔC_2H_2) (2114 cm^{-1}),

Figure 5.5 : $\Delta\phi$ HPt/Pt(111) - Doser "far away" from crystal

The exposure at which the $\Delta\phi$ saturates can change depending on whether the doser was moved closer to or further away from the crystal during dosing. $\Delta\phi$ saturates at 0.2 L when the doser is moved close up to the crystal.

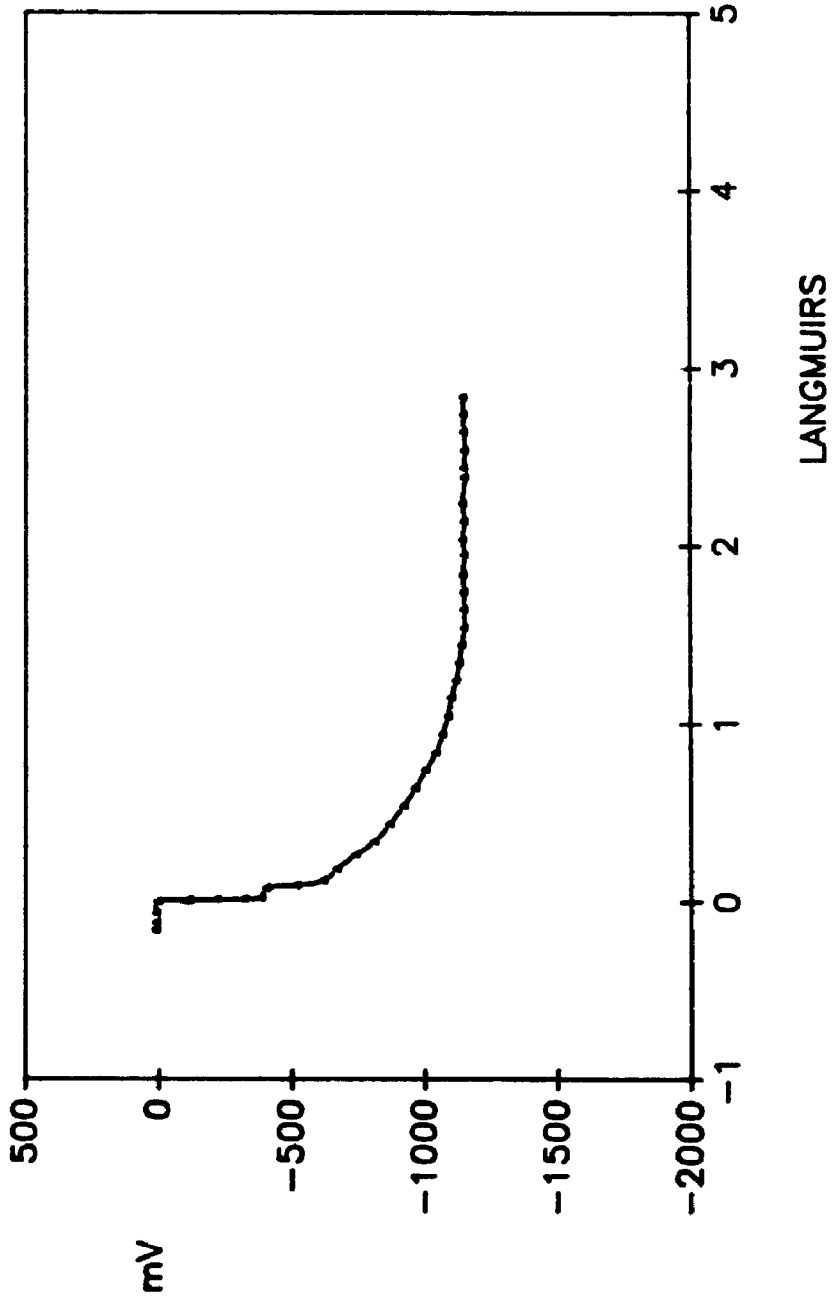
500
0
−500
−1000
−1500
−2000
mV
−1
0
1
2
3
4
5
LANGMUIRS

Figure 5.6 : FTIR-RAS of *cis*-dimethyl platinum diisocyanide on Pt(111) in the spectral ranges of 3020-2750 and 2300-2000 cm^{-1}.

(T_{ads} = 110 K).

Spectrum 1 : 0.26 L exposure of HPt on Pt(111).

Spectrum 2 : 0.6 L exposure of DPt on Pt(111).

Spectrum 3 : 1.17 L exposure of DPt on Pt(111).

Spectrum 4 : 2.5 L exposure of HPt on Pt(111).

Note: The number to the left of each spectrum accompanied by a "×", are the factors by which the displayed spectrum should be multiplied to compare with spectrum 1.

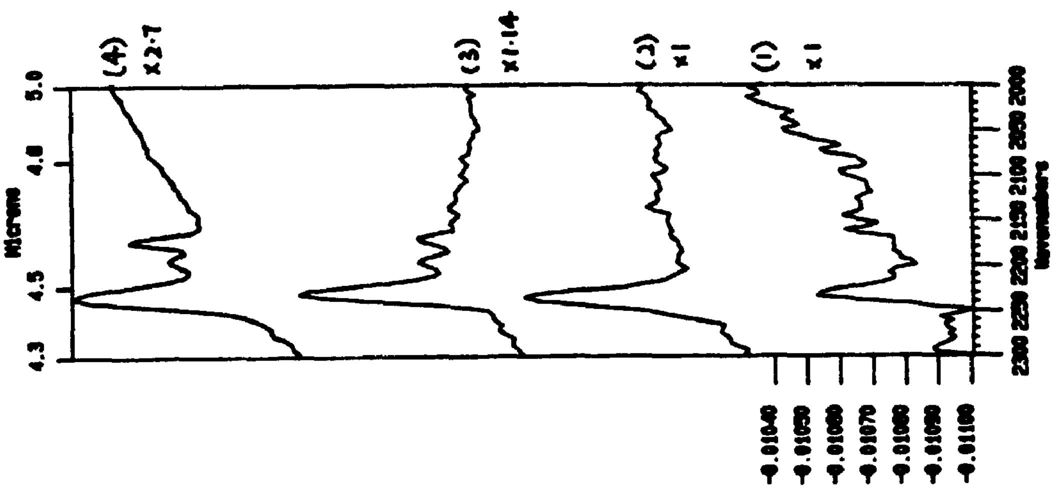
(4)
x2·7
(3)
x1·14
(2)
x1
(1)
x1
Microns
4.3
4.5
4.8
5.0
-0.01040
-0.01050
-0.01060
-0.01070
-0.01080
-0.01090
-0.01100

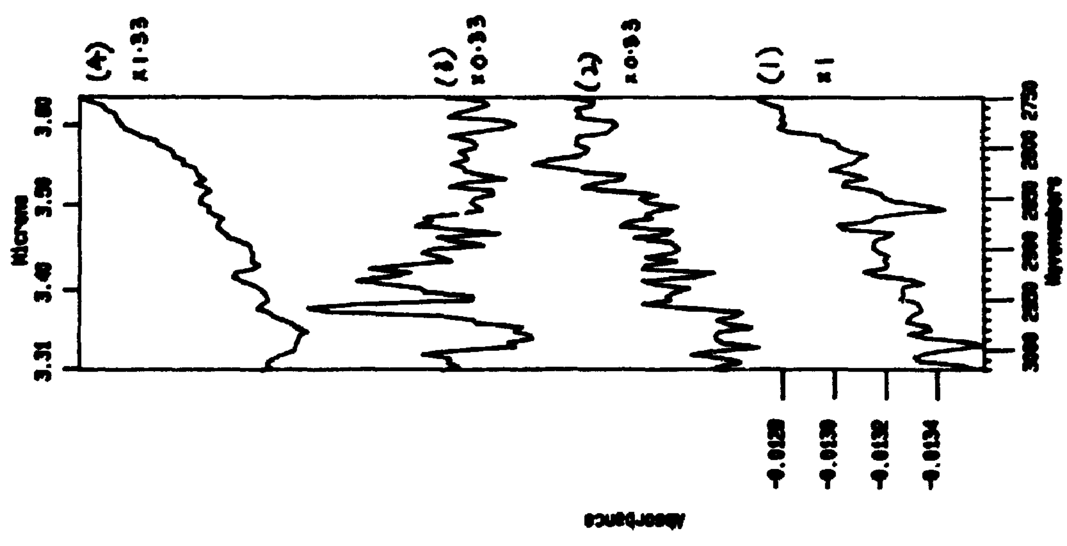
(4)
x1·33
(3)
x0·33
(2)
x0·33
(1)
x1
Microns
3.31
3.40
3.50
3.60
-0.0128
-0.0130
-0.0132
-0.0134
Absorbance

D'Pt (2141, 2111 cm^{-1}) and DPt (2102, 2052 cm^{-1}) in the gas phase. [2] This indicates that there is some CH/CD exchange in the monolayer. A 1.53 L exposure of D'Pt/Pt(111) shows no ν(C-D) stretches, consistent with the 1.17 L exposure DPt/Pt(111) while the band at 2234 cm^{-1} is still present.

Spectrum 4 shows a 2.5 L HPt/Pt(111) exposure on Pt(111). While the CN stretches are clearly observed (0.0016 a.u.), the C-H stretches are weak ($\leq$ 0.0001 a.u.).

[2] Supra footnote 1, chapter 5.

c. After Annealing - FTIR-RAS

Figure 5.7 show TD-FTIR-RAS spectra of a 7 L exposure of HPt on Pt(111), in the spectral ranges of 3020 - 2750 and 2300 - 2000 cm^{-1}. The temperature was held for 1 minute at each elevated temperature and was reset to 110 K for the FTIR-RAS measurement. On annealing to 143 K (Spectrum 1), the ν(C≡N) doublet [ν_{as}(C≡N) and ν_{s}(C≡N)] bonded to the platinum atom decreased in intensity. The CH_3 bends at 1450 cm^{-1} also decrease in intensity. On further annealing to 153 K (Spectrum 2), the C≡N doublet and CH_3 bend were no longer detectable. This is consistent with multilayer desorption (see Section 5.3.3d).

Heat treatment to 175 K (Spectrum 3) reduced the intensity of all peaks, including the ν(C≡N) of terminally bonded CH_3NC except for the C-H stretches at 2917, 2850 cm^{-1} which were no longer observed at 325 K. This temperature coincided with the lower temperature of the hydrogen desorption as described in Section 5.3.3d.

Avery and Matheson [3] have shown that terminally bonded CH_3NC on Pt(111) is not reversibly desorbed. In fact the products of dissociation are H_2 and HCN. Using HREELS, for low coverage experiments of CH_3NC, they observed that all spectral changes occurred below 360 K. They believe that disproportionation or association reactions could explain the spectral changes (attenuation of ν_{s}(C≡N)) before the desorption products are observed above 400 K. Similar disproportionation

---

[3] See Avery, N. R. and T. W. Matheson, **Surf. Sci.**, 143 (1984), 110 - 124.

Figure 5.7 : TD-FTIR-RAS spectra of a 7 L exposure of HPt on Pt(111), in the spectral ranges of 3020 - 2750 and 2300 - 2000 cm^{-1}.

T_{ads}=110 K

Spectrum 1 : multilayer warmed to 143 K

Spectrum 2 : multilayer warmed to 152 K

Spectrum 3 : multilayer warmed to 175 K

Spectrum 4 : multilayer warmed to 196 K

Spectrum 5 : multilayer warmed to 224 K

Spectrum 6 : multilayer warmed to 325 K

Note: The number to the side of each spectrum accompanied by a "×", are the factors by which the displayed spectrum should be multiplied to compare with spectrum 6.

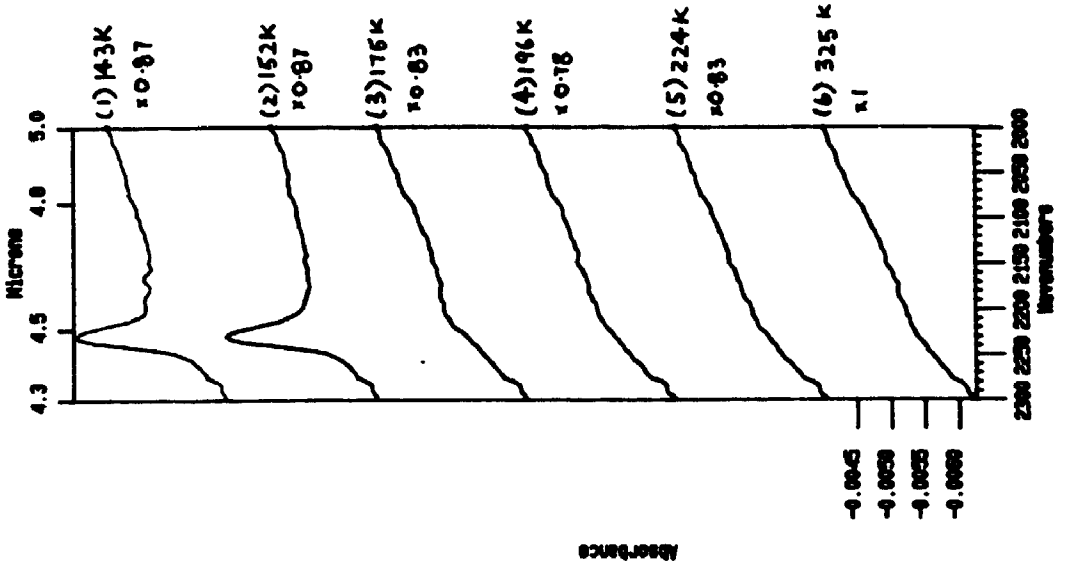
(1) 143K
×0·97
(2) 152K
×0·87
(3) 176K
×0·83
(4) 196K
×0·78
(5) 224K
×0·83
(6) 325 K
×1
Microns
5.0
4.0
4.5
4.3
Absorbance
-0.005
-0.0050
-0.0055
-0.0060

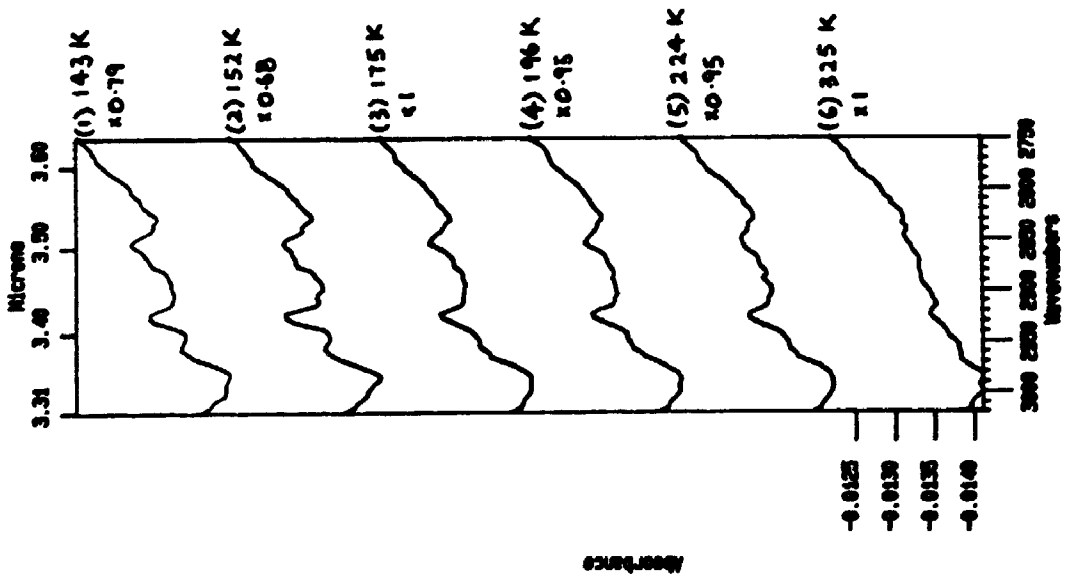
(1) 143 K
×0·79
(2) 152 K
×0·68
(3) 175 K
×1
(4) 196 K
×0·93
(5) 224 K
×0·95
(6) 325 K
×1
Microns
3.80
3.50
3.40
3.31
Absorbance
-0.0125
-0.0130
-0.0135
-0.0140

or association reactions could also be responsible for the spectral changes observedwith HPt/Pt(111).

d. Adsorption - TPD

Figure 5.8 shows TPD spectra of 0.08 L exposure HPt on Pt(111). The m/e 2 and 27 show desorption peaks at 435 K and (525, 660 K) respectively. Two desorption peaks for m/e 27 are observed. As these are high temperature peaks and occur at different temperatures, these peaks are assigned to decomposition products rather than molecular desorption of the monolayer.

Figure 5.9, (0.36 L exposure of HPt/Pt(111)) again shows two m/e 27 desorption peaks at 510 and 640 K. A low temperature m/e 41 peak at 140 K is observed. There is however no high temperature m/e 41 peak. The low temperature m/e 41 is assigned to a fragment from the HPt multilayer desorption.

The m/e 2 is assigned to H_2 desorption, m/e 27 is assigned to HCN and m/e 41 is assigned to CH_3NC. Avery and Matheson showed that CH_3NC decomposes to H_2 and HCN with peak temperatures of 460 K and (520 K, 610 K) respectively. [4] The H_2 desorption from CH_3NC decomposition on Pt(111) at 460 K had a full width half maximum (FWHM) of about 75 K. Henderson et al. showed that H_2 desorption from CH_3 decomposition on Pt(111) had a FWHM of 60 K and peak desorption

[4] Supra footnote 3, chapter 5.

Figure 5.8 : TPD spectra of 0.08 L exposure HPt on Pt(111)

(m/e = 2, 27, 41 ; T_{ads} = 110 K).

Multiplier Voltage = 1850 V

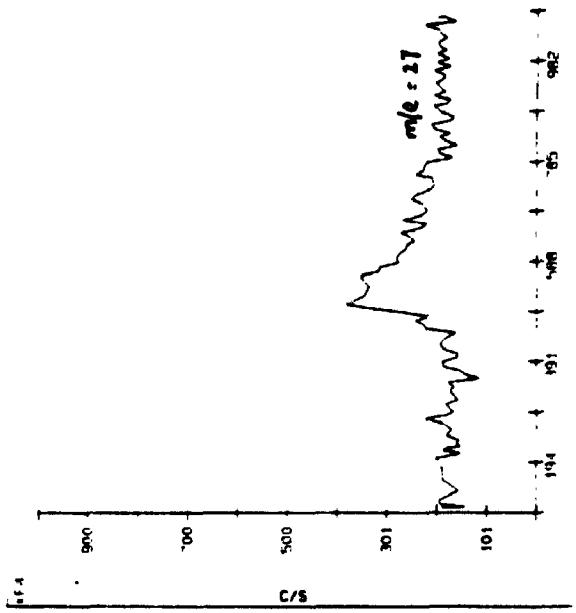
m/e = 27
C/S
Kelvin

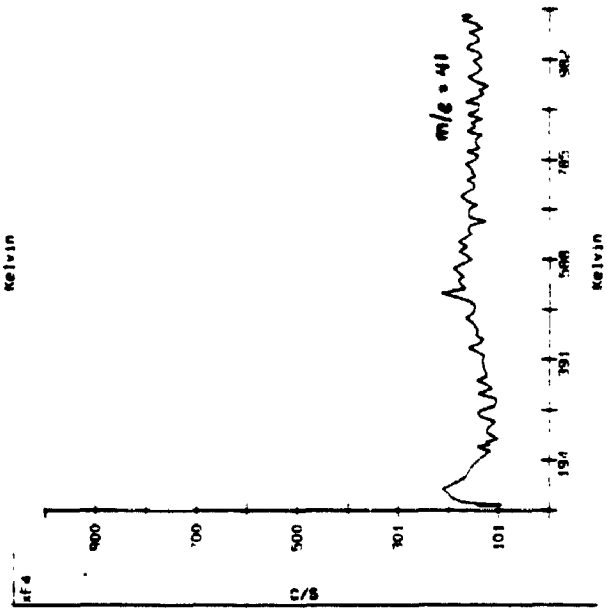
m/e = 41
C/S
Kelvin

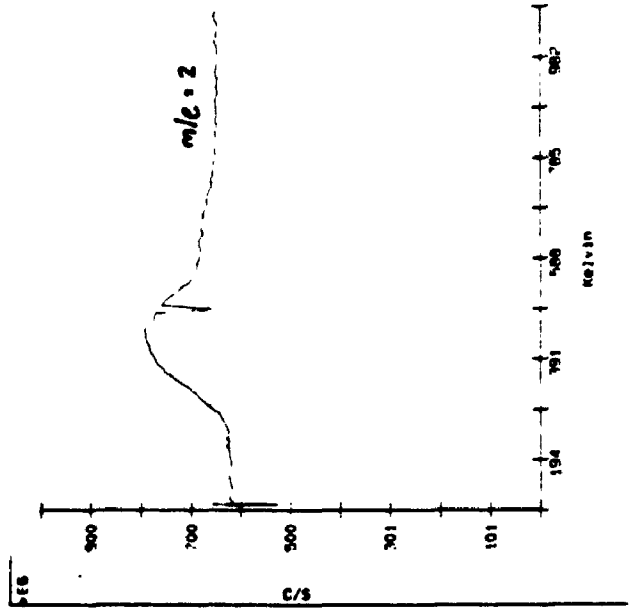
m/e = 2
C/S
Kelvin

Figure 5.9 : TPD spectra of 0.36 L exposure of HPt on Pt(111)

(m/e = 27, 41 ; T_{ads} = 110 K)

Multiplier Voltage = 1850 V

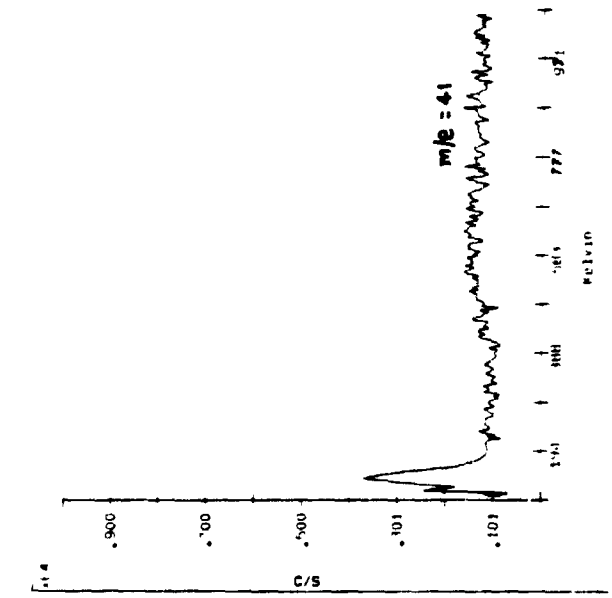
m/e = 41
C/S
.900
.700
.500
.301
.101

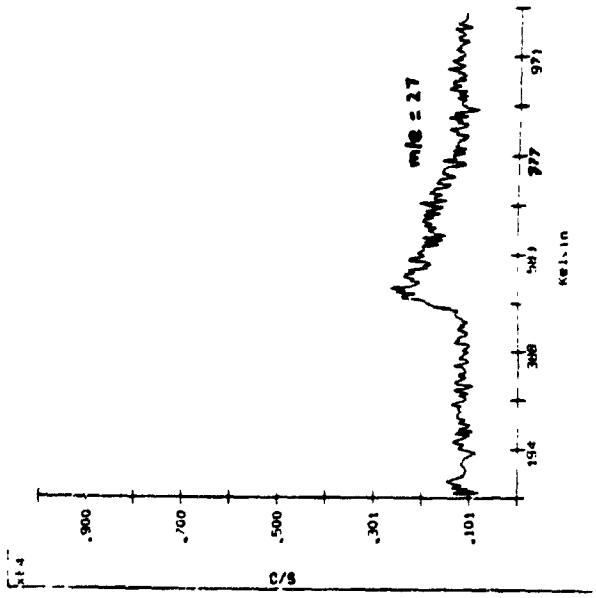
m/e = 27
C/S
.900
.700
.500
.301
.101

temperatures of 360 K.[5] When these results are compared with the TPD data for $H_2$and HCN desorption in the HPt/Pt(111) system, they imply that the HPt must have chemisorbed dissociatively to give CH_3NC adsorbed on Pt(111) as it is the monolayer CH_3NC adsorbed on Pt(111) that decomposes to H_2 and HCN on heating. Furthermore, the FWHM value of about 200 K for H_2 desorption at a peak temperature of 435 K (HPt/Pt(111) system) indicates that the H_2 desorption signal in HPt decomposition is an overlap of H_2 desorption from CH_3NC and CH_3 platinum decomposition on Pt(111).

d. Auger Spectroscopy

The crystal was dosed with about 28 L of HPt from the microcapillary array (far away position from the crystal) with the crystal temperature at 110 K, followed by high temperature flash to 725 •C. Finally the crystal was annealed in 1×10^{-7} torr of I_2 at 725 •C for about ten minutes. Spectrum 1 in Figure 5.10 shows the Auger spectrum of the Pt(111) surface recorded after the hydrogen treatment. The carbon peak at 272 eV is observed, showing that the precursor decomposes on annealing and leaves carbon behind on the surface. Spectrum 2 was an Auger spectrum of the crystal after annealing in oxygen pressure of 1×10^{-5} torr at 725 •C for half hour. In contrast to Spectrum 1, the carbon peak has been removed.

---

[5] Henderson, M.A., G.E. Mitchell and J.M. White, **Surf. Sci.**, 248 (1991), 279 - 286.

Figure 5.10 : Auger spectra

Spectrum 1 : Auger Spectrum after decomposition of 28 L HPt on Pt(111), followed by annealing in hydrogen pressure of 1×10^{-7} torr at 725 •C for ten minutes

Spectrum 2 : Auger Spectrum after annealing in oxygen pressure of 1×10^{-5} torr at 725 •C for half hour.

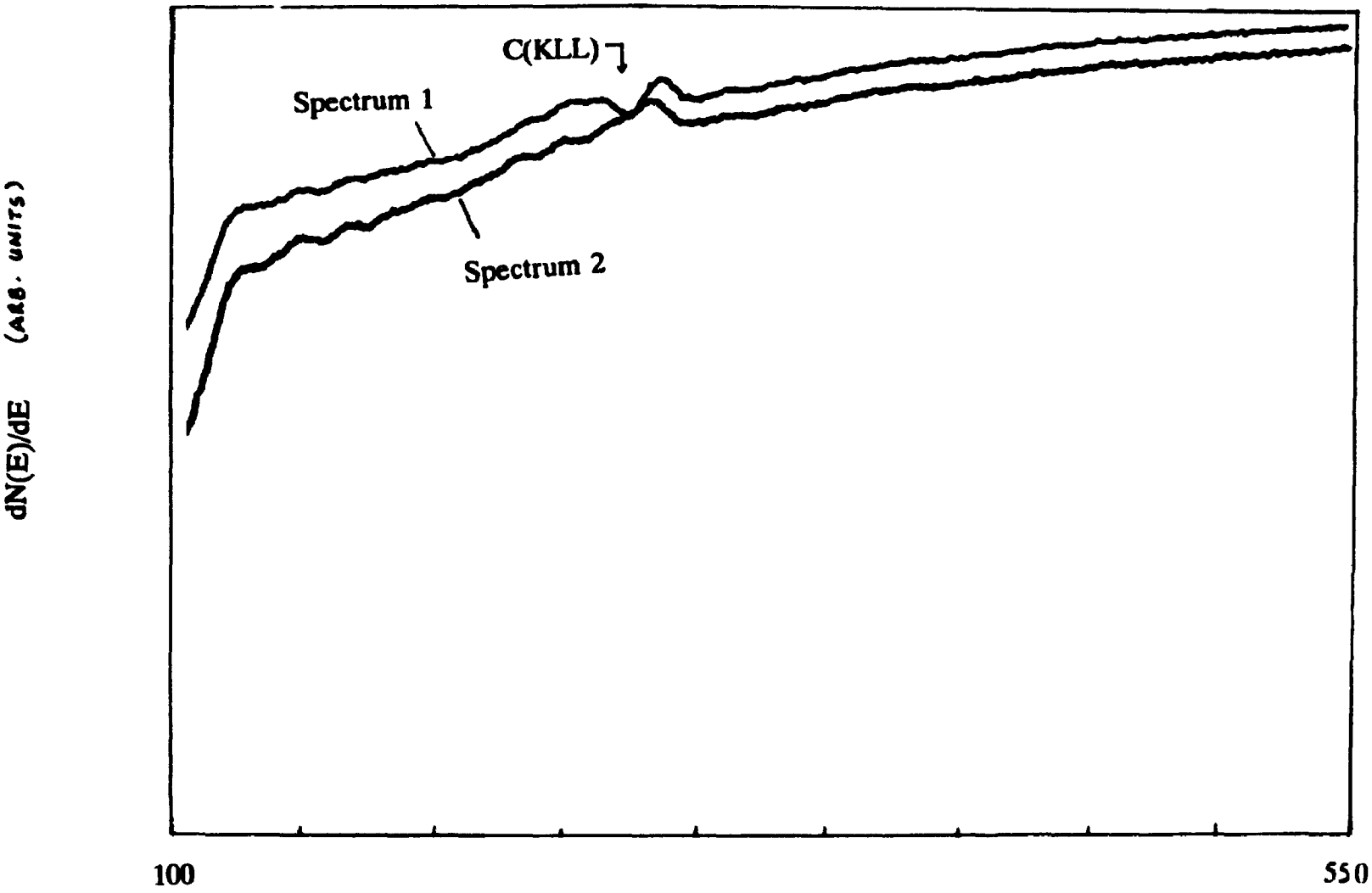
C(KLL)
Spectrum 1
Spectrum 2
dN(E)/dE (ARB. UNITS)
100
550
electron energy (eV)

5.3.4 Coverage Studies of HPt/Pt(111)-C(ΔC_2H_6)

The platinum crystal was heated in an ethane atmosphere of 1×10^{-5} Torr at 800 °C. The Pt(111) surface with carbon incorporation from the decomposition of ethane is referred to as Pt(111)-C(ΔC_2H_6). This treatment produces a carbon containing surface, but no graphitic rings were observed, pointing to a disordered structure. Pt-Auger transitions could still be detected on this surface.

a. Adsorption - FTIR-RAS

Figure 5.11 shows FTIR-RAS spectra for *cis*-dimethyl platinum diisocyanide on Pt(111)-C(ΔC_2H_6) for the spectral ranges of 3020 - 2750, 2300 -2080, 1550 - 1320 and 1100 -900 cm^{-1}.

Spectrum 1 shows a 0.08 L exposure of DPt on Pt(111)-C(ΔC_2H_6). The C-H stretches due to the methyl on the ligand are observed, together with the C-H rock at 1030 cm^{-1}. There is also a contribution to this band from the CD_3 deformation from the CD_3 platinum group. No C≡N or C=N stretches were observed.

In a 0.21 L HPt/Pt(111)-C(ΔC_2H_6), the C-H stretches are observed as well as the C-H rock at 1030 cm^{-1}. The C≡N stretch at 2234 cm^{-1} and C=N stretch are below our detection limit. The CH_3 deformation is also observed. No C≡N or C=N stretch could be observed for a 0.36 L DPt/Pt(111)-C(ΔC_2H_6). Spectrum 2 is a 0.83 L HPt/Pt(111)-C(ΔC_2H_6) and the CN doublet at 2190 and 2170 for the multilayer

Figure 5.11 : FTIR-RAS spectra for *cis*-dimethyl platinum diisocyanide on Pt(111)-C(ΔC_2H_6) for the spectral ranges of 3020 - 2750, 2300 -2080, 1550 - 1320 and 1100 - 900 cm^{-1}. T_{ads} = 110 K

Spectrum 1 : 0.08 L DPt on Pt(111)-C(ΔC_2H_6)

Spectrum 2 : 0.83 L HPt on Pt(111)-C(ΔC_2H_6)

Spectrum 3 : 0.85 L DPt on Pt(111)-C(ΔC_2H_6)

Note: The number to the left of each spectrum accompanied by a "×", are the factors by which the displayed spectrum should be multiplied to compare with spectrum 1.

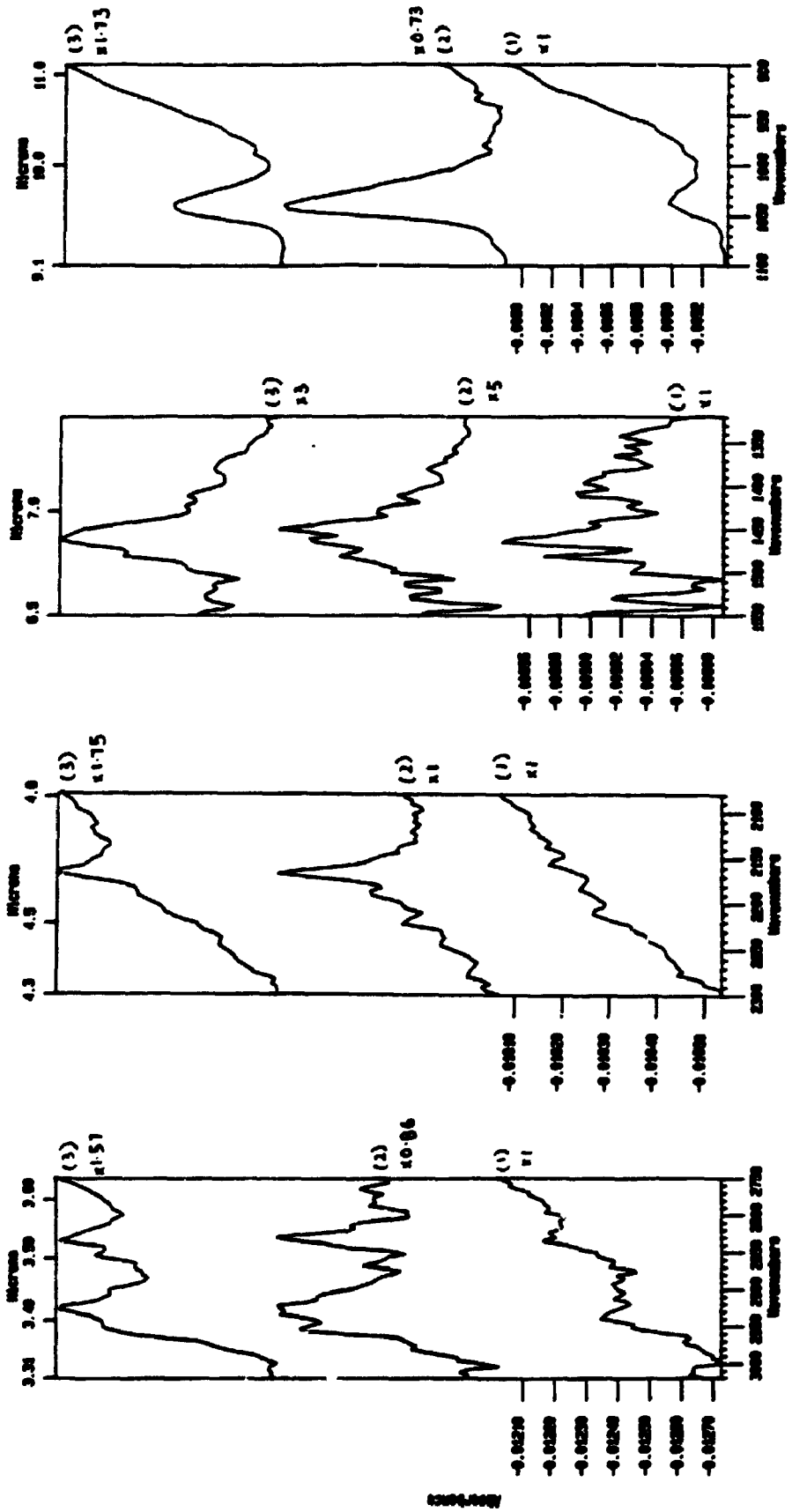

have just begun to grow in.

Spectrum 3 is a 0.85 L exposure of DPt/Pt(111)-C(ΔC_2H_6). The C≡N doublet at around 2160 is observed but is not as well resolved as in HPt. This band is assigned to the C≡N doublet in the multilayer DPt. With higher exposures the C≡N doublet, CH_3 deformation, C-H rock and C-N bands grow in.

b. Adsorption - TPD

Figure 5.12 is a 0.38 L exposure of HPt/Pt(111)-C(ΔC_2H_6). A low temperature m/e 41 and 57 peak is observed. There is a high temperature m/e 41 peak at 520 K but no accompanying high temperature m/e 57. The m/e 2 and 27 desorption peaks present in HPt/Pt(111), has been reduced nearly into the noise level.

Figure 5.13 is a 0.56 L HPt/Pt(111)-C(ΔC_2H_6). The high temperature m/e 41 is clearly present, while the m/e 57 still shows no high temperature feature. The high temperature m/e 41 is thus not due to molecular desorption of the monolayer. Thus monolayer desorption is non molecular. The low temperature m/e 41 is assigned to multilayer desorption and the high temperature m/e 41 is assigned to monolayer decomposition. However, the high temperature m/e 41 does not appear to saturate with the appearance of the low temperature m/e 41 in the coverage studies.

Figure 5.12 : TPD of 0.38 L exposure of HPt on Pt(111)-C(ΔC_2H_6).

(β = 7 K/s)

Multiplier Voltage = 1850 V

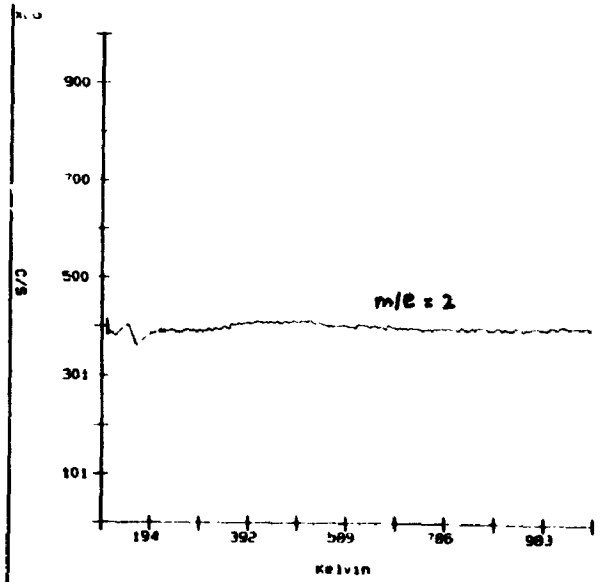
900
700
500
301
101
C/S
m/e = 2
194
392
589
786
983
Kelvin

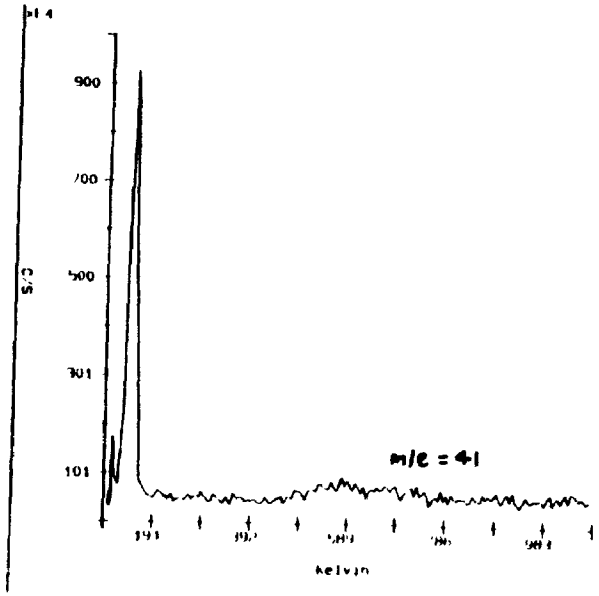
900
700
500
301
101
C/S
m/e = 41
Kelvin

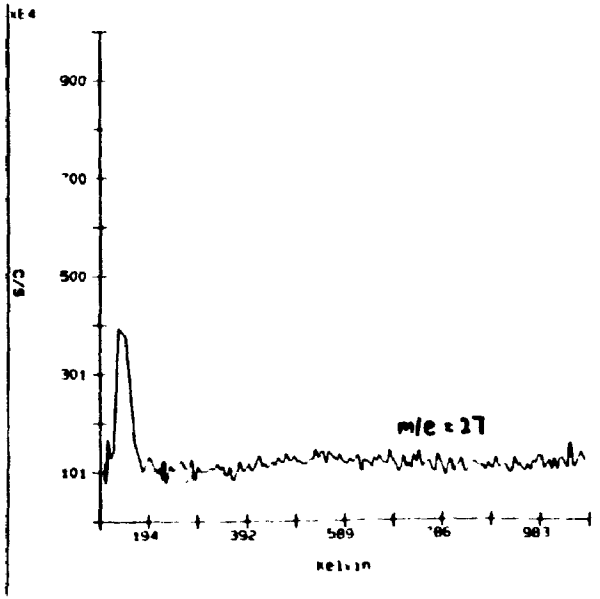
900
700
500
301
101
C/S
m/e = 27
194
392
589
786
983
Kelvin

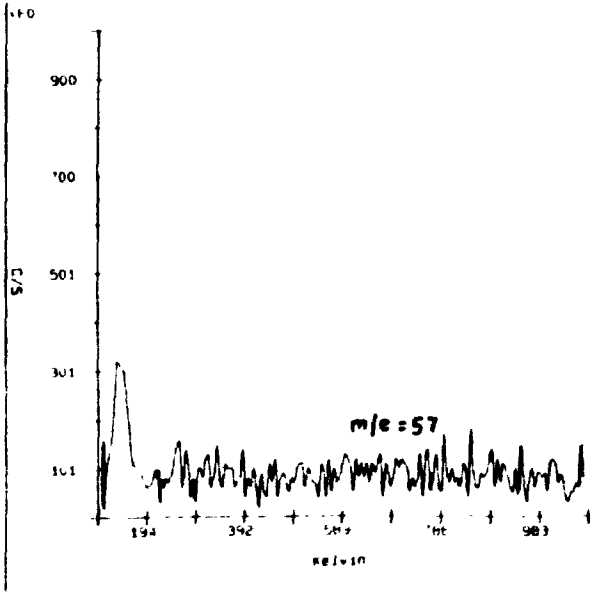
900
700
501
301
101
C/S
m/e = 57
194
392
Kelvin

Figure 5.13 : TPD of 0.56 L exposure of HPt on Pt(111)-C(ΔC_2H_6).

(β = 7 K/s)

Multiplier Voltage = 1850 V

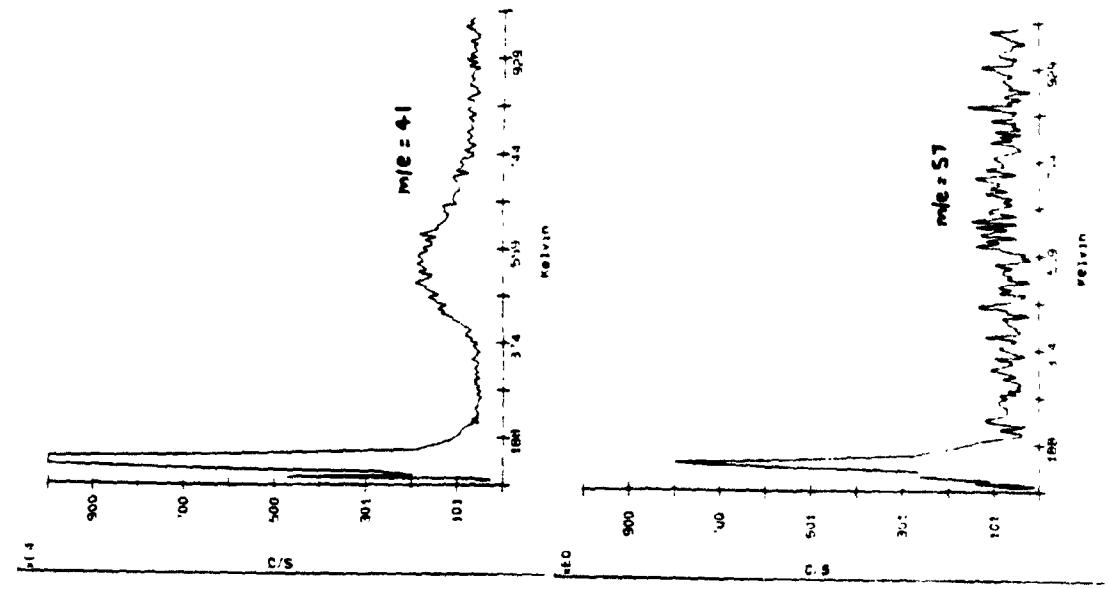
m/e = 41
m/e = 57
C/S
Kelvin

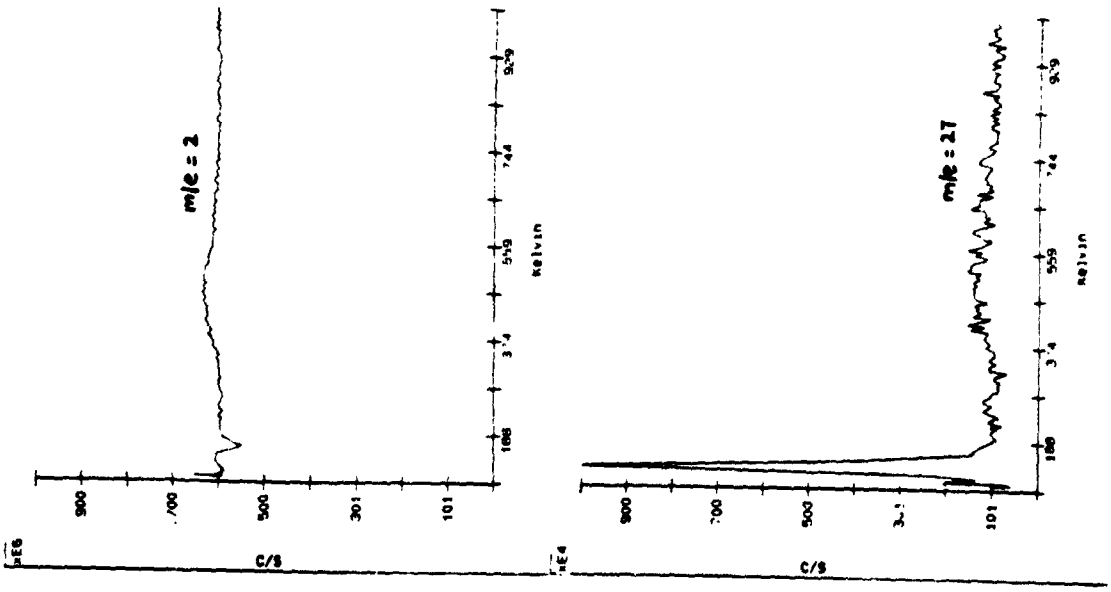
m/e = 2
m/e = 27
C/S
Kelvin

5.3.5 Coverage Studies on Pt(111)-C(ΔHPt)

In these experiments, carbon atoms were incorporated on the Pt(111) surface via decomposition of the organometallic precursor. The surface is referred to as Pt(111)-C(ΔHPt).

a. Adsorption at 110 K - FTIR-RAS

Figure 5.14 show the FTIR-RAS spectra of HPt adsorption on Pt(111)-C(ΔHPt) for the spectral ranges of 3020 - 2750, 2300 - 2100 and 1900 -1300 cm^{-1}. In these experiments, the position of the microcapillary was moved "far" away from the crystal (i.e. the LTM carrying the doser was in the fully retracted position). Accordingly, these exposures are higher than those reported above for the same coverage of HPt on the surface.

Spectrum 1 shows a 1.5 L exposure of HPt/Pt(111)-C(ΔHPt). The 2234 cm^{-1} band is the first one to grow in. Spectrum 2 (a 6 L exposure) shows the C-H triplet grows in next.

Spectrum 3 is a 21 L exposure of HPt/Pt(111)-C(ΔHPt). In addition to the monolayer bands, those characteristic of the multilayer are clearly observed; the CN doublet at 2190 and 2170 cm^{-1}, the $\delta(CH_3)$ at 1450 cm^{-1} and C-N stretch at 900 cm^{-1} (not displayed) is also observed. There is a C=N stretch at 1650 cm^{-1} which could arise from weak interaction of the complex with the surface (compare with multilayer

Figure 5.14 : FTIR-RAS spectra of HPt adsorption on Pt(111)-C(ΔHPt) for the spectral ranges of 3020 - 2750, 2300 - 2100 and 1900 -1300 cm^{-1}.

(T_{ads} = 110K)

Spectrum 1 : 1.5 L exposure FTIR-RAS spectrum

Spectrum 2 : 6 L exposure FTIR-RAS spectrum

Spectrum 3 : 21 L exposure FTIR-RAS spectrum

Note: The number to the side of each spectrum accompanied by a "×", are the factors by which the displayed spectrum should be multiplied to compare with spectrum 1.

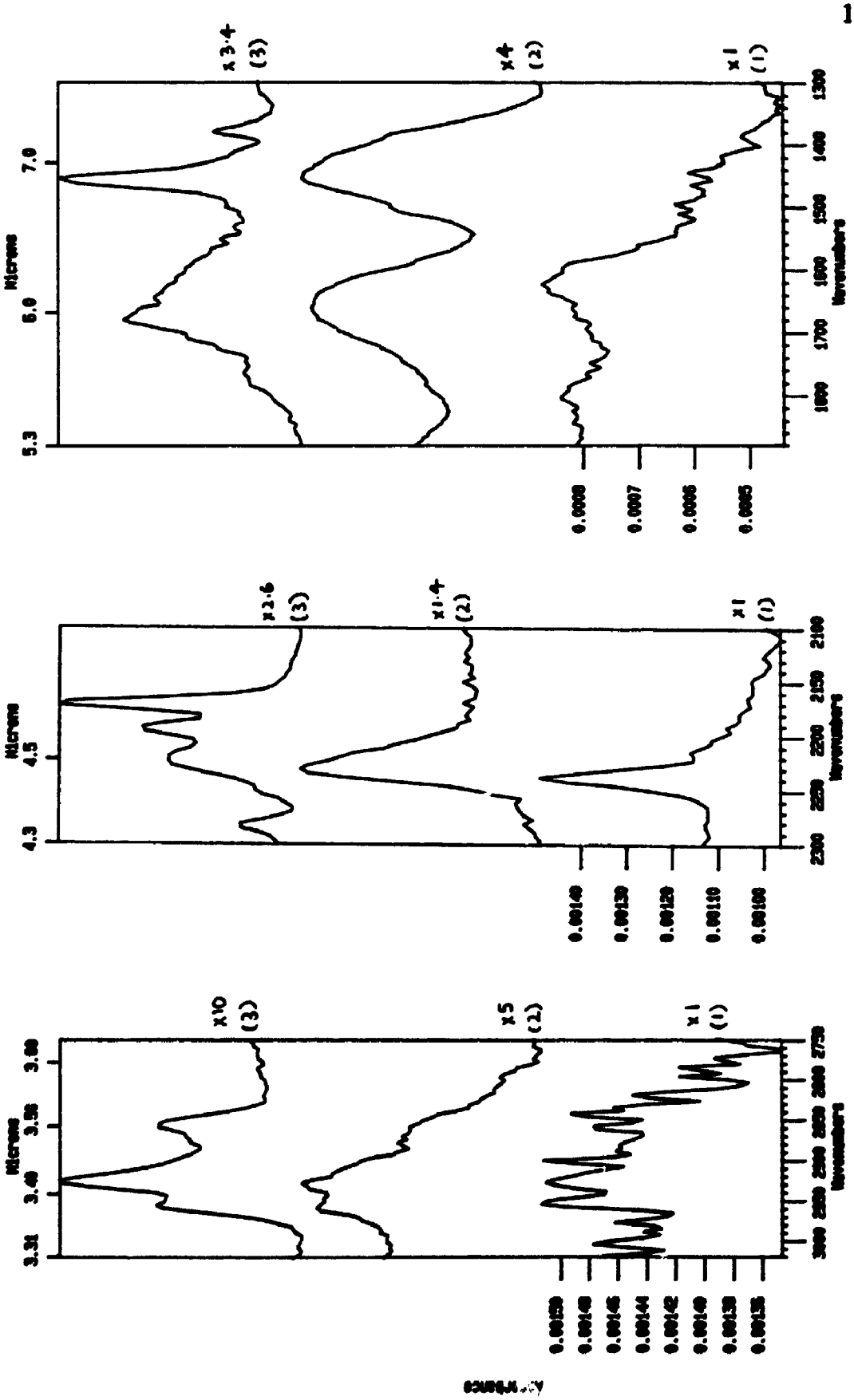
x3.4
(3)
x4
(2)
x1
(1)
Microns
7.0
6.0
5.3
Wavelength
1300
1400
1500
1600
1700
1800
0.0008
0.0007
0.0006
0.0005
x2.6
(3)
x1.4
(2)
x1
(1)
Microns
4.5
4.3
Wavelength
2100
2150
2200
2250
2300
0.0140
0.0130
0.0120
0.0110
0.0100
x10
(3)
x5
(2)
x1
(1)
Microns
3.80
3.58
3.40
3.31
Wavelength
2750
2700
2650
2600
2550
2500
2450
2400
2350
2300
0.0050
0.0048
0.0046
0.0044
0.0042
0.0040
0.0038
0.0036

FTIR-RAS of HPt/Pt(111)-C(ΔC_2H_2) discussed in Section 5.3.2a).

b. After Annealing - TD-FTIR-RAS

Figure 5.15 shows a TD-FTIR-RAS spectra of a 24 L exposure of HPt/Pt(111)-C(ΔHPt) in the spectral ranges of 3020 - 2750, 2300 - 2100 and 1850 - 1300 cm^{-1}. This multilayer was obtained by dosing the crystal with the capillary array "far" away.

Spectrum 1 shows the multilayer (24 L exposure) on Pt(111)-C(ΔHPt) warmed to 135 K. The C-H stretches are larger in intensity than the C≡N stretch at 2234 cm^{-1} (approximately 4:1).

Spectrum 2 shows the multilayer warmed to 152 K. The CN doublet decreases in intensity, but not the C-H stretches (0.0025 a.u.), or the CN stretches at 2234 (0.001 a.u.) and 1650 cm^{-1}.

On warming to 175 K (Spectrum 3), the band at 1650 cm^{-1} is reduced in intensity while no changes in intensity were observed for the C-H stretches and CN stretch at 2234 cm^{-1}. These bands are thus assigned to the vibrational modes in the monolayer.

On warming to 223 K (Spectrum 5) shows the band at 2234 cm^{-1} changes in its shape while the C-H stretches remain unchanged in shape and intensity. At 325

Figure 5.15 : TD-FTIR-RAS spectra of a 24 L multilayer HPt/Pt(111)-C(ΔHPt) in the spectral ranges of 3020 - 2750, 2300 - 2100 and 1850 - 1300 cm^{-1}.

(T_{ads} = 110 K)

Spectrum 1 : multilayer (24 L exposure) on Pt(111)-C(ΔHPt) warmed to 135 K.

Spectrum 2 : multilayer warmed to 152 K.

Spectrum 3 : multilayer warmed to 175 K.

Spectrum 4 : multilayer warmed to 197 K.

Spectrum 5 : multilayer warmed to 223 K.

Spectrum 6 : multilayer warmed to 325 K.

Note: The number to the side of each spectrum accompanied by a "×", are the factors by which the displayed spectrum should be multiplied to compare with spectrum 6.

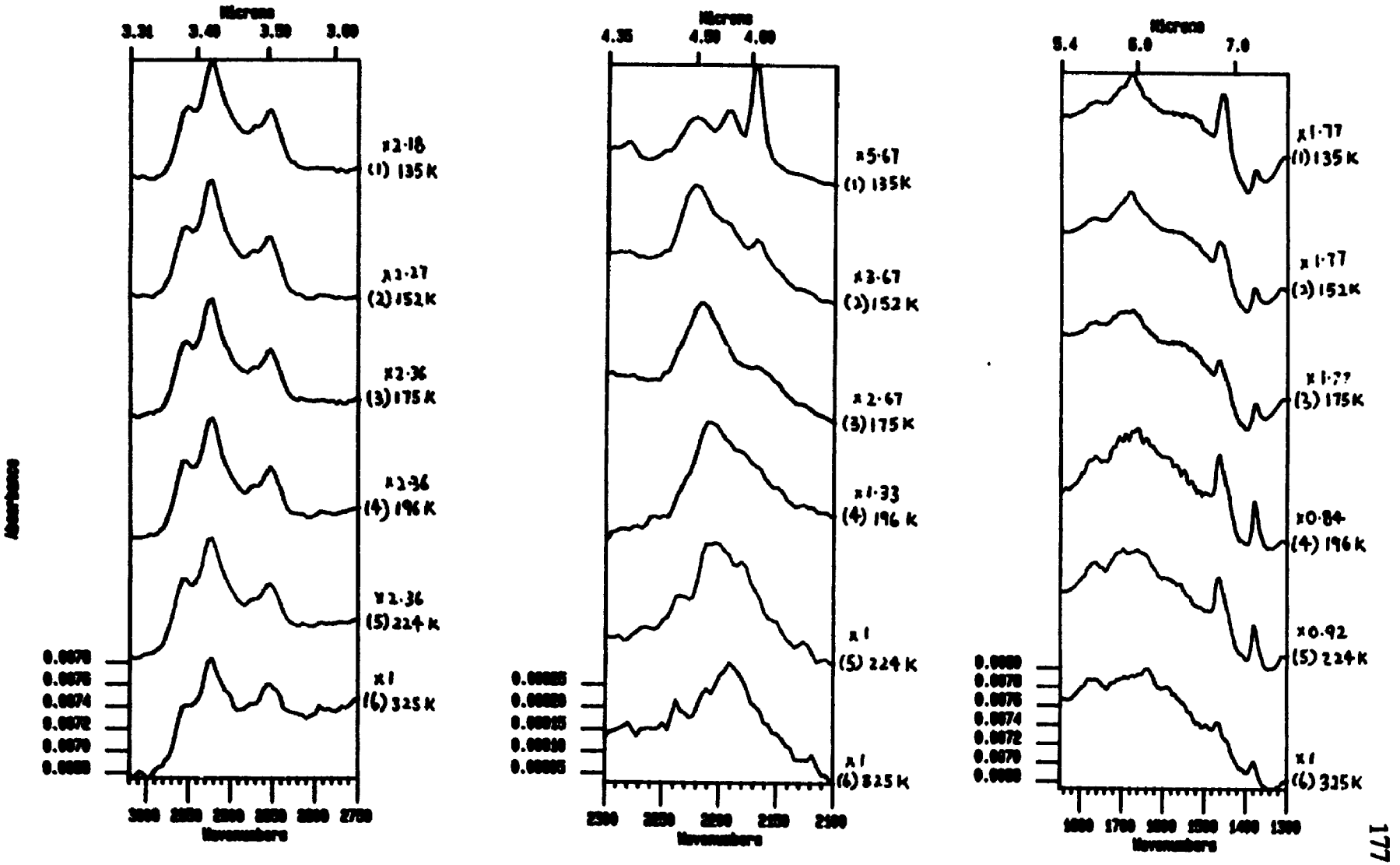
Microns
3.31
3.40
3.50
3.60
x2·18
(1) 135K
x1·27
(2) 152K
x2·36
(3) 175K
x2·36
(4) 196K
x2·36
(5) 224K
x1
(6) 325K
Absorbance
0.0078
0.0076
0.0074
0.0072
0.0070
0.0068
3000
2800
2600
2400
2200
2000
Wavenumbers
Microns
4.35
4.50
4.60
x5·67
(1) 135K
x3·67
(2) 152K
x2·67
(3) 175K
x1·33
(4) 196K
x1
(5) 224K
x1
(6) 325K
2300
2200
2100
2000
Wavenumbers
Microns
5.4
6.0
7.0
x1·77
(1) 135K
x1·77
(2) 152K
x1·77
(3) 175K
x0·84
(4) 196K
x0·92
(5) 224K
x1
(6) 325K
0.0080
0.0078
0.0076
0.0074
0.0072
0.0070
0.0068
1800
1700
1600
1500
1400
1300
Wavenumbers

K, the C-H stretches finally begin to lose intensity.

Spectrum 6 shows the multilayer warmed to 325 K. The C-H stretches are still observed, in sharp contrast to the situation on clean Pt(111).

5.4 Discussion

5.4.1 Platinum Deposition on Pt(111)

While it is easy to prove or disproof platinum deposition on a substrate other platinum, for example on gold or nickel, it is impossible to distinguish the deposited platinum from the platinum substrate using an Auger Spectrometer with a retarding field analyzer. The problem is compounded in the *cis*-dimethyl platinum diisocyanide/Pt(111) system because each complex may sit on 10-20 platinum atoms on the substrate (5 % - 10 % of a monolayer). The Auger signal from the platinum in the complex will be very small in comparison to the platinum signal from the substrate. However, there is indirect evidence form FTIR-RAS and TPD that there is successful deposition of platinum on Pt(111) from the decomposition of *cis*-dimethyl platinum diisocyanide, which will be described below.

In the TPD experiments of HPt from Pt(111)-C(ΔC_2H_2), no high temperture peaks were observed, and the cracking pattern of the complex shows up as the low temperature desorption of masses 15, 27, 41 and 207 at about 150-190 K). The observation of m/e 207 (a Pt-C fragment of the parent molecule), shows that the complex carrying the platinum atom has been successfully transported to the crystal surface. Furthermore, the FTIR-RAS spectra of HPt on Pt(111)-C(ΔC_2H_2) does show a CN doublet. This is the asymmetric and symmetric CN stretch band and indicates that both ligand groups must be bonded to the platinum atom in the complex. It is noted that these data are only for the precursor adsorption on a

passivated surface and thus in a strict sense there is no platinum deposition on the passivated surface as only multilayer desorption was observed.

In contrast on a Pt(111) surface, the FTIR-RAS data shows only one C≡N stretch at 2234 cm^{-1}. This indicates that the two methyl isocyanide ligands in the precursor are no longer bonded to the same platinum atom. In fact they are each terminally bonded to one platinum atom on Pt(111), (c.f. $CH_3NC/Pt(111)$). This may either generate a $(CH_3)_2Pt(MeNC)$ or $(CH_3)_2Pt$ species which adsorbs onto a reactive site on Pt(111). On warming the TPD data shows a mass 2 signal due to molecular hydrogen at 435 K and mass 27 due to hydrogen cyanide at about 525 and 660 K. No mass 15, 41 or 207 were detected. Deuteration experiments with DPt showed a mass 3 (HD) signal but no mass 2 or 4. This means that the C-H bonds on the methyl platinum and methyl ligand must have been activated by the surface with subsequent hydrogen migration to the surface, followed by molecular hydrogen desorption. Comparing this data tc that from the $Pt(111)-C(\Delta C_2H_2)$ it must mean that the precursor must have suffered thermal decomposition on the surface. The absence of any mass 207 TPD signal means that the platinum atom in the complex must have remained on the surface, proving that platinum atoms are deposited on the Pt(111) surface.

5.4.2 Impurity Deposition on Pt(111)

The HPt decomposition on Pt(111) deposited platinum atoms as well as impurities on the surface. Auger spectroscopy detected carbon on the surface.

The work function change during adsorption was measured, in between high temperature flashes of HPt. The work function change became smaller with each successive HPt adsorption-desorption cycle on Pt(111). This indicates that the reactivity of the surface was slowly switched off as impurities began to accumulate on the surface.

5.4.3 HPt chemistry dependence on surface reactivity

In order to understand the decomposition mechanism more fully, the effect of surface reactivity on the interaction of HPt was studied. The following surfaces in order of decreasing chemical reactivity were prepared:

(1) Pt(111) was prepared by argon bombardment, followed by heating in high pressure of oxygen (6×10^{-6} torr) at 800 °C, followed by a high temperature anneal in vacuo.

(2) Pt(111)-C(ΔHPt) was prepared by adsorption of the complex HPt, followed by high temperature anneal to initiate decomposition of HPt on the surface. This procedure was repeated several times.

(3) Pt(111)-C(ΔC_2H_6) was prepared by annealing the reactive surface in high pressures of ethane (4×10^{-6} torr) at 800 °C.

(4) Pt(111)-C(ΔC_2H_2) was prepared by annealing in acetylene at high pressures

of 5×10^{-6} torr and 800 °C.

(5) Pt(111)-p(2×2)-O was prepared by cooling a Pt(111) surface to 110 K in O_2 pressures of 6.4×10^{-7} torr.

On the Pt(111) surface, the methyl isocyanide coordinated to the platinum atom cleaved on chemisorption and coordinated to the platinum (111) surface instead, in a terminally bonded position. The multilayer grew in at apparent exposures greater than 0.2 L. On warming the monolayer, association or disproportionation reactions reduced the infrared intensity of the C≡N stretch into the noise level at 175 K. Further warming yielded H_2 and HCN as products of decomposition. Both methyl platinum and methyl ligand groups suffered dehydrogenation to give a m/e TPD signal at 435 K with a FWHM of 200 K. A low temperature m/e 41 peak was assigned to multilayer desorption of the complex. No high temperature m/e 41 peak was observed.

The FTIR-RAS data of monolayer HPt on Pt(111)-C(ΔHPt) shows a band at 2234 cm^{-1}, with an accompanying ν(C-H) triplet at 2800 to 3000 cm^{-1} of larger intensity (4:1). The band at 2234 cm^{-1} was observed on Pt(111) and had been assigned to terminally bonded methyl isocyanide from the dissociation of HPt on Pt(111).

The large ν(C-H) triplet at 2800 to 3000 cm^{-1} appeared to grow in with surface

carbon contamination. *The carbon was left behind from the decomposition of HPt on Pt(111) - Auger spectroscopy showed the presence of carbon and the magnitude of the work function change during adsorp.. n decreased with each subsequent dose and high temperature flash in vacuo.* Furthermore in contrast to Pt(111) the C≡N stretch at 2234 $cm^{-1}$was observed at 175 K and the ν(C-H) stretches were persistent till 325 K. To investigate the effect of the surface carbon, the Pt(111) surface was annealed in 4×10^{-6} torr of ethane at 800 °C for a few hours. This is a less reactive surface than Pt(111)-C(ΔHPt).

On the Pt(111)-C(ΔC_2H_6) surface, the 2234 cm^{-1} peak which appeared at exposures of 0.5 L on the reactive Pt(111) surface was not observed for equivalent exposures. This is also in contrast to the situation on Pt(111)-C(ΔHPt), where the 2234 cm^{-1} peak is observed. No C≡N or C=N stretches were observed for exposures ≤ 0.36 L and applying the surface selection rule, this implies that the complex, which has dsp^2 configuration around the platinum atom, lies with its square planar molecular plane with the two CN bond axes parallel to the surface. The CN bonds are probably bonded to the surface via π bonding as they already sigma bonded to the platinum atom in the complex. The C-H stretches were observed and the methyl groups are probably farther away from the surface, such that the C-H bond has a non zero dipole moment perpendicular to the surface. The TPD spectra for a 0.56 L exposure showed a high temperature m/e 41 at a peak desorption temperature of 520 K while the m/e 27 high temperature peak was relatively weaker. Furthermore, the

high temperature m/e 41 was not accompanied by a high temperature m/e 57 (trimethyl imine). This fragment is observed in the mass spectrum of HPt (MAT 8230). In other words, the high temperature m/e 41 observed in these spectra is due to monolayer decomposition as its peak desorption temperature is 520 K. This temperature is close to the regime of explosive isomerization of methyl isocyanide to acetonitrile in the gas phase. Besides the high temperature loss of m/e 41 on the Pt(111)-C(ΔC_2H_6), m/e 2 show a very weak signal at 460 K. The surface carbon appears to passivate the dissociative sites for dehydrogenation and this observation is consistent with the TD-FTIR-RAS data for HPt/Pt(111)-C(ΔHPt), which shows a persistent C-H stretch up to 325 K.

The multilayer and monolayer appeared to grow together on a Pt(111)-C(ΔC_2H_6). HPt growth on this surface has limited diffusion of adsorbed species. If $\theta_{HPt} < 1$ ML is the coverage of HPt on the surface, then $1-\theta_{HPt}$ is the probability that the flux of HPt will arrive at a bare surface and θ_{HPt} is the probability that the multilayer will begin to grow on top of the monolayer.

When HPt was adsorbed on Pt(111)-C(ΔC_2H_2), the FTIR-RAS did not show the 2234 cm^{-1} peak at all. FTIR-RAS of the multilayer agreed well with the gas phase spectra except for a band at 1650 cm^{-1}. As the surface was passivated by heating in acetylene, no strong interaction was expected and the band at 1650 cm^{-1} indicated weak interaction. For a 0.7 L exposure, there was no m/e 41 high

temperature peak observed, indicating no monolayer desorption.

In summary, the presence of surface carbon can be realised in both adsorption and desorption experiments. In adsorption, surface carbon turns off the reactivity so that there is reduced dissociative chemisorption. In desorption, surface carbon turns off the dehydrogenation pathway.

5.4.4 Dehydrogenation of *cis*-dimethyl platinum diisocyanide on Pt(111)

Hydrogen is produced in the high temperature anneal of HPt on clean Pt(111). The desorption temperature of hydrogen was greater than the desorption temperature of chemisorbed hydrogen, pointing to reaction limited desorption of hydrogen in HPt decomposition. Clearly, hydrogen is not produced on chemisorption at 110 K as it would otherwise desorb at 223 and 325 K (H_2 desorption temperature from Pt(111)).

The H_2 desorption signal from HPt/Pt(111) has a large FWHM of approximately 200 K. In contrast, H_2 desorption signal from CH_3NC [6] and CH_3 [7] decomposition on Pt(111) has a FWHM of about 80 K and 60 K respectively. It would appear therefore that the H_2 desorption signal from the decomposition of HPt

---

[6] Supra footnote 3, chapter 5.

[7] Supra footnote 5, chapter 5.

on Pt(111) is an overlap of H_2 desorption signal from CH_3NC and CH_3 decomposition on Pt(111) with peak temperatures of 460 K and 360 K respectively. The peak temperature in H_2 desorption from HPt/Pt(111) is 435 K.

FTIR-RAS is the ideal tool to study the mechanism of dehydrogenation. However, the C-H stretch region of monolayer HPt/Pt(111) is unfortunately complicated as a ν(C-H) triplet is usually observed in the 2800 to 3000 cm^{-1} region. Deuteration of the methyl groups on the ligand and the methyl ligands on the platinum has not been successful in detecting a ν(C-D) stretch due to possible CH/CD exchanges on the surface. The C-H stretches of methyl isocyanide on Pt(111) are also weak in intensity.

The interaction of acetonitrile (the isomer of methyl isocyanide) with Pt(111) was studied in chapter 4. There is evidence for C-H bond interaction in chemisorption at 110 K for the CH_3CN/Pt(111) system. This information taken together with HPt dehydrogenation on Pt(111) indicates that the mechanism of dehydrogenation may involve a hydride shift from the methyl on the ligand to the platinum (111). It is also conceivable that a hydride shift from the methyl platinum may also be involved. Hydride shifts in the decomposition of triisobutyl aluminum

on Al(111) and Al(100) signal crystal surfaces have been reported by Bent et al. [8]

5.5 Conclusions

FTIR-RAS, TPD and $\Delta\phi$ have been used to investigate the interaction of *cis*-dimethyl platinum dissocyanide on Pt(111) and Pt(111)-C surfaces.

The main conclusions in this chapter are:

(1) Impurity deposition on Pt(111) as evidenced by smaller work function change and C-Auger signals after each high temperature anneal of HPt on Pt(111).

(2) The interaction of HPt with the surface changes as the reactivity is changed:

- On a Pt(111) surface, the precursor dissociates on chemisorption at 110 K. On heating the monolayer, it decomposes and reaction products HCN and H_2 are detected. HCN arises from CH_3NC decomposition on Pt(111) while H_2 arises from decomposition of methyl platinum groups and decomposition of CH_3NC on Pt(111).
- On a Pt(111)-C(ΔC_2H_6) surface, the precursor adsorbs molecularly with its square planar molecular plane parallel to the surface or at least with the CN bond axis of the MeNC groups close to parallel with the

[8] Bent B. E., R. G. Nuzzo and L. H. Dubois, J. Am. Chem. Soc., Vol. III, No. 5, 1989, 1634 - 1644.

surface. On warming the crystal, the precursor desorbs non-molecularly with a loss of a methyl isocyanide ligand. The growth of HPt on Pt(111)-C(ΔC_2H_6) follows a "hit and stick" model.

- On a Pt(111)-C(ΔHPt) surface, some precursor finds dissociative sites and others find non-dissociative sites.

Dehydrogenation was reaction limited. The mechanistic study of the dehydrogenation was frustrated by the complexity of the C-H stretches at 3000 cm^{-1} (for HPt) and CH/CD exchanges (for DPt and D'Pt), making the detection of the ν(C-D) stretch difficult. However, the acetonitrile interaction with Pt(111) shows evidence of the participation of C-H bond in chemisorption. It is quite possible that the dehydrogenation may involve a β hydride shift to the surface not unlike those observed in the work done by Bent et al. [9]

[9] Supra footnote 8, chapter 5.

CHAPTER 6

CONCLUSIONS

6.1 Summary of results

The decomposition mechanism of *cis*-[$(CH_3)_2Pt(MeNC)_2$] for deposition of platinum thin films has been studied in the gas phase and on the platinum (111) surface. Its co-decomposition with hydrogen has also been studied.

The first step in the gas phase decomposition involves the reversible dissociation of a MeNC ligand to give an intermediate [$Me_2Pt(MeNC)$]. Methane is the only volatile hydrocarbon detected and it is formed by combination of the methyl from the Me-Pt groups and a hydrogen atom probably from the cell walls. The isocyanide ligand probably isomerizes to acetonitrile or polymerizes to an oily polymer with CN stretches at 2232 and 2172 cm^{-1}. The reaction kinetics is first order in the complex (HPt). The theoretical rate law derived from the proposed mechanism agrees well with that determined experimentally and is expressed in the following equation:

$$\frac{d[CH_4]}{dt} = \frac{kK[HPt]}{[MeNC]} \qquad (6.1)$$

The HPt co-decomposition with hydrogen gas produces methane gas and an oily polymeric material as before in HPt decomposition. In addition, there appears

to be an additional volatile product, which is probably ammonia. The MeNC ligand is lost from HPt and isomerizes to CH_3CN which on hydrogenation and subsequent decomposition gives ammonia. The methane is produced from the combination of a methyl platinum group and a hydrogen atom from hydrogen gas.

The rate of methane evolution is increased when *cis*-dimethyl platinum diisocyanide is codecomposed with hydrogen. The kinetics become more complicated. The order of reaction with respect to the complex changed from 1 to 0.5. The kinetic data almost certainly points to catalysis. The growing platinum film is a highly reactive surface. Indeed, the rate of methane evolution was increased when *cis*-dimethyl platinum diisocyanide was codecomposed with hydrogen over a preformed platinum film. Hydrogen gas probably adsorbs dissociately on the platinum surface to provide a source of hydrogen atoms. Acetonitrile from the isomerization of methyl isocyanide quite likely adsorbs in an η^2(C,N) fashion. Hydrogenation of the η^2(C,N) could give the following surface species:

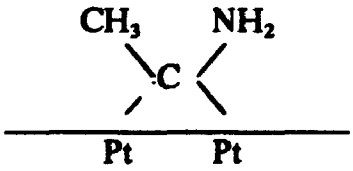

which on decomposition gives ammonia. The methyl platinum group when cleaved from the platinum atom in the complex combines with the hydrogen atoms on the surface to give methane. This model is consistent with the observations of increased methane evolution and cleaner platinum films when *cis*-dimethyl platinum

diisocyanide was decomposed in the presence of hydrogen.

On a reactive platinum(111) surface, monolayer HPt dissociates on chemisorption to give a terminally bonded MeNC ligand on Pt(111) and some Pt containing hydrocarbon fragment. The assignment was based on the FTIR-RAS study of monolayer CH_3NC/Pt(111) which showed a band at 2234 cm^{-1}. On warming association and disproportionation reactions reduce the infrared intensity of the C≡N stretch into the noise level. Further warming yields the decomposition products of hydrogen, hydrogen cyanide and carbon impurity on the surface. The hydrogen desorption shows a peak desorption temperature at 435 K with a high temperature shoulder while the HCN has two peak desorption temperatures at 525 K and 660 K respectively. The CH_3NC/Pt(111) system involved decomposition to give H_2 and HCN on warming. However, the FWHM for H_2 desorption from the HPt/Pt(111) system is much larger (at about 200 K compared to 75 K for CH_3NC decomposition on Pt(111)). Thermal decomposition of the methyl platinum groups could account for the large FWHM. H_2 desorption from CH_3 decomposition on Pt(111) was shown to have peak desorption temperature of 360 K and FWHM of 60 K. The H_2 desorption peak from the decomposition of *cis*-dimethyl platinum diisocyanide is thus an overlap of H_2 signals from CH_3NC and CH_3 decomposition on Pt(111). There is evidence from the interaction of acetonitrile on Pt(111) that the C-H bond is activated by the surface. The mechanism of dehydrogenation may involve a hydride shift to the surface.

Surface carbon on Pt(111) (Pt(111)-C(ΔHPt) surface), caused a ν(C-H) triplet of strong intensity to be observed together with the 2234 cm^{-1} band. The strong ν(C-H) intensity was shown to be due to molecular adsorption of the complex.

When carbon was deposited on the surface by heating the crystal in ethane, the HPt was found to adsorb molecularly with the CN bond axis parallel to the surface. On annealing the crystal, there is non-molecular desorption of HPt. The MeNC ligand is lost at about 520 K. The growth of HPt on a platinum (111) surface with surface carbon appears to agree with a "hit and stick" model.

In the interaction of acetonitrile with Pt(111), we have used temperature programmed desorption, work function measurements and infrared reflection absorption spectroscopy in the investigation. We have shown that the η^2(C,N) state in the monolayer can have intermolecular screening of its dynamic dipole moments, resulting in a reduction in the intensities of the infrared bands. The properties of the submonolayer have been shown to depend on how the submonolayer was prepared. In an "unannealed" submonolayer, the layer adopts an η^{2*}(C,N) bonding configuration, where the CN vector lies parallel to the surface and the β-hydrogens are also involved in chemisorption. In an "annealed" submonolayer, the layer adopts a different bonding configuration, with both terminal and bridge forms of acetonitrile bonded to Pt(111) via the nitrogen atom.

6.2 Further Work

6.2.1 Co-decomposition of HPt with H_2 on Pt(111)

The codecomposition of HPt and H_2 described in Chapter 3 was shown to have a heterogenous component in the reaction mechanism. Thus coadsorption studies of HPt and H_2 on Pt(111) will contribute significantly to the understanding of decomposition mechanisms in OMCVD.

6.2.2 STM Imaging

STM can produce images of surfaces with atomic resolution. "Seeing" the atoms in real space can greatly enhance our understanding of the adsorption and decomposition of the organometallic precursor on surfaces. Furthermore, the microscope can image atoms and molecules on semiconductor surfaces. This will enable study of initial metal growth on semiconductor surfaces. Such work is planned in the group.

6.2.3 HPt interaction with semiconductor surfaces

As already alluded to in the previous sub-section, HPt interaction with semiconductor surfaces will determine the initial growth of platinum on the surface. This current work has used IRRAS to study the adsorption and decomposition of HPt on a metal surface (Pt(111) surface). For semiconductor surfaces, the infrared light has to be coupled into the crystal via a bevelled edge of the silicon crystal and allowed to make multiple internal reflections in the crystal. This is in contrast to

IRRAS where the light makes a single external reflection off the surface. The UV chamber has two 4½ inch ports constructed for this work. They allow the light to focus on the bevelled edge rather than at the centre of the crystal.

6.2.4 XPS

It was pointed out in section 5.4.1 of chapter 5 that it was difficult to prove platinum deposition on a platinum surface. The Auger spectrometer is a retarding field analyser which gives poor energy resolution.

An XPS instrument has better energy resolution and can resolve core level shifts which are sensitive to the chemical environment of the atom. Thus using XPS, a platinum atom in the Pt(111) surface lattice can be distinguished from the platinum atom bonded in the complex. Furthermore, changes in chemical shifts as the platinum atom is incorporated into the surface lattice may yield information regarding the decomposition mechanism of HPt on the surface.

BIBLIOGRAPHY

Avery, N.R., Matheson, T.W. and Sexton, B.A. "Bonding configuration on Pt(111)". **Appl. Surf. Sci.**, 22-23/1 (1985), 384.

Avery, N.R., Matheson, T.W. "Adsorption and decomposition of methyl iso-cyanide on Pt(111)". **Surf. Sci.**, 143 (1984), 110.

Basset, J.M., J.P. Candy, A. Choplin, C. Nedez, F. Quignard, C.C. Sautini, A. Theolier. "From clusters and surfaces to clusters on surfaces -- an opening toward surface organometallic chemistry. " **Mater. Chem. and Phys.**, 29/1-4 (1991), 5.

Bent, B.E., R.G. Nuzzo and L.H. Dubios. "Surface organometallic chemistry in the chemical vapour deposition of aluminum films using triisobutyl aluminum : β-allyl elimination reactions of surface allyl intermediates" . **J. Am. Chem. Soc.**, 111/5 (1989), 1634.

Blass, P.M., S. Akhter, C.M. Seymour, J.J. Lagowskin and J.M. White. "The adsorption and decomposition of bis(benzene) chromium on Ni(100). **Surf. Sci.**, 217 (1989), 85.

Blech, I., H. Sello and L.V. Gregor, in "Handbook of Thin Film Technology". (Maissel L.I. and Glang R., eds.), (1970), 23-1.

Bradley, D.C. "New metallo-organic precursors for surface processing." **Appl. Surf. Sci.**, 46 (1990), 1.

Braichotte, D., C. Garrido and H. van den Bergh. "The photolytic laser chemical vapour deposition rate of platinum, its dependences on wavelength, precursor vapour pressure, light intensity, and laser beam diameter". **Appl. Surf. Sci.**, 46 (1990), 9.

Brillson, L.J., R.E. Viturro, C. Mailhiot, J.L. Shaw, N. Tache, J. McKinley, G. Margaritondo, J.M. Woodall, P.D. Kirchner, G.D. Pettit and S.L. Wright, "Unpinned Schottky barrier formation at metal-GaAs interfaces". **J. Vac. Sci. Technol. B**, 6 (1988), 1263.

Brookhart, M. and M.L.H. Green. "Carbon-hydrogen-transition metal bonds". **J. Organometallic Chem.**, 250 (1983), 395.

Brubaker, M.E. and M. Trenary. "Absorbate ordering processes and infrared spectroscopy : An FT-IRAS study of N_2 chemisorbed on the Ni(110) surface. **J. Chem. Phys.**, 85/10 (1986), 6100.

Chesters, M.A., P. Gardner and E.M. McCash, "The reflection-adsorption infrared spectra of n-alkanes adsorbed on Pt(111)". **Surf. Sci.**, 209 (1989), 89.

Christmann, K., G. Ertl and T. Pignet. "Adsorption of hydrogen on a Pt(111) surface". **Surf. Sci.**, 54 (1976), 365.

Cichy, H. and E. Fromm. "Oxidation kinetics of metal films at 300 K studied by the piezo electric quartz crystal microbalance". **Thin Solid Films**, 195/1-2 (1991), 147.

Creighton, J.R. "Chemisorption and decomposition of trimethyl gallium on GaAs(100)". **Surf. Sci.**, 234 (1990), 287.

Dowrey, A.E. and C. Marcott. "A double modulation Fourier transform infrared approach to studying adsorbates on metal surfaces." **Appl. Spect.**, 36/4 (1982), 414.

Dryden, N.H., R. Kumar, E. Ou, M. Rashidi, S. Roy, P.R. Norton, R.J. Puddephatt and J.D. Scott. "Chemical vapour deposition of platinum: New precursors and their properties". **Chem. Mater.**, 3/4 (1991), 677.

Dubois, L.H., B.R. Zegarski, C.T. Kao and R.G. Nuzzo. "The adsorption and thermal decomposition of trimethylamine alane on aluminum and silicon single crystal surfaces: kinetics and mechanistic studies". **Surf. Sci.**, 236 (1990), 77.

Dubois, L.H., B.R. Zegarski, M.E. Gross and R.G. Nuzzo. "Aluminum thin film growth by the thermal decomposition of triethylamine alane". **Surf. Sci.**, 244 (1991), 89.

Esrom, Hilmar and Ulrich Kogelschatz. "Investigation of the mechanism of the UV-induced palladium deposition process from thin solid palladium acetate films". **Appl. Surf. Sci.**, 46 (1990), 158.

Farnaam, M.K., D.R. Olander. "The surface chemistry of the thermal cracking of silane on silicon (111)". **Surf. Sci.**, 145 (1984), 390.

Fedyk, J.D., P. Mahaffy and M.J. Dignam. "Applications of IR ellipsometric spectroscopy to surface studies". **Surf. Sci.**, 89 (1979), 404.

Feulner, P. and Menzel, D. "Simple ways to improve "flash desorption" measurements from single crystal surfaces". **J. Vac. Sci. Technol.**, 17/2 (1980), 662.

Flitsch, F.A., J.R. Swanson. and C.M. Friend. "Thermal and photo-induced decomposition of $Mo(CO)_6$ on W(110)". **Surf. Sci.**, 245 (1991), 85.

Friend, C.M., E.L. Muetterties and J.L. Gland. "Vibrational studies of CH_3CN and CH_3NC adsorbed on Ni(111) and Ni(111)-C surfaces". **J. Phys. Chem.**, 85 (1981), 3256.

Froitzheim, H., H. Hopster, H. Ibach and S. Lehwald. "Adsorption sites of CO on Pt(111)". **Appl. Phys.**, 13 (1977), 147.

Gaspar, P.P., **Reactive Intermed.**, 3 (1985), 333.

Gates, S.M., J.N. Russell, Jr. and J.T. Yates, Jr. "Observation of a deuterium kinetic isotope effect in the chemisorption and reaction of methanol on Ni(111)". **Surf. Sci.**, 146 (1984), 199.

Garwood, G.A. and A.T. Hubbard. "Superlattices formed by interaction of polar solvents with Pt(111) surfaces studied by LEED, Auger Spectroscopy and thermal desorption mass spectrometry". **Surf. Sci.**, 118 (1982), 223.

Germer, T.A. and W. Ho. "The adsorption and photochemistry of $Mo(CO)_6$ on Rh(100)". **J. Chem. Phys.**, 89/1 (1988), 562.

Golden, W.G. and Saperstein. "Infrared reflection-adsorption spectroscopy of surface species : A comparison of Fourier Transform and Dispersion methods". **J. Phys. Chem.**, 88 (1984), 574.

Golden, W.G., D.S. Dunn and J. Overend. "A method for measuring Infrared Reflection-Absorption Spectra of molecules adsorbed on low- area surfaces at monolayer and submonolayer concentrations". **J. of Catal.**, 71 (1981), 395.

Gozum, J.E., D.M. Pollina, J.A. Jensen and G.S. Girlani. "'Tailored' Organometallics as precursors for the chemical vapour deposition of high purity palladium and platinum thin films". **Thin Solid Films**, 195/1-2 (1991), 147.

Greenler, R.G. "Infrared study of adsorbed molecules on metal surfaces by reflection techniques". **J. Chem. Phys.**, 44/1 (1966), 310.

Griffiths, P.R. and J.A. de Haseth. "Fourier transform infrared spectrometry" **Chemical analysis**, 83 Wiley, (1986).

Gupta, P., A.C. Dillion, A.S. Bracker and S.M. George. "FTIR studies of H_2O and D_2O decomposition on porous silicon surfaces". **Surf. Sci.**, 245/3 (1991), 360.

Henderson, M.A., Ramsier, R.D. and J.T. Yates,Jr. "Minimizing ultra high vacuum wall reactions of $Fe(CO)_5$ by chemical pretreatment of dosing system". **J. Vac. Sci. Technol. A**, 9/5 (1991), 2785.

Higashi, G.S. "The chemistry of allkyl-aluminum compounds during laser-assisted chemical vapour deposition". **Appl. Surf. Sci.**, 43 (1989), 6.

Higashi, G.S. " Mechanism of surface selectivity in aluminum chemical vapour deposition". **J. Vac. Sci. Technol. B.**, 8 (1990), 103.

Hottier, F. and R. Cadoret. "Surface processes in low pressure chemical vapour deposition." **J. Crystal Growth**, 52 (1981), 199.

Jagannathan, G.V., A. Merrill and A.T. Habig. "Hydrogen beam stimulated low temperature dissociation of organometallics -- application for lowering the growth temperature in a metalorganic chemical vapour deposition process". **Appl. Phys. Lett.**, 56/20 (1990), 2019.

Jenks, C.J., C.M. Chiang and B.E. Bent. "Alkyl iodide decomposition on copper surfaces : α-elimination and β-hydride elimination from adsorbed alkyls". **J. Am. Chem. Soc.**, 113 (1991), 6308.

Jo, S.K. and J.M. White. "Adsorption and UV-induced dissociation of $ClCH_2$-CH_2Br on Pt(111). **Surf. Sci.**, 245/3 (1991), 305.

Joyce, B.A., R.R. Bradley, "Epitaxial growth of silicon from the pyrolysis of monosilane on silicon substrates". **J. Electrochem. Soc.**, 110 (1963), 1235.

Koerts, T. and R.A. Vansanten. "The reaction path for recombination of surface CH_x species". **J. Molec. Catal.**, 70/1 (1991), 119.

Konstantinov, L. and R. Nowack and P. Hess. "Gas phase transport and kinetics in pulsed laser CVD". **Appl. Surf. Sci.**, 46 (1990), 102.

Kuech, T.F., E. Veuhoff. "Mechanism of carbon incorporation in MOCVD GaAs". **J. Cryst. Growth**, 68 (1984), 148.

Kulkarni, S.K., S.M. Gates, B.A. Scott and H.H. Sawin. "Modulated molecular beam scattering of disilane and silicon". **Surf. Sci.**, 239 (1990), 13.

Kulkarni, S.K., S.M. Gates, C.M. Greenlief and H.H. Sawin. "Mechanisms of disilane decomposition on Si(111)-7×7". **Surf. Sci.**, 239 (1990), 26.

Larciprete R. "Photoprocesses in organometallics". **Appl. Surf. Sci.**, 46 (1990), 19.

Liu, Z.M., X.L. Zhou and J.M. White. "Adsorption and decomposition of trimethyl gallium on Pt(111)". **Appl. Surf. Sci.**, 52/3 (1991), 249.

Malik, I.J. and M. Trenary. "Infrared reflection-adsorption study of the absorbate-substrate stretch of CO on Pt(111)". **Surf. Sci.**, 214 (1989), L237.

Maruca, R., T. Kusuma, V. Hicks and A. Companion. " Theoretical studies of molecules on metal surfaces: I site stability and vibrational frequencies of CO on Ni(111), Ni(110) and Ni(100)". **Surf. Sci.**, 236 (1990), 210.

Memmert, U. and M.L. Yu. "Pyrolysis of trimethylgallium on GaAs(100) surfaces". **Appl. Phys. Lett.**, 56 (1990), 1883.

Moritz, H. and H. Lüth. "Interactions in the co-adsorption system, CO/acetonitrile on Pt(111) : an IRAS investigation". **Vacuum**, 41/1-3 (1990), 63.

Morgen, P., M. Szymonski, J. Onsgaard, B. Jorgensen, G. Rossi. "Formation of the Pt-Si(111) interface". **Surf. Sci.**, 197 (1988), 347.

Pemble, M.E., J.T. Allen, D.S. Buhaenko, S.M. Francis, P.A. Goulding, J. Lee and M.J. Parott. "The adsorption of trimethylgallium on GaAs(100) at 300 K: adsorption kinetics from optical second harmonic generation transients". **Appl. Surf. Sci.**, 46 (1990), 32.

Purnell, J.H., R. Walsh. "Some comments on kinetics and mechanism in the pyrolysis of monosilane". **Chem. Phys. Lett.**, 110 (1984), 330.

Raynaud, P., J.P. Booth, and C. Pomot. "Hydrogen plasma treatment of silicon surfaces studied by in-situ spectroscopic ellipsometry.". **Appl. Surf. Sci.**, 46 (1990), 435.

Sault, A.G. " Reactions of silane with the W(110) surface". **Surf. Sci.**, 235 (1990), 28.

Schüle, J., P. Siegbahn and U. Wahlgren. "A theoretical study of methyl chemisorption on Ni(111)". **J. Chem. Phys.**, 89 (1988), 6982.

Sexton, B.A. and N.R. Avery. "Coordination of acetonitrile (CH_3CN) to platinum(111) : evidence for an η^2(C,N) species". **Surf. Sci.**, 129 (1983), 21.

Simpson, J. and J.O. Williams. "Preferential (111) orientation of ZnSe on (100) GaAs deposited by laser-induced MOCVD." **Appl. Surf. Sci.**, 46 (1990), 27.

Solomun T., K. Christmann and H. Baumgärtel. "Interaction of acetonitrile and benzonitrile with the Au(100) surface"., **J. Phys. Chem.**, 93 (1989), 3256.

Solomun T., H. Baumgärtel and K. Christmann. "The interaction of nitriles with a potassium-promoted gold(100) surface"., **J. Phys. Chem.**, 95/24 (1991), 10041.

Solymosi, F. and K. Revesz. "Thermal stability of the CH_3 group adsorbed on the Pd(100) surface". **J. Am. Chem. Soc.**, 113/24 (1991), 9145.

Spencer, E.G., P.H. Schmidt. "Ion beam technique for device fabrication". **J. Vac. Sci. Technol.**, 8 (1971) S52.

Sywe, B.S., J.R. Schlup and J.H. Edgar. "Fourier transform infrared spectroscopic study of predeposition reactions in metalloorganic chemical vapour deposition of gallium nitride, 2". **Chem. Mater.**, 3/6 (1991), 1093.

Swanson, J.R. and C.M. Friend, Y.J. Chabal. "Laser-assisted deposition of iron on Si(111)-(7×7): The mechanism and energetics of $Fe(CO)_5$ decomposition". **J. Chem. Phys.**, 87/8 (1987), 5028.

Szilágyi, T., "Infrared spectra of methyl cyanide and methyl isocyanide adsorbed on Pt/SO_2". **Appl. Surf. Sci.**, 35/1 (1988), 19.

Trenary, M., K.J. Uram, F. Bozso and J.T. Yates, Jr. "Temperature dependence of the vibrational lineshape of CO chemisorbed on the Ni(111) surface". **Surf. Sci.**, 146 (1984), 269.

Watson, I.M., J.A. Connor and R. Whyman. "Chromium-phosphorus films deposited by the pyrolysis of an organometallic precursor". **Thin Solid Films** , 196/1 (1991), L21.

Xin, X. and Steinfeld. "UV-laser photodeposition of iron films from $Fe(CO)_5$: role of gas-phase and surface dissociation process". **Appl. Surf. Sci.**, 45 (1990), 281.

Xue, Z., M.J. Stouse, D.K. Shah, C.B. Knobler, H.D. Kaesz, R.F. Hicks and W. R. Stanley. "Characterization of (methyl cyclopentadienyl) trimethyl platinum and low temperature organometallic chemical vapour deposition of platinum metal". **J. Am. Chem. Soc.**, 112/10 (1990), 4090.

Zaera, F. "Reversibility of C_1 hydrogenation-dehydrogenation reactions on platinum surfaces under vacuum." **Langmuir**, 7 (1991), 1998.

Zaera, F. and H. Hoffmann. "Detection of chemisorbed methyl and methylene groups: surface chemistry of methyl iodide on Pt(111)." **J. Phys. Chem.**, 95 (1991), 6297.

Zeper, W.B., F.J.A.M., Greidanus and P.F. Carcia, "Evaporated Co/Pt layered structures for magneto-optical recording". **IEEE Transactions on Magnetics** 25/5 (1989), 3764.